FABRICATION OF METAMATERIAL FILTERS FOR TERAHERTZ WAVE APPLICATIONS BY E-BEAM PATTERNING

A Thesis submitted to
The Graduate School of Engineering and Science of
İzmir Institute of Technology
in Partial Fulfillment of the Requirements for the Degree of

DOCTOR OF PHILOSOPHY

in Materials Science and Engineering

by
Yasemin DEMİRHAN

July 2017
İZMİR

We approve the thesis of **Yasemin DEMİRHAN**

Examining Committee Members:

Prof. Dr. Lütfi ÖZYÜZER
Department of Physics, İzmir Institute of Technology

Prof. Dr. Necdet BAŞTÜRK
Department of Physics Engineering, Hacettepe University

Assoc. Prof. Dr. Devrim PESEN OKVUR
Department of Moleculer Biology and Genetics, İzmir Institute of Technology

Asst. Prof. Dr. Enver TARHAN
Department of Physics, İzmir Institute of Technology

Prof. Dr. Hakan ALTAN
Department of Physics, Middle East Technical University

31 July 2017

Prof. Dr. Lütfi ÖZYÜZER
Supervisor, Department of Physics
Izmir Institute of Technology

Asst. Prof. Dr. Gürcan ARAL
Co-Supervisor, Department of Physics
Izmir Institute of Technology

Prof. Dr. Mustafa M. DEMİR
Head of the Department of
Material Science and Engineering

Prof. Dr. Aysun SOFUOĞLU
Dean of the Graduate School of
Engineering and Sciences

To my Family…

ACKNOWLEDGEMENTS

First of all, I would like to express my deepest gratitude to Professor Lütfi Özyüzer for his supervision throughout the past 15 years, for leading my way with his vast knowledge. I appreciate him, for his endless patient, encouragement, unconditional support and I could not have finished this thesis without his inspiring suggestions and constant guidance. It was an honor of me studying all the laboratories leadership of him and to benefit from his experience. I hope that I also have acquired some of his scientific thinking along the way.

I would like to express my sincere gratitude to Assoc. Prof. Gülnur Aygün Özyüzer, not only for her time and extreme patience, but also for valuable contributions to my thesis.

I wish to extend my thanks to Assoc. Prof. Hakan Altan for his guidance, valuable reading and comments on my thesis and articles.

I am also grateful to Hakan Altan's METU Terahertz Laboratory research group for the Terahertz Time Domain Measurements, especially Mehmet Ali Nebioğlu and Merve Akkaya.

I am thankful to Assoc. Prof. Dr. Cumali Sabah and Batuhan Mulla for their contributions to my thesis.

I would like to thank also the members of my thesis committee Prof. Necdet Baştürk, Assoc. Prof. Devrim Pesen Okvur and Asst. Prof. Gürcan Aral for helpful comments and constructive feedback.

I would like to thank also Assoc. Prof. Yusuf Selamet for his contributions during my master and PhD education.

As teamwork is essential, I am very thankful to my lab mates, especially Hakan Alaboz, Hurriyet Yüce and Şehriban Zeybek for their kindness and support while studying together.

I wish to thank to all my labmates, and to each of my friends at Izmir Institute of Technology for providing a great atmosphere and a wonderful workplace. We have unforgettable memories at the end of fifteen years and now each of them is very important for me.

I acknowledge TUBITAK (Scientific and Technical Research Council of Turkey) since this project is supported by TUBITAK with project number 114F091 and thanks also to AQUREC (Applied Quantum Research Center) at IZTECH for provi
me clean room facilities and as e-beam lithography system.

Last, but not least I want to thank my family for their unconditional love, unending support and understanding me during my whole life and providing me with more than I can ever repay them for.

ABSTRACT

FABRICATION OF METAMATERIAL FILTERS
FOR TERAHERTZ WAVE APPLICATIONS
BY E-BEAM PATTERNING

In the electromagnetic spectrum, terahertz (THz) radiation falls into the region among microwaves and the far-IR. The unique properties of superconducting materials allow them to be utilized in a number of ways for THz device applications. In the first part of this thesis, the spectral performance of THz bandpass filters were produced from titanium, copper and indium tin oxide thin films with a metal-mesh shape on fused silica substrates by uv lithography were investigated. For metamaterial filter fabrication, $Bi_2Sr_2CaCu_2O_{8+x}$ thin films were deposited by DC and RF magnetron sputtering system on saphirre and MgO substrates. After thin film characterizations, it is obtained that the films were not in single phase and could not be used for filter fabrication. A new, unique fourcross shaped metamaterial THz filter was designed and fabricated from both gold thin films and $YBa_2Cu_3O_{7-d}$ high T_c superconducting thin films. The designed fourcross shaped rectangular filter structure consists of periodic metallic rings where strip lines are located at the sides of the ring. CST Microwave Studio, is used to design and optimize the metamaterial filter structures. To investigate the temperature-dependent resonance behavior and confirm the measurements, simulations are carried out at temperatures above and well below T_c. Fourcross metamaterial filters are fabricated by using e-beam lithography and ion beam etching techniques. The resonance switching of the transmission spectra was investigated by lowering the temperature below the critical transition temperature. This novel fourcross filter holds great potential for active, tunable and lowloss THz devices for imaging, sensing, and detection applications.

ÖZET

TERAHERTZ DALGA UYGULAMALARI İÇİN E-DEMETİ ŞEKİLLENDİRMESİ İLE METAMALZEME FİLTRE FABRİKASYONU

Elektromanyetik spektrumda, terahertz (THz) radyasyonu mikrodalgalar ve uzak IR arasındaki bölgede yeralır. Süperiletken malzemelerin benzersiz özellikleri, THz aygıt uygulamaları için çeşitli şekillerde kullanılmasına olanak sağlar. Bu tezin ilk bölümünde, titanyum, bakır ve indiyum kalay oksit ince filmlerinden uv litografisi ile fused silika alttaş üzerine metal-örgü şekilli üretilen THz bant geçiren filtrelerin spektral performansı araştırılmıştır. Metamalzeme filtre üretimi için, $Bi_2Sr_2CaCu_2O_{8+x}$ ince filmleri, safir ve MgO altaşlarına DC ve RF magnetron saçtırma sistemi ile kaplanmıştır. İnce film karakterizasyonları sonrasında, filmlerin tek fazda olmadıkları ve filtre üretimi için kullanılamayacağı anlaşılmıştır. Yeni, özgün, dört köşeli THz metamalzeme filtre yapısı tasarlanmış ve hem altın ince filmlerden hem de $YBa_2Cu_3O_{7-d}$ yüksek T_c süperiletken ince filmlerden üretilmiştir. Tasarlanan dörtlü çapraz şekilli dikdörtgen filtre yapısı, şerit hatların kenarlarına yerleştirildiği periyodik metalik halka yapıdan oluşur. CST Mikrodalga Stüdyosu, metamalzeme filtre yapılarını tasarlamak ve optimize etmek için kullanılmıştır. Sıcaklığa bağlı rezonans davranışını araştırmak ve ölçümleri doğrulamak için, simülasyonlar T_c'nin üstünde ve altında sıcaklıklarda gerçekleştirilmiştir. Dörtlü çapraz metamalzeme filtreler, e-demeti litografisi ve iyon demeti aşındırma teknikleri kullanılarak üretilmiştir. Geçirgenlik spektrumlarında rezonans anahtarlaması, sıcaklığı kritik geçiş sıcaklığının altına düşürerek incelenmiştir. Bu özgün dörtlü çapraz dikdörtgen filtre, görüntüleme, algılama ve spektroskopi uygulamalarında aktif, ayarlanabilir ve düşük kayıplı THz cihazları için büyük potansiyel taşımaktadır.

TABLE OF CONTENTS

LIST OF FIGURES

Figures **Page**

LIST OF TABLES

Table **Page**

LIST OF ABBREVIATIONS

BCS theory: Bardeen–Cooper–Schrieffer theory

Bi2212: $Bi_2Sr_2CaCu_2O_{8+\delta}$

Bi2223: $Bi_2Sr_2Ca_2Cu_3O_{10+x}$

BPFs: Bandpass filters

CSRRs: Complementary split ring resonators

EBL: Electron beam lithography

EDX: Energy Dissipative X-Ray Microanalysis Spectrometer

EOT: Extraordinary optical transmission

FIR: Far infrared

FTIR: Fourier transform infrared spectrometer

FWHM: Full width half maximum

$H_c(1)$: Lower critical field

$H_c(2)$: Upper critical field

H_c: Critical magnetic field

Hg1223: $HgBa_2Ca_2Cu_3O_{8+x}$

HTSs: High Temperature Superconductors

IL: Insertion loss

IR: Near infrared

ITO: Indium Tin Oxide

J_c: Critical current density

$La_{2-x}Ba_xCuO_4$: Lanthanum barium copper oxide

MIR: Medium infrared

MKS: Mass flow controller

PR: Photoresist

Rs : Sheet resistances

R-T: Resistance-Temperature

SEM: Scanning Electron Microscope

SNR: Signal to noise ratio

SRRs: Split-ring resonators

Tc: Critical transition temperature

THz: Terahertz

THz-TDS: Terahertz time-domain spectroscopy

Tl2223: $Tl_2Ba_2Ca_2Cu_3O$

Y123: $YBa_2Cu_3O_{7-x}$

CHAPTER 1

INTRODUCTION

1.1. Terahertz (THz) Region

The region of the electromagnetic spectrum in the 0.3 to 10 THz frequency range is called Terahertz waves or T-rays (THz) (Figure 1.1.).

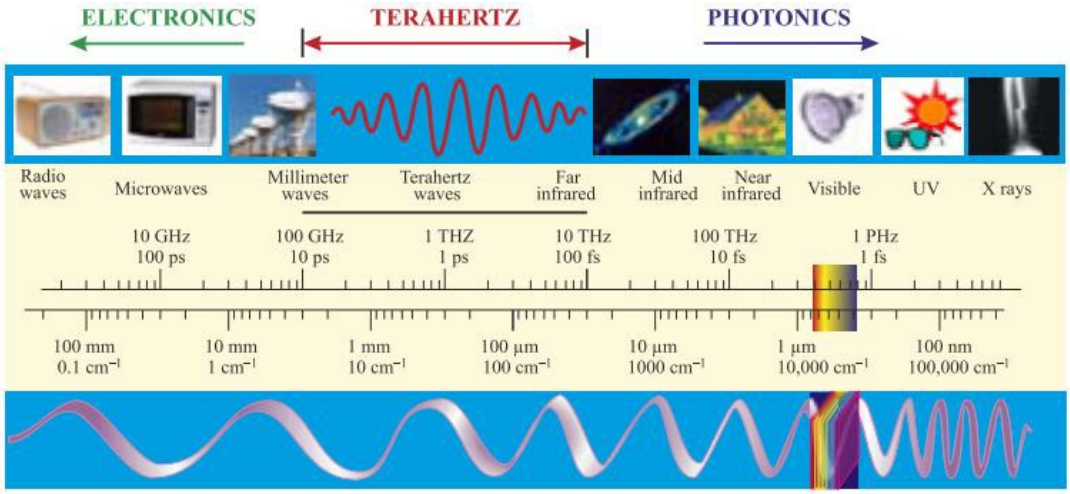

Figure 1.1. The Electromagnetic Spectrum with THz gap.
(Source: Rogalskii et al., 2011)

The low photon energy of the terahertz wavelength (1 THz = 4.1 meV) is one billionth of a meter of the wavelength that X-rays have. When it touches the human body, it prevents the biological tissues from being damaged because it does not ionize the atoms. The use of THz waves allows imaging and spectroscopy applications to cover a wide range of areas such as biology and medical diagnostics, detection of threats against terrorism and trafficking, natural and industrial sensors, battlefield surveillance, airport landing systems, detection of chemical warfare agents, monitoring and airspace security (Kawase et al., 2004; Tonouchi et al., 2007; Ozyuzer et al., 2007; Ozyuzer et al., 1999;

Alaboz et al., 2017). Currently there are many active or passive devices operate in the region, which is often referred as "THz" gap.

Technologies based on terahertz wavelengths are developing rapidly today. One of the most important developments in recent years is seen in the field of terahertz communication technologies. Particularly in the western countries, developments towards the opening of communication bands towards terahertz frequencies are taking place. Base local companies in our country have already made efforts to develop transceiver systems in millimeter wave length (<100 GHz) and integrate existing communication networks for mobile phone users. The importance of developing passive and active devices based on terahertz and millimeter wavelength technologies is rapidly increasing in this intense interest environment. In recent years, especially in our country, micro-scale production techniques based on semiconductor devices are developing rapidly. Using these techniques in the terahertz field, many different devices have been developed that affect terahertz beams, and one of the successful examples is metamaterial structures in terms of ease of fabrication compared to other shorter wavelengths. The Terahertz (THz) region (0.3 and 10 THz) is often referred to as the THz gap, and despite the fact that the materials contain many natural frequencies of vibration, the absence of efficient devices, detectors and components operating in this region makes the THz region unexplored.

In Terahertz technology, metamaterials have an important place in the design of artificial optical elements since they exhibit electromagnetic properties that can not be obtained from natural materials and can be designed with the desired functionality. In recent years, much research has been done in the field of metamaterials for various applications at different frequencies of the electromagnetic spectrum and these studies have received great attention.

However, the success rate in application areas depends on the sensitivity of the materials to losses. Metamaterials can be geometrically scaled and thus operate in a wide range of frequencies including radio, microwave, millimeter wave, far infrared (FIR), medium infrared (MIR), near infrared (IR) frequencies and even visible wave lengths. The Terahertz gap can be thought of as a transitional region between electronic and photonic areas, since metamaterial structures are frequency-tunable, they can easily be drawn from the microwave to the THz region. Numerous scientific researches have been published on analytical, numerical and experimental approaches, original metamaterial effects and superconductivity-based metamaterials. The resonant effects that the

metamaterials show at different terahertz frequencies have started to gain a very important place especially in terms of the detection and spectroscopic methods. In addition to these, the superconducting materials-based devices have developed in recent years at high temperatures have generated a new field of technology development in terahertz wave lengths.

1.2. Applications of THz Radiation

Terahertz radiation is useful in many areas such as scientific studies on material characterization at the universities, pharmaceutical imaging pills, and defense issues of states. Other uses for trade are dentistry (tooth decay detention), T-ray imaging, medical diagnostics (early diagnosis of skin cancer), terahertz time domain spectroscopy, pharmaceutical process control (pill examination). The unique characteristic of the terahertz radiation is not found in other regions of the spectrum. Due to low photon energies of THz waves (1 THz = 4.1 meV, one million times weaker than X-rays) do not cause harmful photoionization in biological tissues (Kawase 2004). Furthermore, since water absorbs Terahertz radiation, it can be used to determine differences in water content and tissue densities. Interacting the terahertz waves with living tissues makes it possible to early diagnose the tooth decay and breast or skin cancer, or to understand dynamical features of cell using a less painful and safer system together with the help of imaging. Terahertz radiation can penetrate into materials which are generally opaque in the case of visible and infrared radiation. This is very interesting for scientists. Clothes, plastics, fabrics, wood, ceramic, paper and fog are some of the materials that can be passed through Terahertz waves. Terahertz waves' frequency corresponds to the frequency of the motion of many other molecules in a range of chemical and biological materials. The transmitted and reflected THz spectra in such materials include THz absorption information characterizing the THz rotational and vibrational modes and which gives significant spectroscopic information (Fischer et al., 2005). This spectroscopy technique with Terahertz waves is particularly useful in pharmaceutical applications where drug structure must be identified rapidly and accurately. Given these advantages, THz technologies are so significant in today's world in seeking hidded explosives, defects in defense and security application and chemical/biological threats

(Arnone et al., 1999). Additionally, this can potentially be used in ultra-high bandwidth wireless communication networks, atmospheric pollution tracking, vehicle control, and inter-satellite communication (Tonouchi, 2007). In such technological applications, many areas are considered for use which are also listed below. These can be counted as screening passengers at the airports for explosives, weapons, drugs and other contraband. Figure 1.2. shows some images for THz radiation applications.

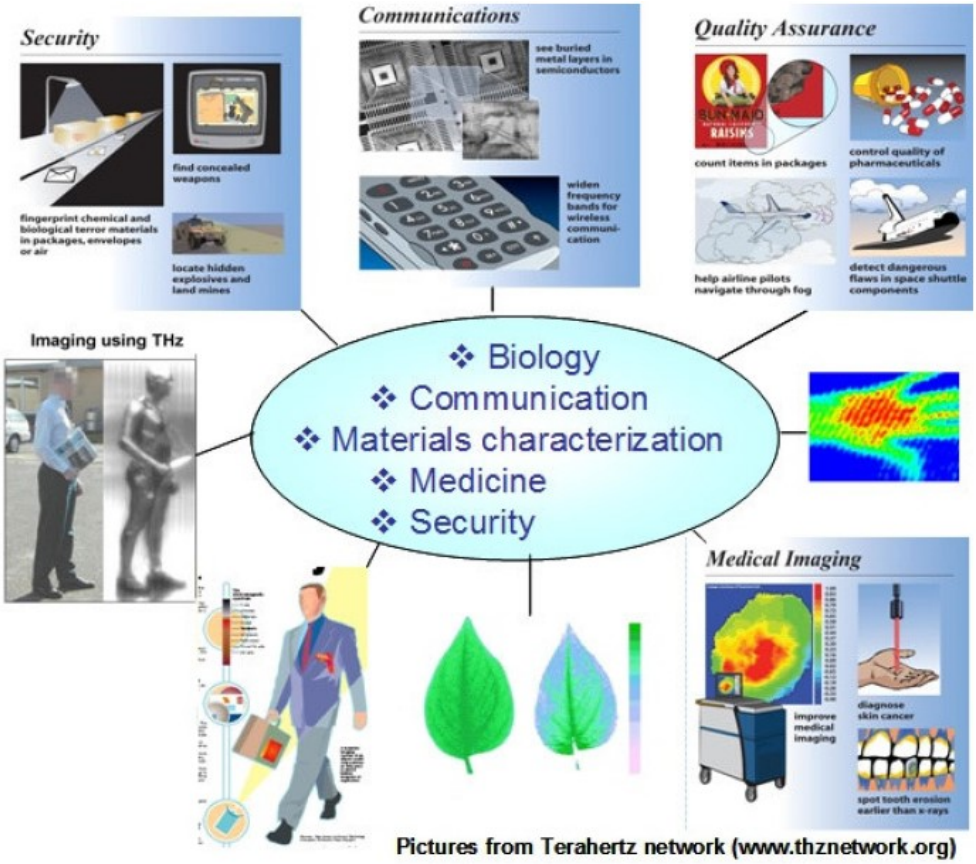

Figure 1.2. Various THz application areas.
(Source: www.thznetwork.org)

1.3. Metamaterial Filters Operating in THz Region

For the fabrication of metamaterial devices, dielectric / normal metal structures are generally preferred (Chen et al., 2006, Chen et al., 2009, Shelby et al., 2001). Alternatively, it has been observed in many studies that periodic photonic crystal structures also have potential for negative refractive index materials. Metamaterials fabricating from conducting elements could show negative refraction at successful junction. But as it is shifted to higher frequencies, problems may arise in devices made of these metamaterials, especially in optical regions. While the metamaterials are expected to be smaller in design and more efficient to work than wavelengths, the application areas of MM devices are limited due to significant losses. This loss in the microwave range is small and the electromagnetic properties can still be achieved. As we go to the higher frequencies, losses in the terahertz region rapidly increase and affect the electromagnetic properties negatively. Applicable metamaterials which can work with low loss in Terahertz region are needed. Ohmic losses in the THz frequency range limit the performance of these materials. Superconductors are excellent candidates to solve this problem (Semerci et al., 2016).

The discovery of superconducting materials by Kamerlingh Onnes (Onnes, 1911), which has zero resistance under a certain temperature, thus preventing energy losses, and at the same time exhibiting perfect diamagnetic properties, has attracted attention to these interesting materials. They also eliminate the problem of overheating in circuits / devices, in the sense that they carry the electric current without resistance / lossless and very low resistance even at high frequencies. The use of high temperature superconductors in 1986 and later and the use of liquid nitrogen (77 K) in the technological field to observe superconductivity at higher temperatures has become widespread. Usually these materials are perovskite. Techniques such as magnetic sputtering, vacuum evaporation, chemical vapor deposition, and metal organic chemical vapor deposition techniques have been used to deposit high temperature superconducting thin films, such as Bi2212 (Yamasaki, 2014; Wild 1998). Superconductors have many electromagnetic properties that are not found in normal metals, and these properties can be used to make almost ideal and unique metamaterials. In previous studies it has been proven that the losses in metamaterials operating at the frequency of THz and at the frequency of GHz are greatly reduced when metal structures are replaced by superconductors.

Contrary to metals, the complex conductivity in superconductors varies with the magnetic field, temperature and applied optical fields. It is possible to produce active metamaterial structures (Ricci, 2007; Zhang, 2012; Chen, 2010; Savinov, 2012) without controlling additional elements by controlling the conductivity of superconducting materials. In addition, at low temperatures superconductors exhibit superior conductivity and it is possible to integrate quantum behavior elements. Surface resistances are low in microwave frequencies. This value is about 100 μΩ (Talanov et al., 2000) for high-temperature superconductors (Knobloch et al., 1998), while Type 2 superconductors such as Nb at 2 K and 1 GHz have a surface resistance value of nano-ohm order (Knobloch et al., 1998). These small losses indicate that superconductors can overcome the limitation problem mentioned earlier. Furthermore, superconductor based metamaterials are very suitable for specific meta-structures. Non-linear behavior can be used for parametric amplification of negative indexed photons, further reducing the negative effects of possible losses. Superconducting meta-atoms are inherently tunable in resonance frequencies due to the change of Josephson induction with magnetic field and temperature. In both cases the adjustable property is due to the density of the Cooper pairs, from the superconductivity parameter. Thus the quality factor of the resonance can be changed by changing the resonance frequency.

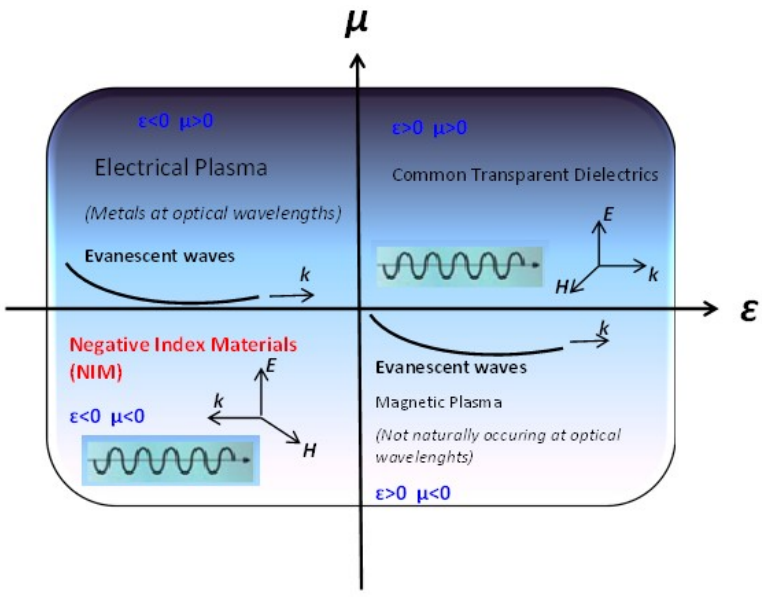

Figure 1.3. Schematic view of μ-ε space.

Zhang et al., have researched on this subject, measured field induced nonlinear behavior of metamaterials made of low-temperature superconducting NbN and unfabricated thin films (Zhang et al., 2013). The THz spectrum, which measures the range of the energy interval frequency of NbN ($f_g = 2\Delta_0/h$, the energy range at Δ_0=0 K and is the Planck constant) is 1.18 THz, the range of frequencies below the energy range frequency is higher than that of the THz spectrum. Since high temperature superconductors have wide energy ranges, they are more suitable for the broadband range and have anisotropic dielectric properties. Moreover, they can operate at liquid nitrogen temperatures because they exhibit superconductivity at higher critical temperatures. In another study on the same subject, the nonlinear permeability property of high temperature $YBa_2Cu_3O_7$ (YBCO) thin films was measured (Zhang et al., 2013). In subsequent studies, the metamaterials are designed to minimize material losses and are designed to provide better impedance matching to empty space, such as split-ring resonators (SRRs). Recent studies have also found superconducting split-ring resonators that can adjust the negative permeability with temperature (Ricci et al., 2006; Pendry et al., 2000; Claire et al., 2012).

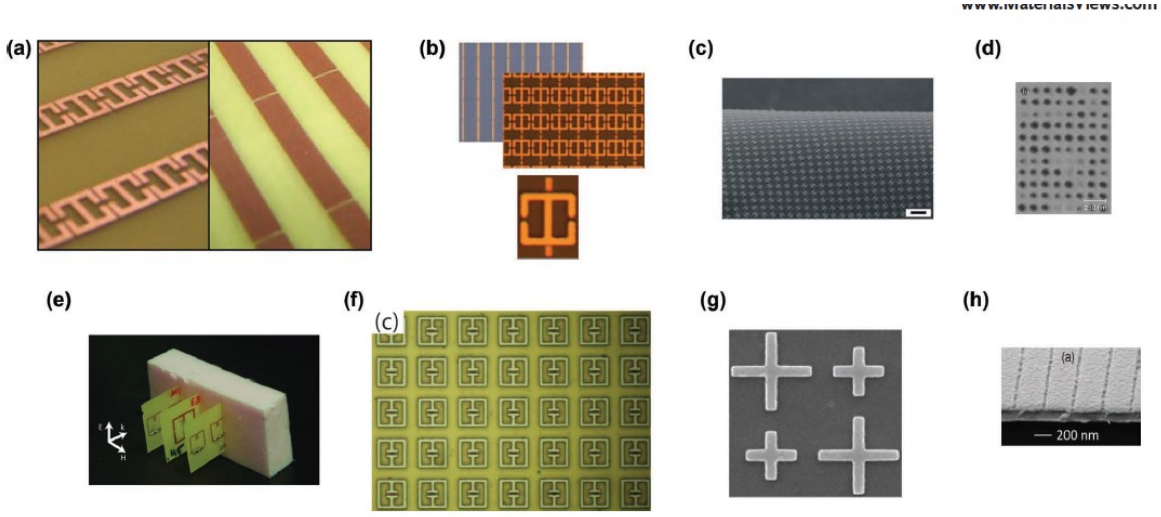

Figure 1.4. Metamaterial filter designs from literature.
(Source: Claire M. Watts et al., 2012)

In Figure 1.4., Scanning electron microscope images and optical photos of different types of metamaterial designs such as split ring resonators, electric split ring resonators are shown. Pendry et al. (Pendry et al., 2000) has shown that periodic artificial metamaterial structures called split ring resonators (SRRs) can provide negative active μ

at frequencies close to the magnetic resonance frequency. SRRs are made up of two half rings. Thanks to the clefts in the ring, the SRR unit can be resonated at larger wavelengths. On the inside, the split part is able to provide high capacitance in the intended small gap area of the ring which is located directly opposite the outer ring. The gap between the two rings prevents current from passing between the rings. However, the high capacitance value between the two rings allows current flow. By joining the split ring resonators in the periodic environment, a strong magnetic interaction occurs between the resonators and unique properties are obtained from this material, isotropy is ensured. It is known from Maxwell's equations that it is necessary to reduce the size of the structures in order to use the designed structures at higher frequency values.

For example, SRR structures previously used in the microwave range can be used at lower frequencies with lower dimensions. Experimental studies have shown that left-handed materials can be made using SRR piles and thin wire constructions (Smith et al., 2004). Split ring resonators exhibit high magnetic characteristics against electromagnetic waves above certain frequencies. Thus, the magnetic resonance of the SRR structure does not allow the electromagnetic waves to propagate in the periodic environment, a stop band occurs. New application areas of superconducting metamaterials in addition to superconducting split rings and wires are classified as superconducting/ferromagnetic composites, DC/RF superconducting metamaterials, SQUID metamaterials and superconducting photonic crystals. In recent metamorphic studies, fishnet and similar structures have been studied to make metamaterials with adjustable and nonlinear characteristics. Devices that can operate at microwave frequencies are designed from these materials (Sabah et al., 2011; Shen et al., 2009). One of the most important features of the studies is that the proposed structures can only exhibit metamaterial characteristics in a certain frequency range. These features apply only to design conditions for design constructions. If the frequency is increased, it is difficult to obtain the same properties. Especially in optical frequencies, the situation is changing a lot and new models and applications are at the forefront. Besides the observed advantages that these properties provide at the working frequencies, the losses and the absence of adjustability make the researchers more inclined to these features.

In particular, the loss of the designed metamaterials leads to a number of serious problems in practice. Losses, especially metals and metal losses from the underlying metal and conductor losses, are antagonistic. Metal losses are supposed to be reduced in a

considerable way using superconducters. Thus, this thesis proposed becomes important at this point.

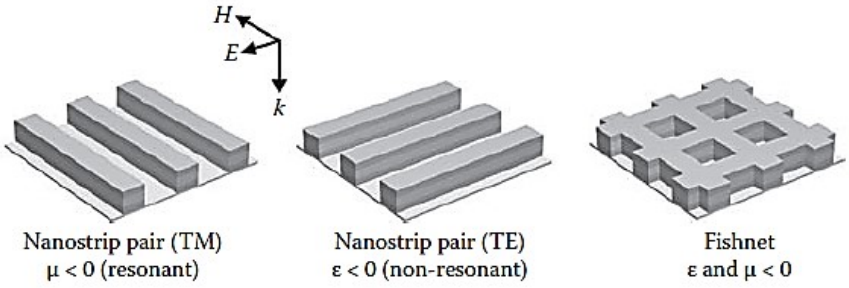

Figure 1.5. Schematic view of Fishnet structure.
(Source:Tutorials in Metamaterials, Mikhail A. Noginov)

In fishnet structures, pairs of wider metal strips provide negative magnetic permeability with asymmetric currents, while narrow metal strips act as diluted metal. As shown in Figure 1.5. the fishnet structure consists of a combination of two resonant and non-resonant structures. In this structure, pairs of narrow metal strips act as off-resonant tangles while magnetic resonance occurs in wide strips, narrow metal pairs are necessary to prepare the substructure for negative dielectric permeability.

Recently, stimulation of modes with weak interaction with external electromagnetic field called trapped modes has been observed in metamaterials. This excitation is demonstrated in surface current distribution simulations. In these modes, the radiation losses are very low to the energy of the field energy stored in the resonance frequency. These modes show similarities such as a sharp phase distribution in the radiation transmitted by electromagnetic induced transparent atomic systems and a narrow transmission band in the wide stop band. These features allow the fabrication of high-selectivity band-pass filters with compact metamaterial size. For Terahertz systems, low insertion loss (IL), sharp cut-off and low cost compact band-pass filters should be designed. Complementary split ring resonators (CSRRs) for filter design that can operate in the microwave range have received great interest as metamaterial components (Shen et al., 2009).

1.4. Motivation

The aim of this thesis is to design terahertz filters from metamaterials. Instead of conventional metal materials, superconducting materials with low ohmic losses have been used in this study. Previous work on metamaterial filter structures has usually used metal materials, but the lack of frequency tunability and the ohmic losses have led researchers to prefer the materials with these properties. In particular, the loss of the designed metamaterials leads to a number of serious problems in practice. It is thought that metal losses will be greatly reduced with superconducting materials. Kinetic inductance and superfluid density are dependent on temperature. Superconducting THz metamaterials have low ohmic losses and adjustable frequency and frequency properties make these materials superior to metamaterials. When the temperature approaches the critical transition temperature (T_c) and is changed at lower temperatures, the resonance frequency adjustability of the filter is increased due to the effective kinetic inductance of the superconducting film.

Within the scope of the proposed thesis, these superior features of superconductors are aimed to used at designing and fabrication of efficient, compact, and highly selective metamaterial base filters working in the THz band. High selectivity filters can prevent the transmission of unwanted signals in the predefined frequency range and can be used for THz applications. This feature will contribute to the broadband THz applications of superconducting metamaterials when combined with the appropriate, unique filter design.

CHAPTER 2

SUPERCONDUCTIVITY

2.1. Basic Characteristics of Superconductors

One important property of superconductors among others is the critical temperature T_c where the resistivity of the material vanishes. Therefore, recent research has focused on discovering new superconducting materials with high critical temperatures.

Another significant feature of superconductors is the critical magnetic field (H_c) they have. This parameter is important because superconducting state cannot exist if an applied magnetic field is greater than a critical value which is called as H_c. A characteristic of the material, this critical magnetic field is strongly correlated with the superconductor's critical temperature. If the critical magnetic field (H_c) increases, then critical temperature T_c decreases. When the material is in a superconducting state, according to Meissner effect, the magnetic field lines are removed from the sample. External field enters into the bulk from the sample's surface, on the other hand magnitude of the penetrating magnetic field decreases and this decrease is in the exponential form. Superconductors are grouped into two as type I and type II in terms of their diamagnetic properties. For type I conductors, H_c works as a limiting factor since the applied magnetic field increases, the magnetization balancing this magnetic field also increases up to H_c is reached. Therefore, in the case applied external magnetic field surpasses H_c, the material is not any more in the superconducting state. If the applied magnetic field is lower than H_c, the material becomes in the Meissner state and expulsion of all magnetic flux from the sample is realized. Mostly pure metals, type I superconductors have a limited practical use due to the small and suddenly disappearing superconducting state of their critical magnetic fields at that temperature. Type II superconductors, on the other hand, pass from the normal state to superconducting state and Meissner effect does not occur suddenly, however it passes through a transitional state where the applied field can penetrate through sample's certain local regimes. This state of transition is called vortex state. Superconducting currents' vortices encompass cores of normal materials and it

bears the features of a mixed state of superconducting and normal regions. In the case the applied magnetic field increases up to the lower critical field, $H_c(1)$ is reached, and the material expels all magnetic flux falling on it. Furthermore, if the applied magnetic field continues to increase up to upper critical field, $H_c(2)$, then the material becomes in the vortex state and magnetic flux lines can go into the sample in some of the regions. The impact of such flux lines are terminated by the supercurrents turning around the walls of the vortices, so that the total magnetic flux is zero. Type II superconductors are mostly alloys and they have higher critical magnetic fields. Another significant parameter called critical current density J_c determines the superconductor quality. The maximum current the material can carry per unit is defined as J_c and it strongly depends on temperature. T_c will usually decrease with the increase of the current which flows through a superconductor. If the current flows through a superconductor, a magnetic field occurs. When it is high enough for the current density, magnetic field located at the sample's surface becomes larger. Therefore, this accelerates the vanishing of the critical magnetic field (H_c) as well as the superconductivity.

Because Cooper pairs' spin is zero, Pauli's exclusion principle cannot be found in the superconductors any more. So that they can take place in the same quantum state, and this occupation of energy state is described by Bose-Einstein distribution law. Although all Cooper pairs have same momentum, it is not possible to know when energy from applied electric field exceeds the energy gap of the Cooper pair. Expressing energy cap (Δ) in a semiconductor and a superconductor is remarkably different than each other. The energy 2Δ can be defined as a binding energy of the Cooper pair in superconductors and this energy is enough to separate a cooper pair in a superconductor. When the pairs are broken, single electrons occur and these are called quasi-particles. Experimentally, energy gap can vary with the temperature, and BCS (Bardeen–Cooper–Schrieffer theory) theory also predicts this. At $T_c=0$, the ratio $2\Delta(0) /k_BT_c$ variation with superconductor elements are generally between 3.2 and 4.6 however this ratio predicted by BCS theory is equal to 3.5 (Wesche et al., 1998).

2.2. Low Temperature and High Temperature Superconductivity

In 1957, Cooper, Bardeen and Schrieffer suggested a theory (BCS theory) which accomplished to explain the superconductivity on microscopic origins. Quantitatively, BCS theory could predict the superconductors' properties (Bardeen et al., 1957). Their theory takes earlier discovery by Cooper (1956) as basis. In his study Cooper concluded that the ground state of a material is unstable with regards to pairs of 'bound' electrons. Electron phonon interactions form these pairs of electrons and they take the name Cooper pairs. We can briefly describe the mechanism of the Cooper pairs as an electron in the cation lattice distorting the lattice around it and thus creating an area with greater charge density around itself. Then another electron at some distance to lattice is attracted to this charge distortion (phonon) and this process is called electron phonon interaction. So that, electrons are attracted to each other indirectly and form a Cooper pair. To make it clear, the attraction between two electrons is mediated by the lattice thus creating a 'bound' state of two electrons. It is clearly known that electrons being fermions follow the Pauli Exclusion Principle. However, electron pairs can show very different behaviours than single electrons, in other words, they behave more like bosons that can intensify into the same energy level and have one single wave function which describes the behaviours of all cooper pairs. To explain the mechanism of superconductivity in low temperature superconductors, BCS theory was a success. Based on the BCS theory, 30 K is the highest T_c that a superconductor can achieve and therefore the theory could not be a basis for high temperature superconductors with higher T_c values. The most important problem in the superconductor technology is the cooling system. Many superconducting devices have been suggested, however using them widespread is only possible through a discovery of new superconducting materials with transition temperatures at around ambient temperature. Thus, producing high temperature superconductors promises for many other technological applications. Nevertheless, cooling the system remains a problem even if increasing the transition temperature with high T_c superconductors is achieved. Superconductors can work with three main regimes. These depend on the zero resistance when superconducting state is maintained, transition between the normal state and superconducting state and Josephson Junctions.

2.3. High Temperature Superconductors

To reach the very low temperatures, use of liquid helium by H.K. Onnes in 1911 has allowed to discover new superconducting materials by increasing their critical temperature (T_c) in following years. Physicists has believed until 1986 that BCS theory used to forbid superconductivity at temperatures between 30 K and 40 K due to thermal vibrations. However, Bednorz and Muller published in that year an interesting research renewing the superconductivity in a ceramic compound material, lanthanum barium copper oxide ($La_{2-x}Ba_xCuO_4$) with transition temperature of 35 K (Bednorz and Müller 1986). The important thing in discovering this ceramic compound was not only high critical temperature but also the fact that it was the first cuprate in new class superconducting materials also known as copper oxide superconductors. Next year, replacement of lanthanum with yttrium in LBCO materials, yttrium barium copper oxide compound, $YBa_2Cu_3O_{7-x}$ (YBCO), was discovered with T_c about 90 K (Wu et al., 1987). This was commercially important since the produced liquid nitrogen could then cheaply be used as a refrigerant (at atmospheric pressure, the boiling point of nitrogen is 77 K). Same year, a different superconducting compound including bismuth, strontium, calcium and copper (BSCCO) was found. These two superconducting phases were characterized as $Bi_2Sr_2CaCu_2O_{8+x}$ (Bi2212) and $Bi_2Sr_2Ca_2Cu_3O_{10+x}$ (Bi2223) with their T_c 95 K and 110 K respectively (Chu et al., 1998). In a very short time, thallium barium calcium copper oxide compound, $Tl_2Ba_2Ca_2Cu_3O$ (Tl2223) which has around T_c 125 K was discovered in 1988 (Hazen et al., 1988). With maximum transition temperature T_c around 135 K, the last superconductor compound $HgBa_2Ca_2Cu_3O_{8+x}$ (Hg1223) was found in 1993 (Schilling et al., 1993). All HTSs have a layered crystal structure and include copper oxide layers which ensures superconductivity separated by non-superconductor layers. These are based on oxygen defect modification of a perovskite adopted by many oxides that have the chemical formula ABO_2. With the A-cation in the middle of the cube, the B-cation in the corner and the anion, commonly oxygen, in the centre of the face edges, its structure is a primitive cube. Due to such layered structures, HTSs have anisotropic behaviours at critical field, London penetration depth, coherence length and resistivity. These are extremely type II superconductors and only they can be use for energy and magnet applications which can be well defined by Gindzburg-Landau theory (Ginzburg; Landau, 1950). It was found out in 1959 that this theory can be derived from the BCS theory.

Based on their critical fields, London penetration depth λ and coherence length ξ, type I and type II superconductors are different. Although, $\xi>\lambda$ demonstrates the characteristic of type I superconductors, the status of $\xi<\lambda$ is certain in type II superconductors. In the case the ratio λ/ξ called Ginzburg-Landau parameter (κ) is greater than 1/2 , superconductor must be type II (Wesche et al., 1998). Despite their short coherence length values, HTSs have large critical magnetic field. In addition to such different parameters, an unusual behaviour of some superconductor in external magnetic field have been firstly found by Shubnikov. Following 20 years of time to clarify the experiment of Shubnikov, Abrikosov used Gindzburg-Landau theory and proved that two types of superconducting materials are available which are grouped as type-I and type-II superconductor. While type I superconductor materials, for example, remove magnetic flux completely from their interior up to critical magnetic field values, at high presence of an applied external magnetic field, properties of the vortex characterizes a mixed state in type-II superconductor material, which is formed at a point in which the magnetic field penetrates the superconductor in a flux tube through the sample. Because the magnetic flux is penetrated, the region near the core of the vortex behaves as a normal metal. As lower critical magnetic field Bc_1 and the upper critical magnetic field Bc_2, type II superconductors have two critical magnetic fields. In the case of lower applied field than Bc_1, superconductor expel the magnetic field completely as a type I superconductor. The superconductor in the magnetic field between Bc_1 and Bc_2 mixed state is formed and it becomes at normal state at Bc_2 material.

2.3.1. Structure of $Bi_2Sr_2CaCu_2O_{8+\delta}$ (Bi2212)

In this thesis, Bi2212 was initially planned to be used as a superconducting thin film for metamaterials. In superconductors, the structural properties have a significant effect on the superconductivity property of high temperature superconductors (HTSs). All ceramic superconductors consist of similar layers closely related to the classical perovskite ABO_3 structure. One of these layered HTSs's is Bi-based superconductors. The superconductors in this structure have the general formula $Bi_2Sr_2Ca_{n-1}Cu_nO_{2n+4+\delta}$ where n is the number of perovskite units or the number of copper oxide layers in the unit cell.

The complicated HTSs series, $(BiO)_2Si_2Ca_{n-1}Cu_nO_{2+2n}$, contains perovskite-type layers and $(BiO)_2$ layers of bismuth in the unit cell. Number of the perovskite units in other words the number of the consecutive copper oxide layers in the unit cell can be denoted by "n". There exits three phases for BSCCO namely, (n=1) $Bi_2Sr_2CuO_{6+\delta}$ (Bi2201) with $T_c \leq 20$ (Akimitsu et al., 1987), $Bi_2Sr_2CaCu_2O_{8+\delta}$ (n=2, Bi2212 phase) with $T_c \approx 90$ K and $Bi_2Sr_2Ca_2Cu_3O_{10+\delta}$ (Bi2223 phase) with $T_c = 110$ K (Maeda et al., 1988). All of these phases have layered atomic arrangement with planes of weak bonding, the $(BiO)_2$ (Romano et al., 1998). Among the cuprates, or more specifically within the BSCCO family, the Bi-2212 is the most widely studied material and many researchers have been working on it in the recent years. The optimally doped sample of Bi-2212 has an onset critical temperature of approximately 95 K which is the maximum value of T_c for this compound and its transition temperature can be reduced either by additional oxygen content (overdoping) or by the removal of oxygen with vacuum annealing (underdoping). Thus, the phase diagram of this cuprate as well as its physical properties can be investigated by means of doping. There is an important advantage of this material namely, it can be grown in the way of single crystal without any macroscopic defects or dislocations. The above mentioned parameter n also corresponds to the number of superconducting layers in the structure. For example, there are two CuO_2 layers separated by Ca layer in the structure of Bi2212 phase. The unit cell of Bi2212 has a pseudo-tetragonal symmetry with lattice parameter; a = b = 5.4 and c = 31 Å.

Sequence of its stacking atomic layers is like that, $(BiO)_2$/SrO/CuO_2/Ca/CuO_2 /SrO/$(BiO)_2$/SrO/CuO_2/Ca/CuO_2/SrO/$(BiO)_2$. Taking into account to the structure types there exits two kinds of layers in crystal structure of Bi2212. One of which consisting SrO/CuO_2/Ca/CuO_2/SrO has a structure of perovskite type, while another consisiting SrO/$(BiO)_2$/SrO has a structure of NaCl type. The layered structure of Bi2212 HTSs including IJJs (Intrinsic Josephson Junctions) makes the crystal anisotropic material. Consequently, Josephson tunneling occurs along the c axis between superconducting (Cu-O) layers separated by insulating layers unlike electrical behaviors of the crystal at a-b planes. On the other hand, layered HTSs have different coherence lengths and penetration depths at different directions. At a-b planes coherence length ξ_{ab} (between 20 and 40 Å) is larger than coherence length ξ_c ($\approx$1 Å) along to c axis. Although the coherence lengths of Bi2212 is small, λ_{ab} is equal to 2000 Å. Accordingly Bi2212 with the Ginzburg-Landau parameter κ greater than 100 exhibits behaviors of type II superconductors. The crystal is fairly intricate and show excessively anisotropic properties due to its layered structure.

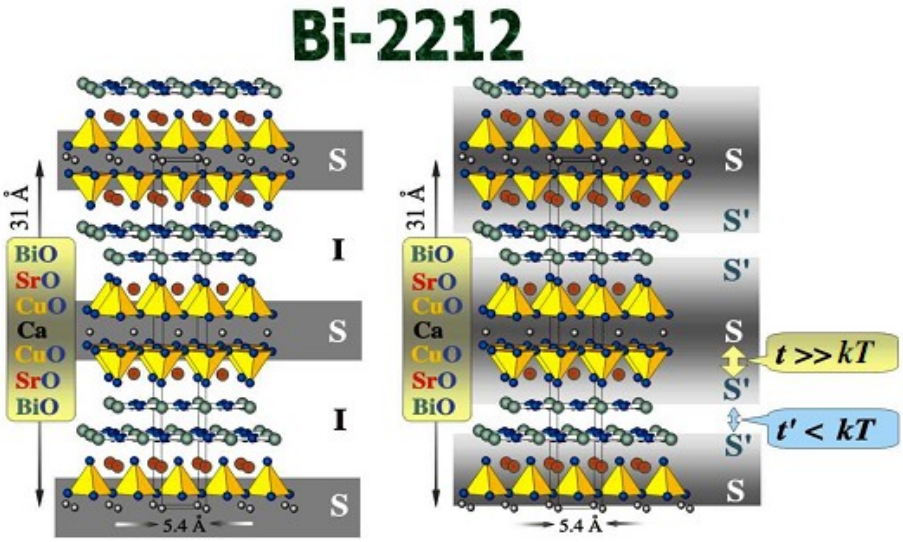

Figure 2.1. The crystal structure of Bi2212. The left image corresponds to basic multilayer model and the right image defines the proximity model.
(Source: Yurgens et al, 1996a)

In order to be able to explain the mechanism of this material two models are developed namely, multilayer model and proximity model (Yurgens et al., 1996a) which are represented in Figure 2.1. According to the multilayer model; Bi-2212 single crystals behave like stacks of Josephson coupled Cu-O double layers with the thickness of 3 Å separated by nonsuperconducting Sr-O and Bi-O layers of thickness 12 Å. This configuration forms natural Josephson tunnel junctions array going on like SISIS... inside the single crystal and enables to observe both DC and AC Josephson effects. Superconducting properties of the multilayered high T_c superconductors stem mainly from the double CuO_2 layers in which coupling occurs, while the role of the other layers can not be defined exactly; it is commonly believed that Sr-O and Bi-O intermediate planes behave as passive spacers or charge reservoirs.

As stated in the preceding lines, the superconducting coherence length for Bi-2212 in the out of plane direction is approximately 0.1 Å, which is relatively small when compared with the distance between two adjacent CuO_2 layers in the Bi-2212 unit cell. This point makes Josephson tunneling of Cooper pairs hard across the insulating layer (Yurgens et al., 1996).

Another model namely proximity model is proposed ; where it is suggested that not only CuO_2 layers but also Bi-O planes make contribution to superconductivity of the HTSs. It is shown by some other experiments that Bi-O layers exhibit metal-like property

or even superconducting features rather than insulating character. According to the proximity effect, there is a strong coupling between the Cu-O and Bi-O layers (S-S') with weak Josephson coupling between neighboring Bi-O layers (S'-S'). There are research workers who claim that the reduced energy gap value of Bi-2212 is the consequence of the proximity induced superconductivity of the Bi-O layers (Yurgens, et al. 1996a).

2.3.2. Structure of $YBa_2Cu_3O_{7-x}$ (Y123)

Yttrium barium copper oxide ($YBa_2Cu_3O_{7-x}$) is discovered as the first superconductor with the property of having Tc > 77 K (liquid nitrogen boiling point) where the mole ratios of the different metals are 1 to 2 to 3 for yttrium to barium to copper respectively and due to this characteristic it is frequently mentioned as 123 superconductor. Since $YBa_2Cu_3O_7$ is the first material with a high transition temperature above 77 K, it is a well-known superconductor. On the other hand YBCO is a type II superconductor, thus has the following properties: 1) higher critical transition temperature, Tc~90K; 2) short coherence length ξ, ξ_{ab}=2.7 nm (77K), ξ_c=0.3 nm (77 K); 3) strong anisotropy, $\xi_{ab}(0)/\xi_c(0)$ =5∼8.In Figure 3.3 YBCO structure is presented and it is observed that the configuration consists of three perovskite unit cells stacked along the c-axis. The construction incorporates a layer of yttrium atoms sandwiched between copper oxide planes, followed by a barium oxide layer, copper oxide chain and another barium oxide layer. The specifications of the superconductor are responsive to the oxygen content of the material namely to the value of (δ). The crystallographic structure and the hole concentration in the CuO_2 planes are governed by the oxygen content in YBCO. In the case of an oxygen content x=6, the compound YBCO is in the tetragonal configuration and behaves like an insulator. However, when the oxygen content is increased up to x=6.6 the compound experiences a phase transition from tetragonal to orthorhombic configuration (Jorgensen, et al.1987, Cogollo, et al. 2003).

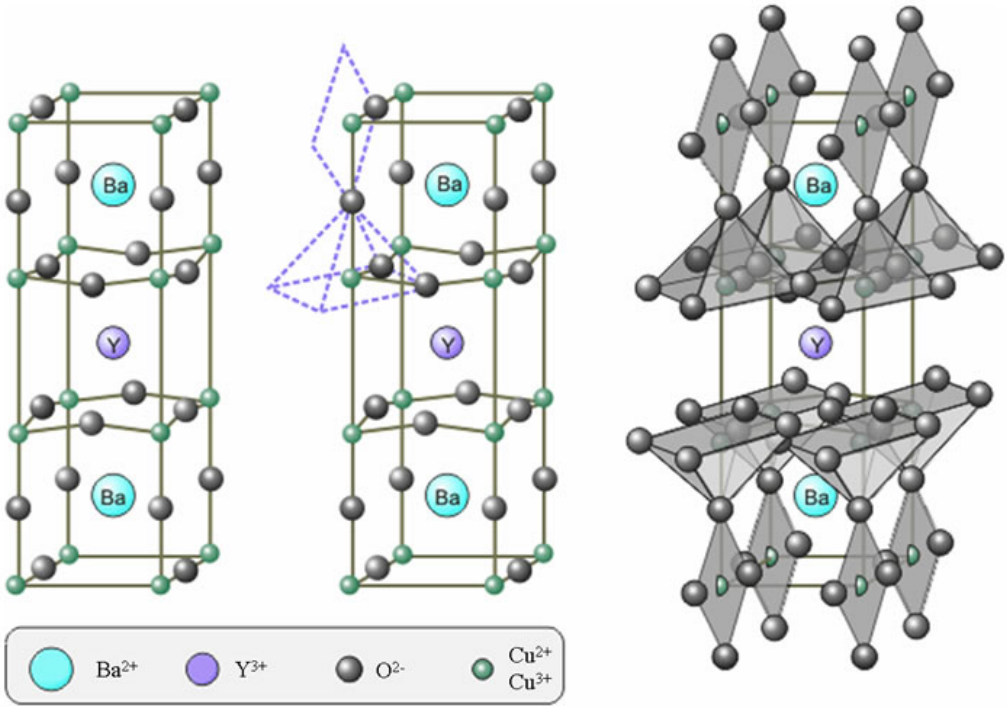

Figure 2.2. The crystal structure of Y123.
(Source:http://www.fusione.enea.it/index.html.en)

By virtue of an optimal hole doping in CuO_2 planes, the maximum value of T_c occurs at resulting in 6.94 is the existence of overdoped state which occurs when the holes in CuO_2 planes go beyond the optimum concentration. The tetragonal phase is detected at high temperatures in a region between 750°C and 900°C. A second-order phase transition from the tetragonal to the orthorhombic phase takes place at the temperature appoximately 700^0C when the temperature is decreased and the oxygen amount of the sample is increased, by oxygen held and diffusion. When the structure of YBCO is orthorhombic then this case is a superconducting transition and the temperature increases nearly up to 92 K. In comparison to parameters along the c-axis, the conductivity, critical current density J_c, and also the unit cell parameter along ab-plane are different. The conduction perpendicular to Cu-O sheet is very weak which is due to the complete absence of oxygen linking to the adjacent Cu-O layers in c-axis direction. In order to accomplish high- quality thin films, appropriate substrates are essential for many important applications of YBaCuO thin films in electronic devices.

In this thesis, superconducting films are planned to be used for metamaterial filter fabrication. For this purpose, Bi2212 superconducting thin films have been deposited and

characterized, the further experimental information about our thin film deposition technique, filter fabrication and characterization is given in next chapter.

CHAPTER 3

EXPERIMENTAL METHODS

3.1. Bi2212 Thin Film Fabrication

Our magnetron sputtering system is a high-vacuum system and the picture of the system is shown in Figure 3.1. and Figure 3.2. DC and RF magnetron systems have been used in different designs in previous projects (Yazici et al., 2015; Koseoğlu et al., 2015). The system has water cooling duct, gas inlet and power supply connections. Mechanical pump and turbo molecular pump are used to operate in high vacuum (below 2.0×10^{-6} Torr). The sample surface on which the sample holder is placed is heated. The pressure of the system is measured with a cold cathode before deposition and the argon gas is sent to the system with the mass flow controller system. DC voltage is applied to create the plasma. The argon gas is ionized, accelerated towards the target, and the target atoms are stripped and deposited in the substrate.

Figure 3.1. DC and RF magnetron sputtering systems.

Figure 3.2. Bi2212 target used in our RF magnetron sputtering system.

3.2. Electron Beam Lithography and UV Lithography Techniques

UV lithography and e-beam lithography techniques are used for fabrication of metamaterial filter designs. Electron beam lithography (EBL) is used to form electron beam resistivity-sensitive features on a thin film. The most important advantage of electron beam lithography is that it can form even under the light diffraction limit, that is, even at the nanometer scale. The short wavelength of the electrons and the small spot size make this possible. Electron beam lithography is an maskless application and can be used to create masks used in photolithography also. The structures designed for metallic and superconducting thin films were transferred to the photoresist (PR) surface by electron beam lithography followed by the ion beam etching process. In the ion beam etching system, the sytem is first pumped by rough pump and turbo molecular pump up to a pressure of 10^{-6} Torr before the etching process starts. Because, low pressure values are needed to increase the acceleration of the free ion beam. When the desired pressure value is reached, the argon gas sent by the MKS (mass flow controller) to the system. Argon gas is sent and our samples are placed at an angle of 67.5^{o} and the areas not protected by the photoresist layer are etched. Since the protected area is the photoresist layer, it can not be etched with the ion beam, thus the designed periodic filter structure is created on the film surface.

We work in class 1000 clean rooms for sample preparation and chemical procedures. The picture of our e-beam lithography system is shown in Figure 3.3.

Schematic presentation of the clean room process and our ion beam etching system are shown in Figure 3.4. and Figure 3.5. respectively.

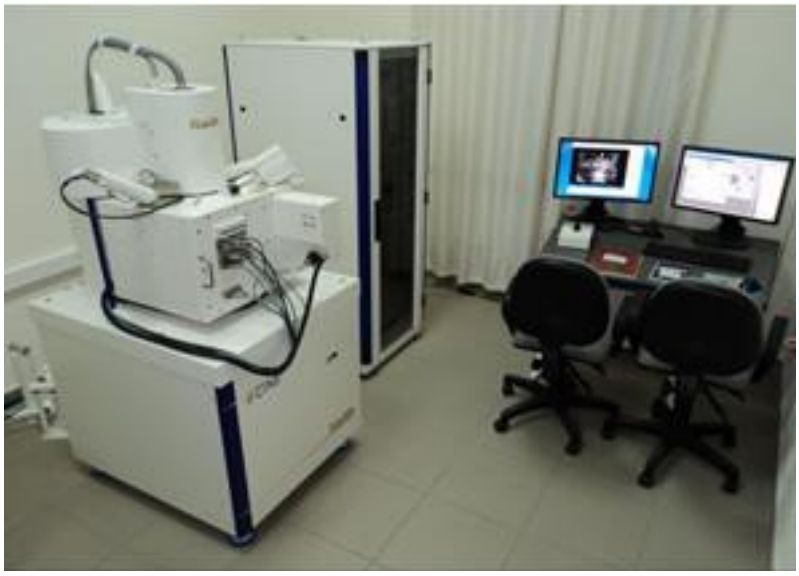

Figure 3.3. Electron beam lithography system.

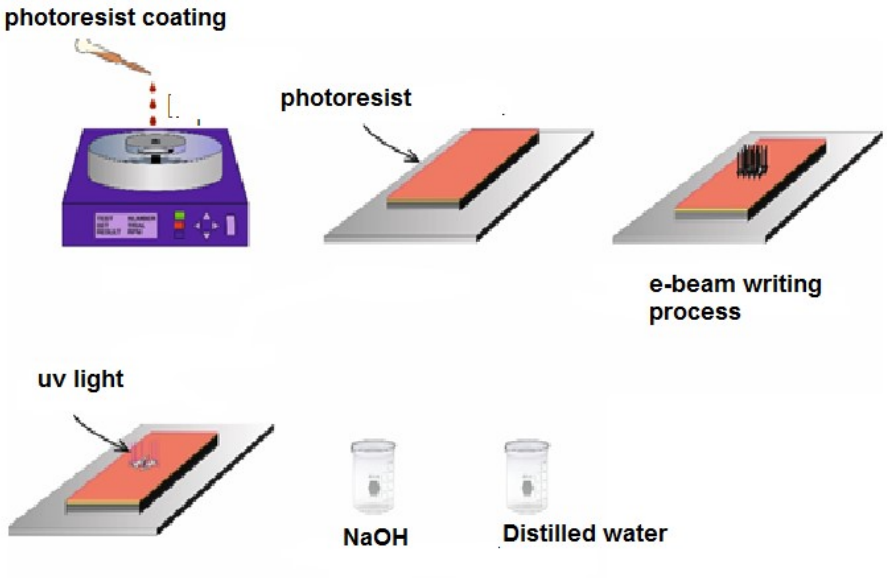

Figure 3.4. Schematic presentation of the clean room process.

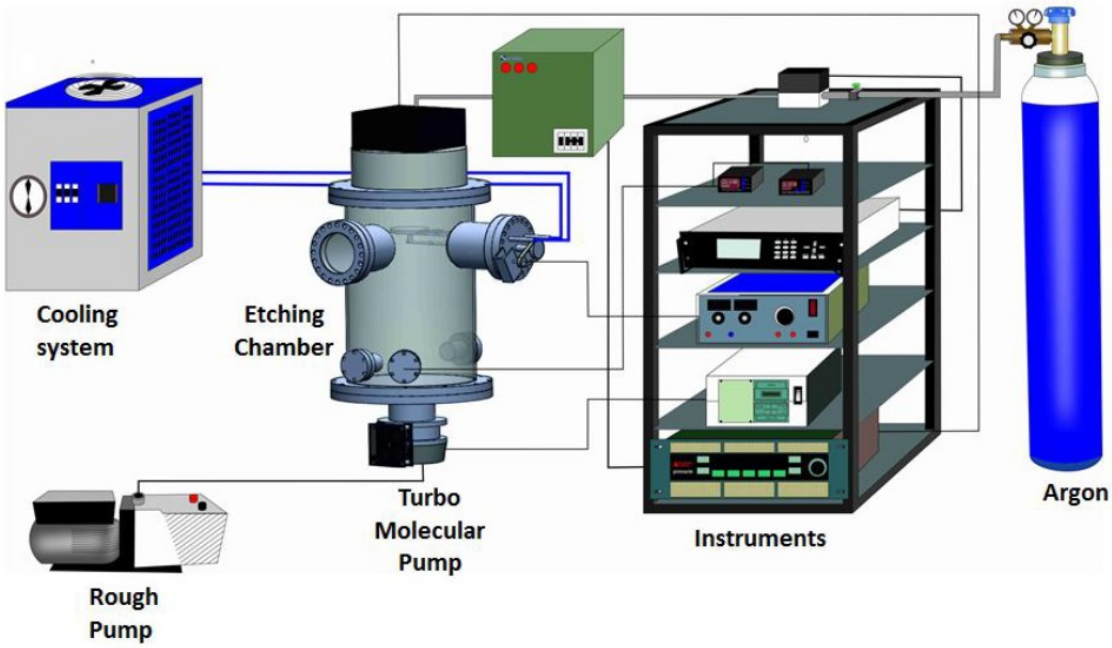

Figure 3.5. Schematic representation of the ion beam etch system.
(Source: Saglam Msc Thesis 2011)

3.3. THz Characterization Methods

In the analysis of the transmission characteristics of the designed THz bandpass metal mesh filters, a standard Fourier transform infrared spectrometer (FTIR) and a home-built terahertz time-domain spectroscopy (THz-TDS) system was utilized. The data obtained from the measurements are in agreement with that of simulation by the commercial software package CST Microwave Studio in terms of predicted center frequency and bandwidth.

3.3.1. Characterization of Terahertz Filters by Terahertz Time-domain Spectroscopy

The filters are characterized by a time-domain spectroscopy system in the Figure 3.6. By the help of a light shaper, the incoming light forms two optical lines of the spectrometer. These are the production and detection of the arm. In the production line s polarized terahertz beam is produced using a multi-dipole photo-detector antenna. The torch beam produced by the torch is directed to the system with the aid of two off-axis parabolic mirrors and two TPX lenses. In this way a THz ray with a beam diameter of 5 mm is focused on the specimen. The THz pulse can be measured by a detection method using the electrooptical detection method with the aid of a photodiode in the detection arm. Phase sensitive lock-in amplifiers were made and the results from the system were obtained by computer and data collection card. The obtained data is 40 GHz resolution.

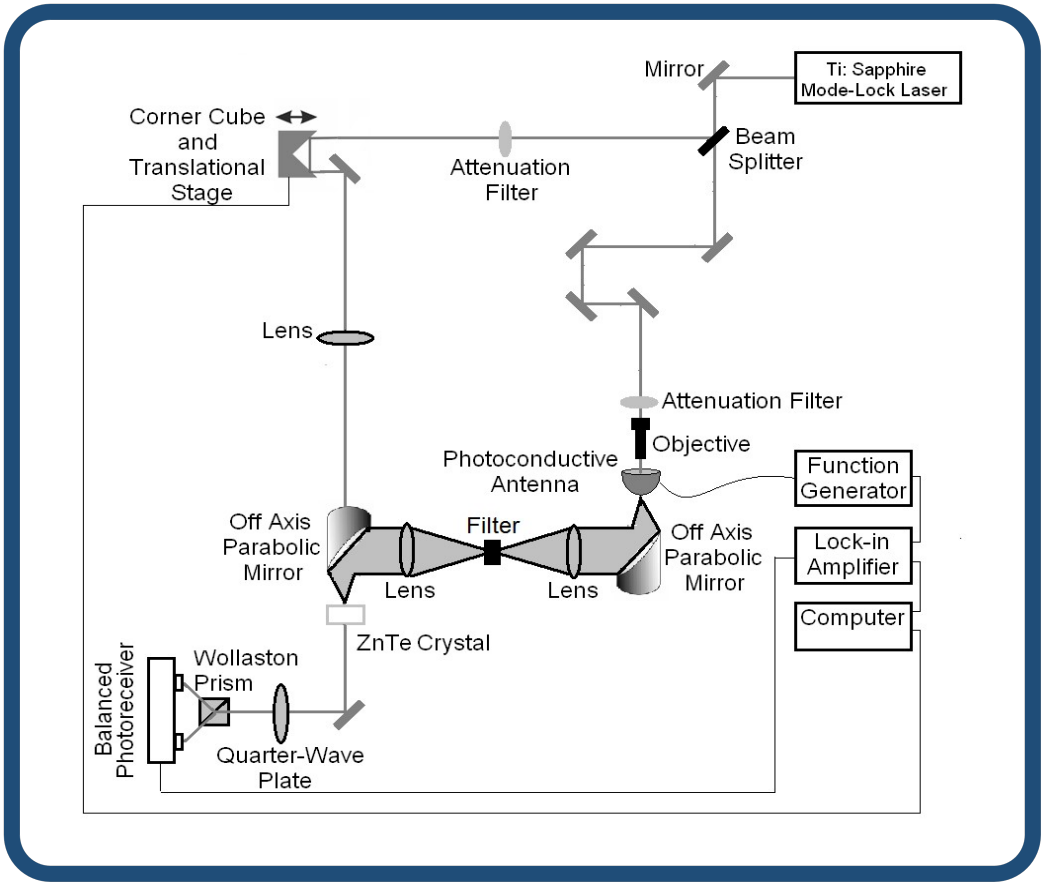

Figure 3.6. Schematic view of THz Time-Domain system.

As mentioned before, the superconducting materials have to be lowered to low temperatures in order to show superconducting properties. According to the literature, YBCO material shows superconductivity between 86 and 93 Kelvin (Vendik et al., 1998). The cooling process was performed with the help of a closed-cycle Helium cryostat integrated into the Terahertz Time-Domain Spectroscopy system. The cryostat system consists of three important systems called pumps, compressors and coldheads. Figure 3.7. and Figure 3.8. shows the system's photos. The compressor is connected to the right head with two pipes. The cooled helium gas sent from the compressor is directed to the cold head by means of the gas inlet tube and cools the head. The heated helium gas is recompressed from the cold head with the gas outlet pipe and cooled again. The inlet and outlet of helium gas with high and low pressures are controlled by means of a piston in the cold head.

The specimens are placed in the sample holder at the end of the cold head and closed with a reservoir with high quality quartz glass. Quartz is highly transparent in the THz range. By pumping, the pressure of the cold head is reduced to $1x10^{-3}$ torr. The sample holder, pump and compressor are shown in Figure 3.8. respectively. CST Microwave studio program was used for simulation of superconducting metamaterials. The modeling of superconducting materials is based on literature (Vendik et al., 1998). Parameters such as characteristic plasma frequency, values and depth of entry required for the model are taken from the literature. Then the surface impedance value is calculated according to the thickness of the sample.

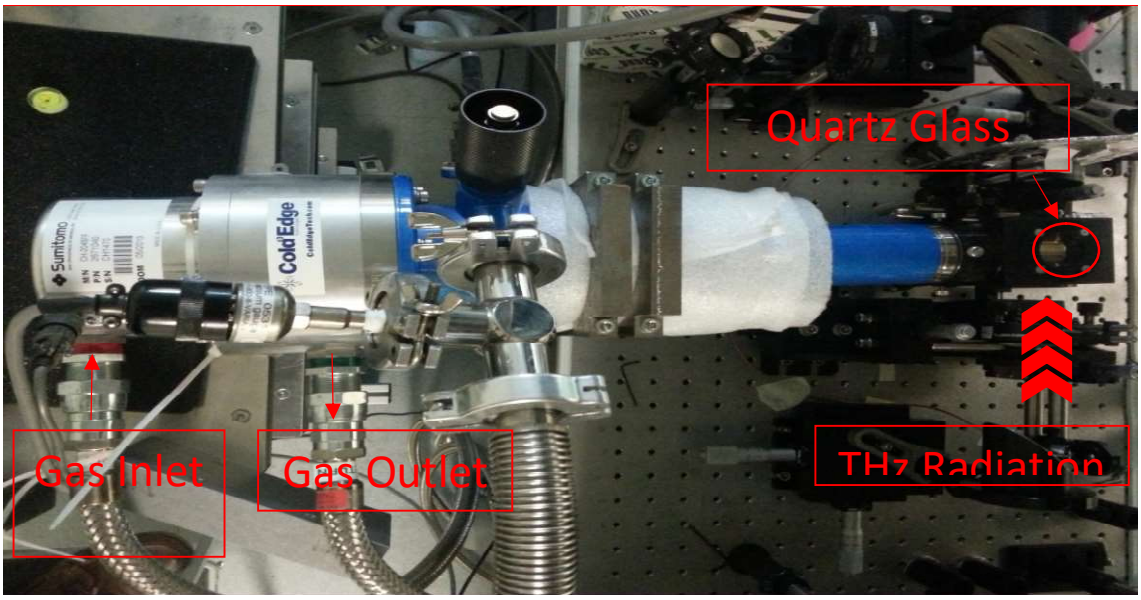

Figure 3.7. Cold head that used during superconducting measurements.

Figure 3.8. Sample holder, compressor and pump.

The temperature value is read through the temperature controller by means of a semiconductor sensor on the sample holder. When the compressor starts to operate, the frequency is reduced and the current is sent from the frequency controller and the frequency is increased with the help of the resistance heater.

3.3.2. Characterization of Terahertz Filters by Fourier Transform Infrared Spectroscopy

The transmssion measurements of the Metal-Mesh Band Pass Filters were also analyzed by Fourier Transform Infrared Spectroscopy (FTIR). It has been observed that the resonance frequency and bandwidth values estimated by CST simulations are compatible with the FTIR measurements. The measurements were made using a Bruker Vertex 80v type FTIR instrument, which has a Mylar beam splitter and DTGS detector. Measurements were carried out under 3 hPa pressure, resolution 2 cm^{-1}. The filters were placed in such a way that the FTIR measurements gave a 90 degree angle with the incident beam.

Designed metamaterial filters were fabricated and characterized using the experimental techniques described above. The filter fabrication studies are began by using the mesh parameter of one of the well-known cross shaped filter design “metal mesh filters” from Porterfield’s study (Porter field et al., 1992). The next chapter involves the experimental and numeric study of fabricated metal mesh filters from titanium, copper and indium tin oxide thin films on fused silica substrates.

CHAPTER 4

METAL MESH FILTERS FOR THE TERAHERTZ WAVES

In this part of the thesis, spectral behaviour of resonant terahertz (THz) bandpass filters has been studied where the filters were fabricated using thin films designed in a metal-mesh shape. The above mentioned filters were produced from titanium, copper and indium tin oxide thin films on fused silica substrates by UV lithography with an array of cross-shaped apertures. Utilizing both a THz time domain spectrometer and a Fourier transform infrared spectrometer (FTIR) it is possible to exhibit the performance of these filters experimentally due to the fact that the spectral characteristics of the filters are determined by the mesh period, cross-arm length and its width. In the verification of the experimental data we have adopted a commercial electromagnetic simulation software, CST Microwave Studio.

The transmission of the filters are in the range 20-55% at their pertinent center frequencies. To the best of our knowledge on the existing literature, in this investigation it is primarily demonstrated that fabricated patterns based on ITO thin films can be used to filter THz radiation.

In the THz region of the electromagnetic spectrum, for a great number of materials the optical specifications are not well known and thus one can find a few number of optically operating devices. Although researchers are conducting experiments with great interest in the THz region of the spectrum yet there is a necessity for new sources, detectors and optical components. Lately, many advances in the development of THz sources (Turkoglu et al., 2013; Turkoglu et al., 2012; Wang et al., 2009) and in the fabrication of THz detectors (Rice et al., 1994; Hu et al., 1989; Du et al., 2008) have been encountered.

In addition, there are numerous attempts in order to improve tunable THz filters, where dispersive media to spatially filter out the unwanted components have been used (Melo et al., 2008; Porterfield et al., 1994; Adeet al., 1994; Tarasovet al., 2009; Park et al., 2010). In customary digital electronics, it is a well known approach to design capricious and compound filters which enables wireless devices operating in the radio and microwave regions of the electromagnetic spectrum. With the purpose of

transmission of only the desired spectral regions, the detection capabilities can be improved by preventing the out-of-band interferences. Hindering the extra thermal radiation, the filtering procedure could be maintained which leads to flattening of the output spectrum of a THz emitter and moreover lowering the output spectrum of a THz emitter.

In the analysis of physical background for the process in the different filter structures the usual theoretical model of extraordinary optical transmission (EOT) has been used. In the development of resonant transmission, surface electromagnetic modes have a crucial function. It has been demonstrated that, these modes are at the origin of the enhanced transmission from single apertures surrounded by periodic corrugations (Takanet al., 2015). The electromagnetic responses of structured conductive surfaces on which the metal-mesh filters are fabricated are far more powerful in comparison to aforesaid digital filters. It is feasible to operate these filters as high pass, low pass, bandpass filters. By modifying the geometry and the dimensional parameters, the optical behavior of these filters can be adjusted (Melo et al., 2012). There are a great number of theoretical and also experimental studies where it has been demonstrated that the extraordinary transmission has a crucial function (Martin-Morenoet al., 2001; Ebbesenet al., 1998). The primary discovery was made on silver, gold, and chromium films at optical frequencies (Kimand et al., 2006).

Succeeding the theoretical studies and experimental attempts, researchers proceeded to investigate fabricating several types of filters which exhibit high-transmission peaks within the range 100 GHz up to 14 THz and having property of bandpass widths between 13 up to 50% of the central frequency (Ma et al., 2009; Kaufmannet al., 2010; Winnewiseret al., 1999). When the bandpass geometry of the metal mesh filters is considered, the customary filter is the cross-shaped type where the dimensions of the cross width (J), length (K), and periodicity (G) determine the frequency profile. Metal mesh filters of this type was introduced and investigated for the first time by Porterfield (Porterfield et al., 1994). The design parameters together with the thickness h of the material determines the transmission performance of the filter. In Fig. 4.1., the resonant metal-mesh filter design is presented.

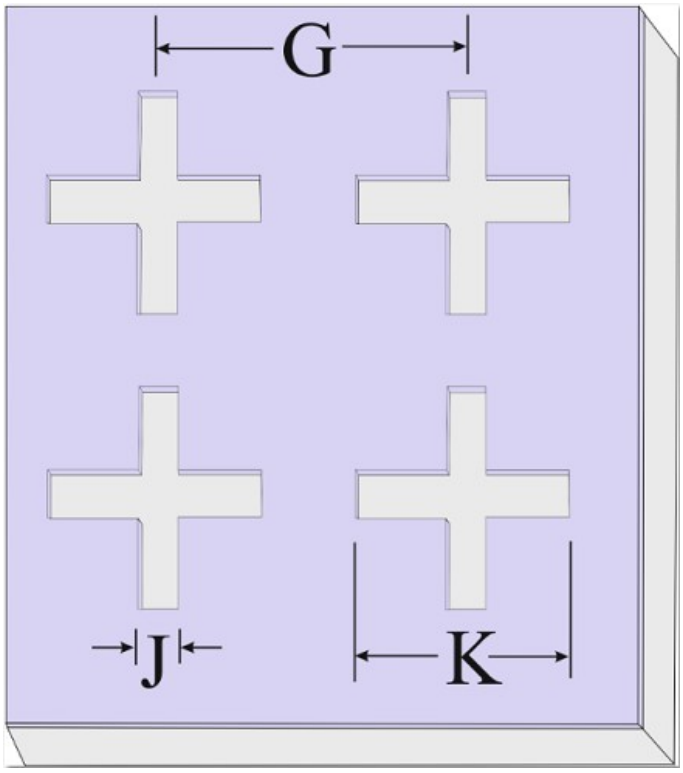

Figure 4.1. Sketch of a cross-shaped bandpass filter with mesh parameters G,J,K and *h*. (Source: Demirhan et al., 2016)

In recent works, for free standing filter structures the resonant empirical expression is given by,

$$\lambda_r = 1.8K - 1.35J + 0.2G$$

where the wavelength of the cross-shaped filter can be calculated (Voisiat et al., 2011). The resonant frequency decreases with an increase in the length of the crosses K however when the width of the crosses J increases the bandwidth also increases and the resonant frequency slightly increases. An increase in substrate thickness h leads to a small decrease in the resonant frequency. Then again, the resonant frequency increases when the corners of the apertures are rounded.

In this study, simulation and transmission measurements of cross shaped Ti, ITO, Cu thin film bandpass THz filters on fused silica substrates with several dimensions have been carried out and these filters are compact, demonstrate an easy and available fabrication process. The obtained measurement data have been discussed in the view of surface conductivity of deposited films.

4.1. Design and Fabrication of Metal Mesh Filters Based on Ti, ITO and Cu Thin Films

Metal mesh filters are frequency selective surfaces with the property of displaying high transmission profiles at designed frequency and turn down out of band radiation. In addition to these properties, the ideal bandpass filters (BPFs) must be vacuum compatible, vibration tolerant and cryogenically stable for most of THz applications. In the filter design the basic targets are: the peak transmission has to be increased where as the peak full width half maximum (FWHM) and out of band transmission have to be decreased. In sensor technologies, a significant fact is that; out of band transmission has to be decreased and this process improves detection capabilities by blocking out of band interferences and allowing transmission of only the desired spectral region. Moreover, it also brings an improvement in signal to noise ratio (SNR) of a detector. Before starting the experimental measurements, CST microwave studio simulations have been carried out where the aim is prescribing the transmission characteristics and also conforming a design with optimum structure.

The free standing filter design is introduced which was given in ref. (Porterfield et al., 1994) to the structures fabricated on fused silica substrates (for commercial use substrate is required, thin metallic film is very sensitive to mechanical stresses). As it was expected, the addition of the dielectric substrate influenced the behavior of the resonant filters (Ma et al., 2009). The numerical results for terahertz wave transmittance of the copper filter are presented in Fig. 4.2., the simulated results gives the terahertz wave transmittance peak of 82.5% at 0.333 THz for402(K)/261(J)/66(G) μm mesh parameter.

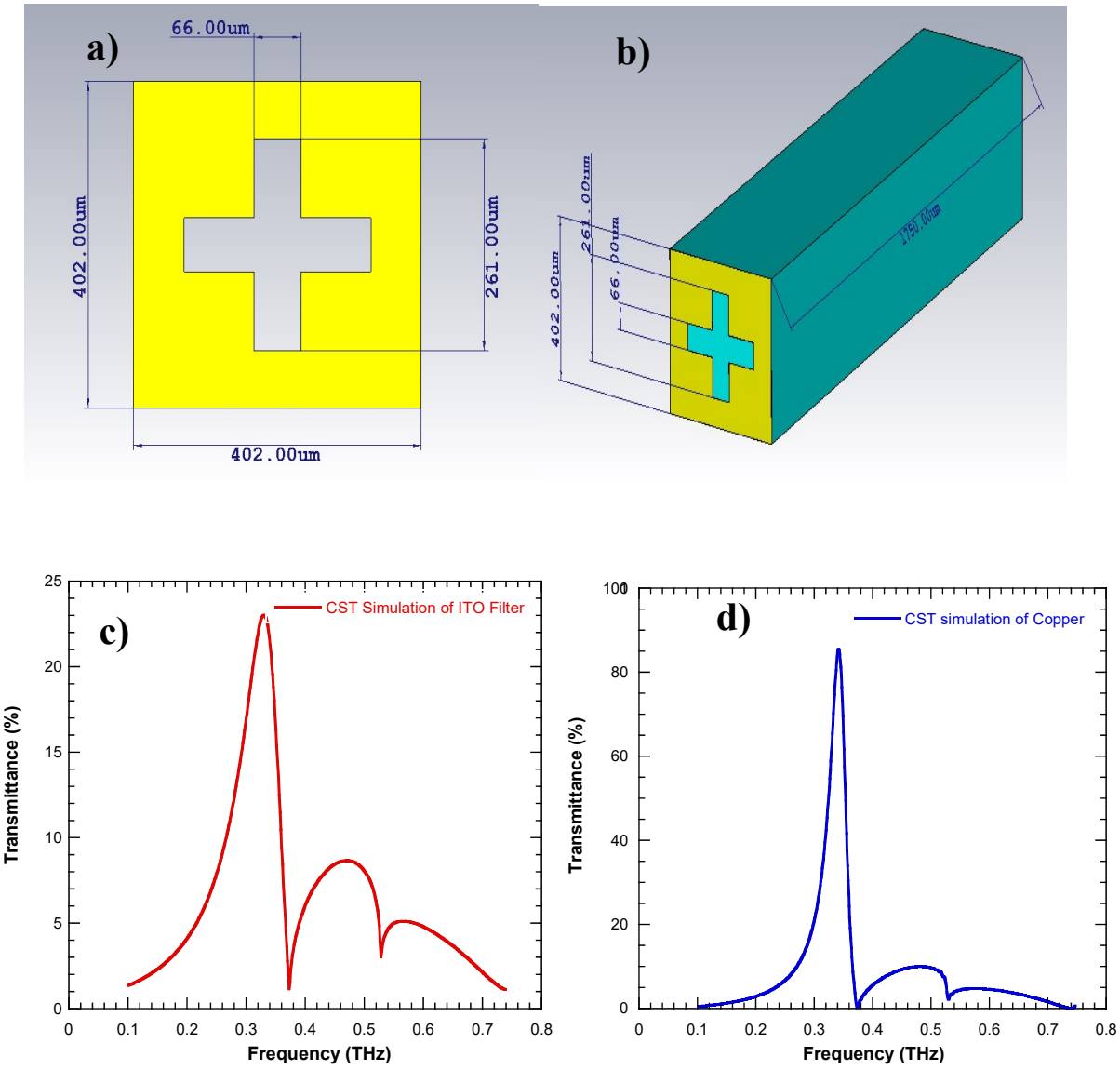

Figure 4.2. (a), (b) Design of metal mesh filters with dimension G/J/K, 402,261,66 µm and substrate thickness of 1.75 mm, respectively. (c), (d) The simulated transmission spectrum of ITO and Cu metal mesh filters with designed parameters. (Source: Demirhan et al., 2016)

Material type of the filter has not any influence on the resonant frequency on the other hand, there was a reduction in the transmittance peak due to reduced film conductivity. With the identical mesh parameters, the simulated ITO conventional cross-shaped filter design exhibits a pass band at 0.340 THz and gives a transmission peak of 24%. In the metal mesh structures under investigation, a resonant frequency shift of 24% was achieved from free-standing structure at 0.582 THz to fabricated structure on fused silica at 0.330 THz. It was demonstrated by the simulations that our conventional metal mesh filters generate the expected filter responses at desired frequencies.

In the experimental process, in order to microfabricate the metal mesh filters , thin film deposition, photolithography, and ion beam etching techniques were employed. Titanium and copper thin films were grown in high vacuum dc magnetron sputtering system on fused silica substrates where a system identical to ref. (Yazici et al., 2015) was utilized. The films were deposited under identical growth conditions namely argon partial pressure, dc power and the deposition time. When a base pressure below 4.5×10^{-6} Torr was achieved, the sputtering process was initiated. Operating pressure was maintained at 2.5×10^{-3} Torr with Ar gas (%99,99 purity), and target-to-substrate distance was fixed at 8 cm. In order to fabricate filter structures, insulators which are basically lossless at THz frequencies were used as substrates. Indium tin oxide which is grown by a sputtering system on fused silica substrates given in ref. (Koseoglu et al., 2015) has an individual feature different than titanium and copper namely the combination of electrical conductivity and optical transparency in visible range. It is not possible to etche the thick films since there is erosion of photoresist during the etching process. In this study, the samples used have the highest thicknesses and lowest surface resistances that can be achieved for each material. Utilizing a four-terminal sensing measurement, we have measured the sheet resistance of deposited films which does not vary with film dimensions. In Table 1, the thickness and sheet resistivity values of the samples are presented.

Subsequently to the thin film deposition, THz resonant metal-mesh filters were fabricated where the UV photolithography and Ar ion beam etching techniques were employed. During the UV lithography process, different imperfections could appear as irregularity in shaperounding etc. In Figure 4.3. the optical photographs of the cross-shaped filters fabricated using Ti, ITO and Cu films are presented.

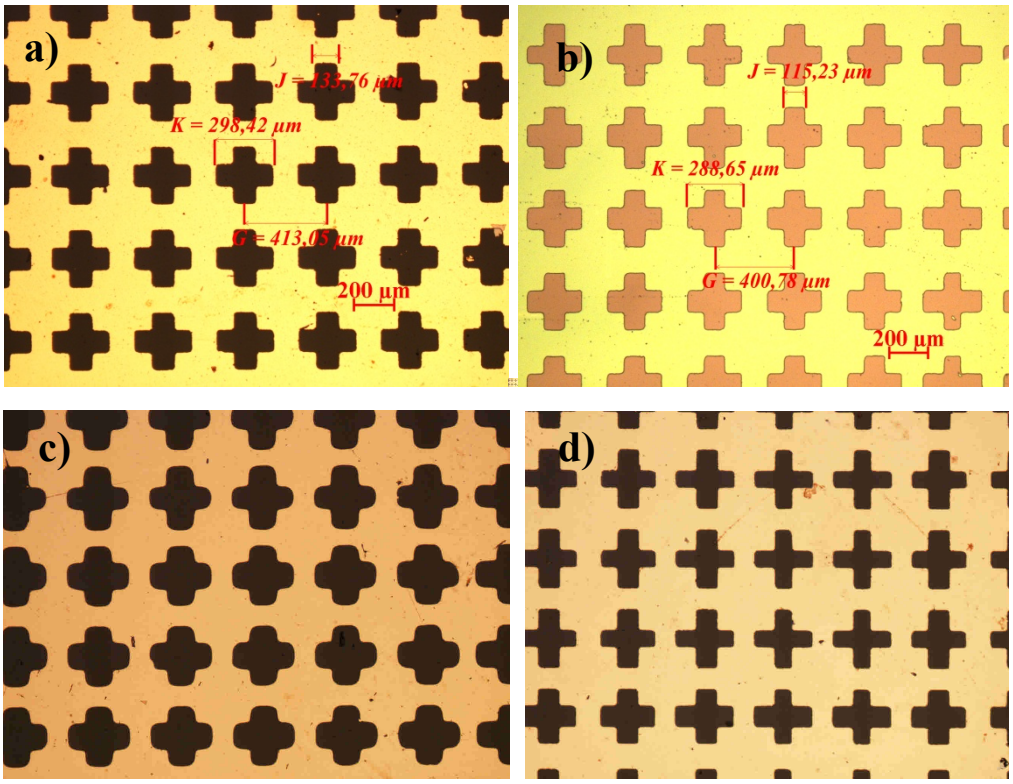

Figure 4.3. (a), (b) Optical microscope images of Cu and ITO metal mesh filters. (c), (d) Optical microscope images of Ti and ITO metal mesh filters with local defects and also showing rounding near the edges. (Source: Demirhan et al., 2016)

Metal mesh structure of the Ti filter displays rounding near the corners as seen in Figure 4.3.(c) however a nearly perfect structure of ITO filter is observed in Figure 4.3.(d). The spectral properties of the THz filters will be influenced by these variations.

4.2. Fourier Transform Infrared Spectrometer Measurements

In Figure 4.4. the transmission profiles for four different filter samples fabricated from Ti, ITO and Cu thin films are demonstrated.

Table 4.1. The thickness and sheet resistivity values of the samples

(Source: Demirhan et al., 2016)

Sample	**Material**	**Thickness(nm)**	**R_s value(Ω/sqr)**
Ti-a	**Ti**	92	14.29
Ti-b	**Ti**	92	14.29
ITO-a	**ITO**	500	7.50
ITO-b	**ITO**	500	7.50
ITO-c	**ITO**	500	7.50
ITO-d	**ITO**	500	7.50
Cu-a	**Cu**	370	0.25
Cu-b	**Cu**	370	0.25
Cu-c	**Cu**	350	0.37
Cu-d	**Cu**	350	0.37
Cu-e	**Cu**	350	0.37
Cu-f	**Cu**	350	0.37

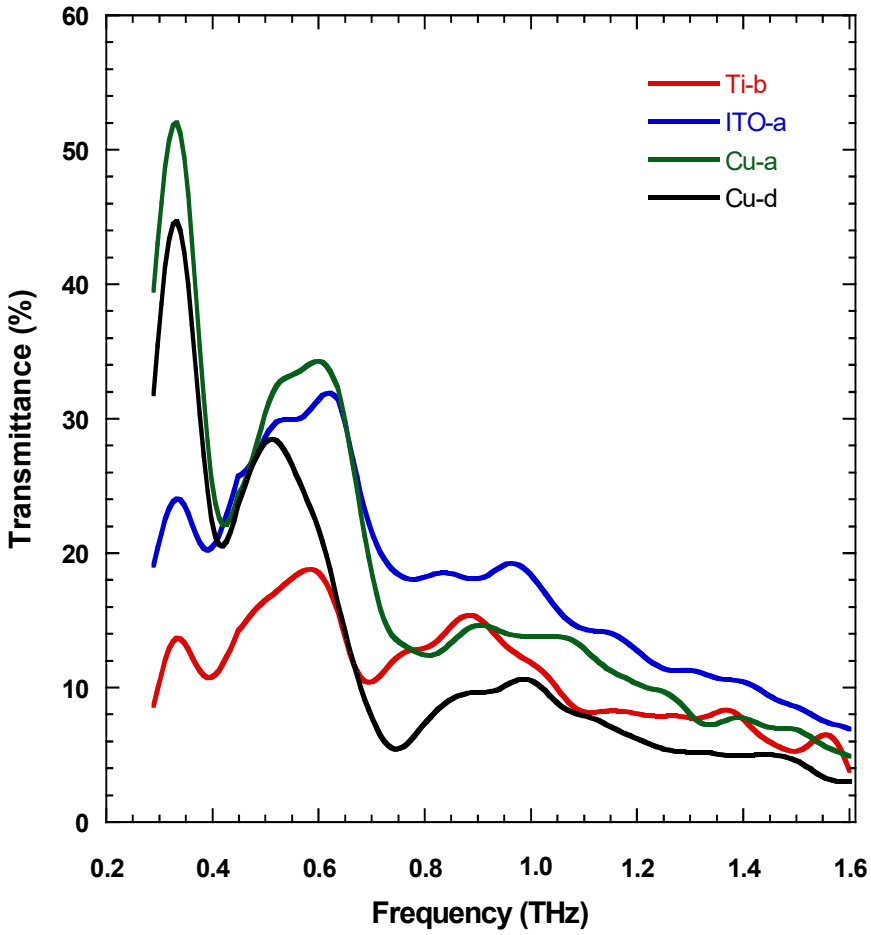

Figure 4.4. FTIR measurements of Ti, ITO and Cu metal mesh filters on the same graph. (Source: Demirhan et al., 2016)

For the sake of clarification, only a subset of samples are presented in this figure. When designed with same mesh parameters, Ti, ITO and Cu filters have approximately the same expected center bandpass frequency value of 0.33 THz. It is noteworthy to state that, certainly the transmittance of the bandpass filters increases with increasing conductivity. The measured peak transmission through a Ti filter is only 15%. One can realize this decrease since it is due to the poor conductivity of Ti films. Transmission of the ITO filters is about 24% and can be enhanced by doping of ITO thin films. When the electrical properties of ITO thin films are taken under consideration doping rate is a critical factor. In between the sheet resistances of the ITO thin films and the amount of oxygen vacancies and microstructure there exits a strong correlation. During the ionization process, at most two free electrons per vacancy to the donor level are generated by the oxygen vacancies and this leads to an increase in conductivity and decrease in sheet resistances (R_s). The relinquishing of some oxygen atoms from the surface of the ITO thin films and the absence of free oxygen in vacuum gives rise to the

decrease in R_s which can be attributed to the alteration in the crystallinity and enhancement of oxygen vacancies.

When the electrical conductivity of ITO thin films is improved higher transmittance of band pass filters for THz waves is furnished. Moreover, it has been demonstrated lately that as a consequence of the fabrication process and individual variation of each mesh parameter G/K/J which can shift the peak frequency and bandwidth in a linear or non linear way the spectral response of metal mesh filters is sensitive to local imperfections (Melo et al., 2012).

In Figure 4.3.(a) one can observe that depending on the over UV exposure in our filter structures equivalent behavior has been achieved. In Figure 4.5., the transmission characteristics of all copper based filters having the same mesh parameters are presented. Due to the rounding of corners, defects and imperfections, variance in the spectral data have been observed. Since Porterfield filters usually have a bandpass width of about 15% of the central frequency, as anticipated variations in the bandwidths is 13% and 18% of the central frequency.

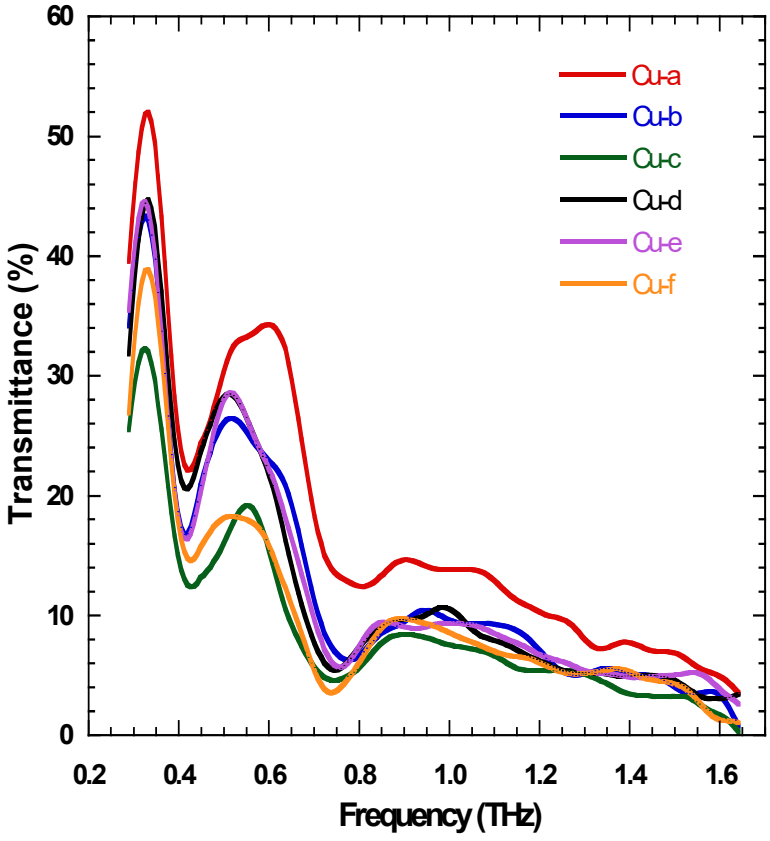

Figure 4.5. FTIR measurements of all Cu metal mesh filters on the same graph. (Source: Demirhan et al., 2016)

Furthermore, in Figure 4.5. it is observed that out-of-band rejection of measured cross-shaped filters is weak. One of the methods for developing the out-of-band rejection is to comprise an inner cross to the design, resulting in trapped-mode excitation, which has the opposite surface current to the outer cross structure (Paul et al., 2009). In order to reduce the bandwidth, aforementioned filters can be fabricated on both sides of the substrate together with multiple filters can be used for the purpose of narrowing the transmitted spectrum in the applications.

4.3. Terahertz Time-Domain Spectroscopy Measurements

The utilized time-domain terahertz spectrometer has a conventional bandwidth of about 3 THz. The usable bandwidth of the system during the measurements was limited to 1 THz by virtue of the slight absorption profile of the fused silica substrate.
Furthermore the employed TPX lenses focused the beam to a diameter of about 5mm on the substrate. The measurements were carried out in a dry nitrogen purged atmosphere.

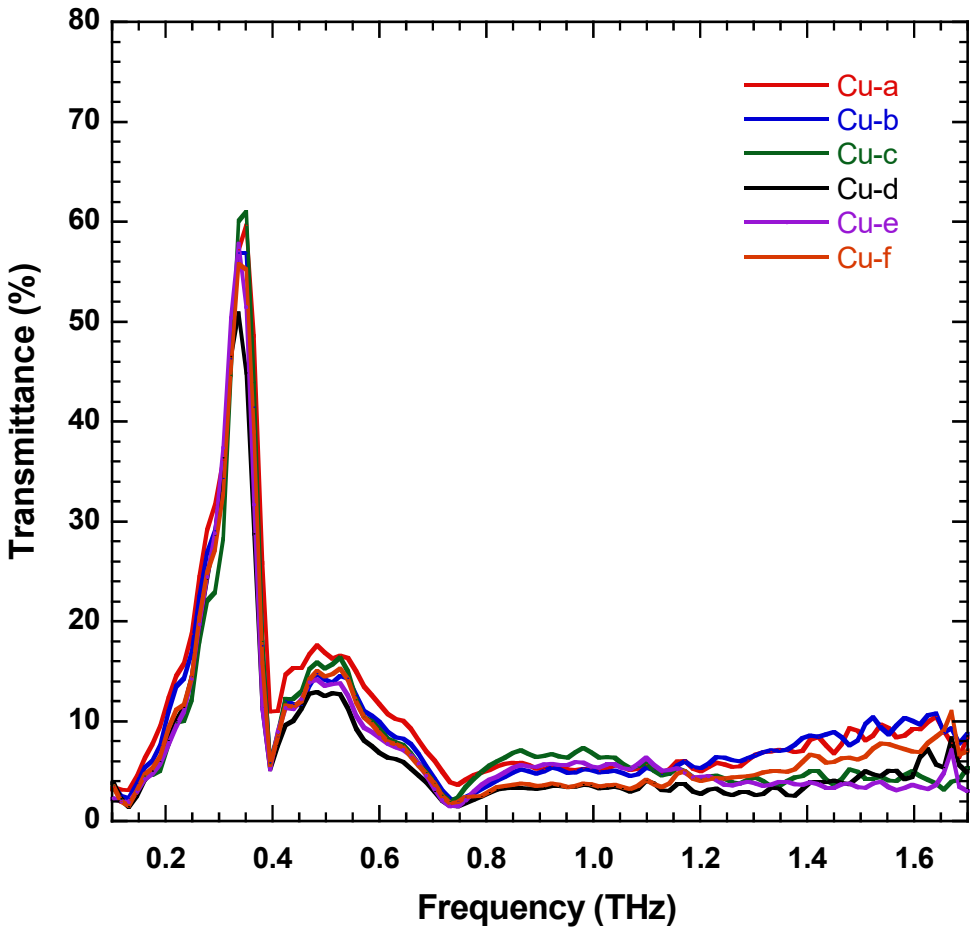

Figure 4.6. THz time-domain measurements of all Cu filters on the same graph. (Source: Demirhan et al., 2016)

In Figure 4.6. it is observed that, the THz transmission displays an apparent peak that coincides with the peak as simulated using CST Microwave Studio which was represented in Fig. 2. Moreover the broad peak observed at 0.5 THz that is due to the substrate is also noticeable however much less in amplitude once more as predicted in the simulation.

Extra measurements were carried out on the same pattern based on ITO as the conductive mesh layer (Nebioğlu et al., 2017). As a result of the smaller conductivity of the ITO film, it is observed in Figure 4.7. that the main peak is less than the transmission through Cu filters.

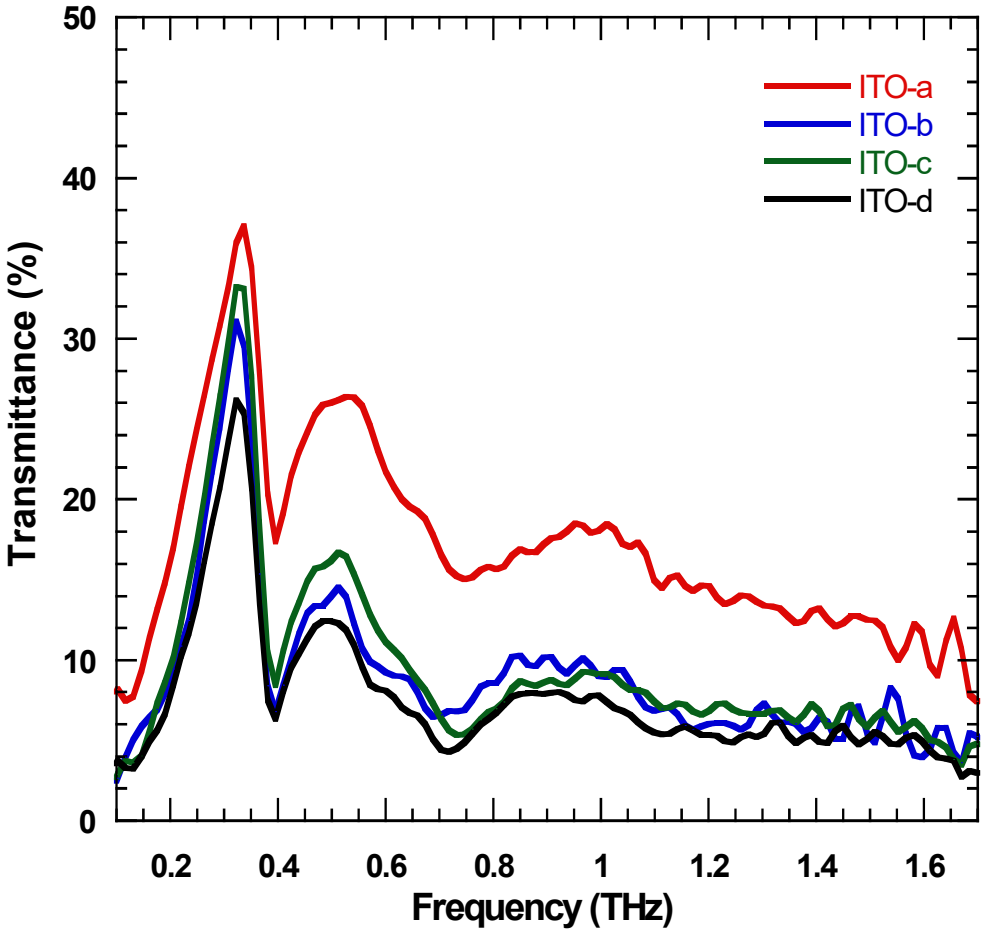

Figure 4.7. THz time-domain measurements of all ITO filters on the same graph. (Source: Demirhan et al., 2016)

The decrease in the main peak leads to getting more articulation of the broad peak near 0.6 THz which is equivalent to the case as observed with FTIR measurement for the same sample and presented in Fig 4.4. The incompatibility in the peak THz transmission intensities about 0.3 THz between the THz-TDS and FTIR measurements are most probably resulting from sample placement along the THz beam path. The thick fused silica substrates on which the films were patterned may cause shifts in the focus of the THz beam that in turn can enhance or reduce the THz transmission. Consequently, these measurements demonstrate that THz-TDS methods have high sensitivity and can be employed in characterization of the response of various filters in phase a long side with amplitude of the propagated field.

In this thesis, since it is aimed to fabricate metamaterial filters from superconducting films that works in terahertz region, deposition studies of superconducting $Bi_2Sr_2CaCu_2O_{8+d}$ (Bi2212) thin films have been carried out

simultaneously. Superconducting film properties is going to be optimized for the filter designs. These studies are given in detail in the Chapter 5.

CHAPTER 5

BSCCO THIN FILM DEPOSITION STUDIES FOR FABRICATION OF THZ METAMATERIAL FILTERS

5.1. Bi2212 Target Preperation Processes

Bi_2O_3, $SrCO_3$, $CaCO_3$ and CuO were used as starting powders to prepare a $Bi_2Sr_2CaCu_2O_{8+d}$ (Bi2212) target. These initial powders were weighted 4.66 for Bi_2O_3, 2.95 for $SrCO_3$, 1.00 for $CaCO_3$ and 1.59 g for CuO according to the molar ratios (Bi: Sr: Ca: Cu: Cu = 2: 2: 1: 2) and beaten up to get homogenous mixture. The resulting powder was placed in a alumina crucible as shown in Figure 5.1. and placed in a cube oven for the calcination process. The purpose of the calcination process is to get rid of the carbon from $SrCO_3$ and $CaCO_3$ as CO_2. Figure 5.2. shows the temperature-time plot of the calcination heat treatment. The resultant powder was heated from room temperature to 800° C at a heating rate of 6.4 °C/ min, held at 800 °C for 17 hours, and then calcined naturally by autogenous cooling. This process has been repeated twice.

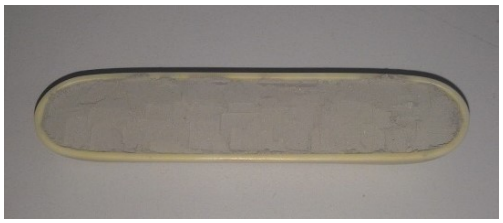

Figure 5.1. The obtained homogenous powder mixture and alumina crucible.

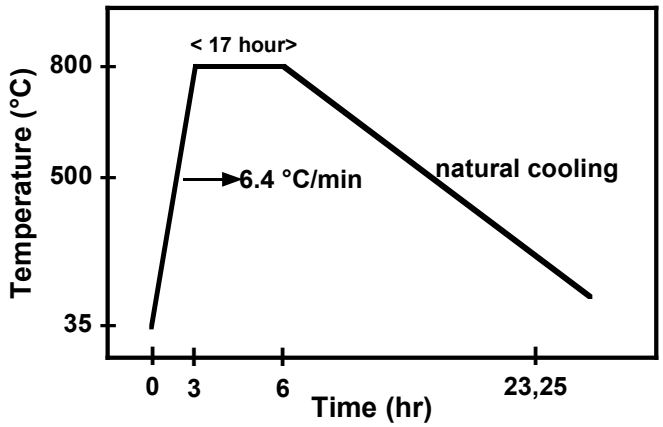

Figure 5.2. Temperature timeline of calcination heat treatment.

The calcined powder was poured into the mold shown in Figure 5.3. and pressure of 80 MPa was applied to obtain a tablet having a diameter of 3 cm and a width of 6.7 mm. This tablet was then placed on the alumina plate and the heat treatment chart in Figure 5.4. was applied to tablet hardening. The tablet is first heated at a heating rate of 4.5 ^{0}C/min, held for 3 hours at 845 ^{0}C. and then spontaneously cooled with a cooling rate of 20 ^{0}C/min. The photo of the obtained Bi2212 target is shown in Figure 5.5. For the DC magnetron deposition, 4 tablets with the dimesions 4 mm in diameter and 3 cm in diameter have been prepared as described above. These prepared tablets were appropriately cut into pieces to obtain a 2 inch (5.08) diameter 4 mm thick target (Figure 5.6.). During the heat treatment, the Bi content is reduced with respect to the other materials and the Bi content of the Bi2212 phase falls below 2. To prevent this, the molar ratio of Bismuth was taken as 2.5.

Figure 5.3. Calcined powder and tablet press mold in the alumina container.

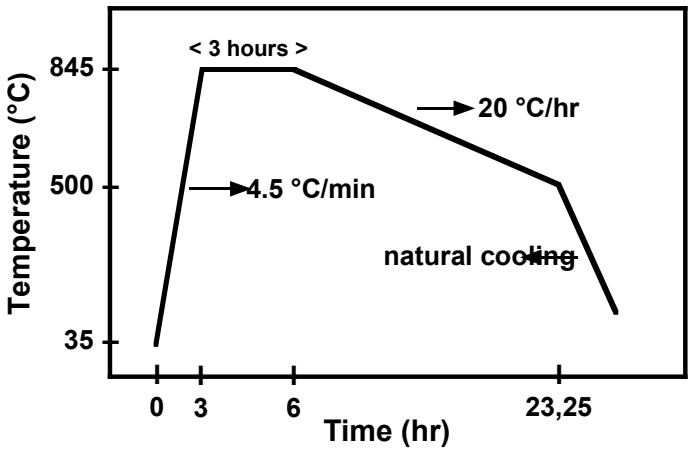

Figure 5.4. Temperature schedules of tablet hardening.

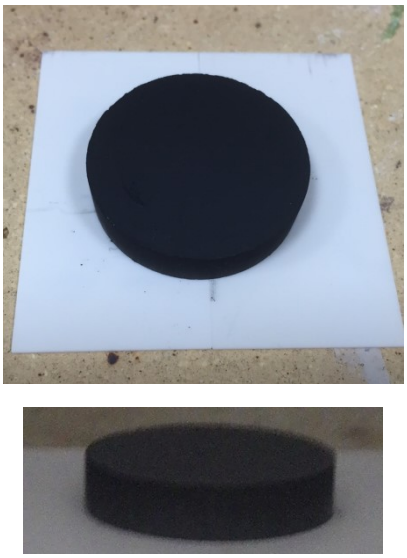

Figure 5.5. Photograph of the prepared Bi2212 target.

In the deposition of the superconducting Bi2212 thin films, over the fifty samples, the target was worn away due to broken particles (Figure 5.7.). Considering that the coating time is 5 hours for most specimens, the wear of the specimen is considered normal. It is also estimated that the reason why the target wears so fast is that the insufficient pressure we can apply causes the formation of porous targets.

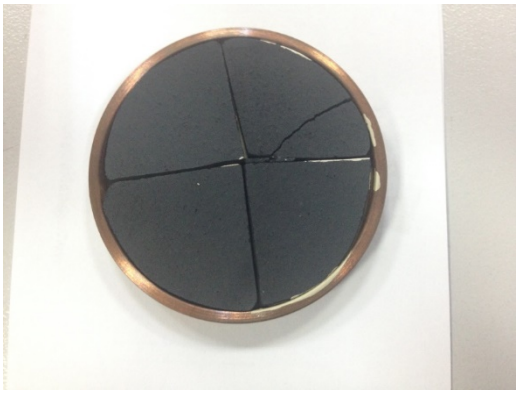

Figure 5.6. Pre-coating photograph of the fabricated Bi2212 target incorporated into a copper metal container

Figure 5.7. Photograph of the prepared Bi2212 target combined in a copper metal container after deposition processes.

5.2. Bi2212 Thin Film Deposition

The Bi2212 target that we prepared was placed in the system and the superconducting thin films are deposited on the sapphire and MgO substrates in our DC magnetron sputtering system using different parameters. In addition, the purchased Bi2212 target was placed in the system and deposition is done with RF magnetron sputtering technique on sapphire and MgO substrate using different parameters. Deposition parameters (power, substrate temperature, pressure value, ratio of Argon and Oxygen gas delivered) are of great importance in terms of superconducting film phase and quality (structural stability, critical temperature, critical current values etc.)

(Uchiyama et al., 2007; Sozeri et al., 2007; Levinson et al., 1988). Thin films coated with DC magnetron sputtering technique are optically and structurally characterized.

5.3. Characterization of Bi2212 Thin Films

Structural and electrical characterizations of the thin films we deposited with Bi2212 target and DC magnetron system were done. SEM images were taken with the Scanning Electron Microscope for surface analysis of BSCCO thin films. With SEM, materials can be displayed in micro and nano dimensions. In the SEM images of the deposited BSCCO thin films, we could not see the microgranular structure that should be observed on the thin film surfaces. The most known method for composition determination is EDX (Energy Dissipative X-Ray Microanalysis Spectrometer) analysis. At the end of the EDX analysis made at the Material Research Center (MAM, IZTECH), the elemental content of our BSCCO thin films was found quantitatively and qualitatively and the distribution of elements over the SEM image was given by mapping. The percentages of the elements in the samples are proportional to the area under the peaks of the elements.

5.3.1. Scanning Electron Microscope Images

The SEM images taken for the surface analysis of Bi2212 thin films coated with the target and the different growth parameters are given in Figures 5.8-5.11., respectively.

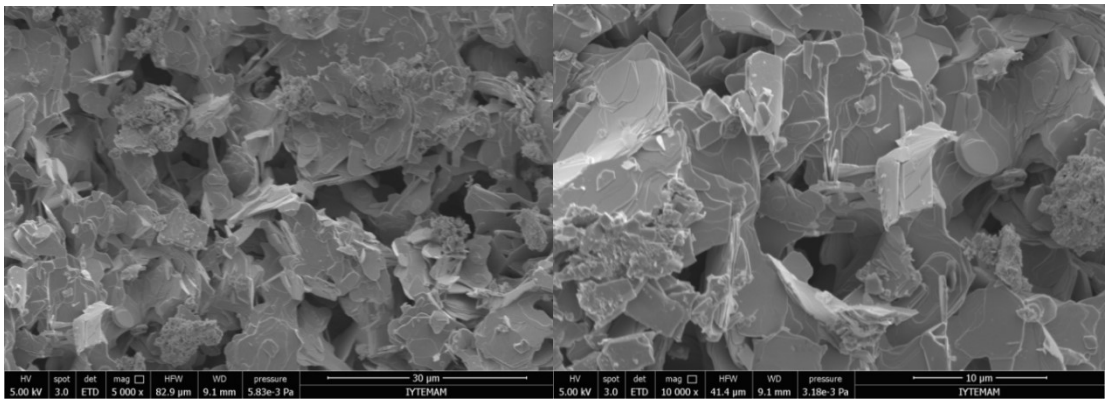

Figure 5.8. SEM image of prepared Bi2212 target.

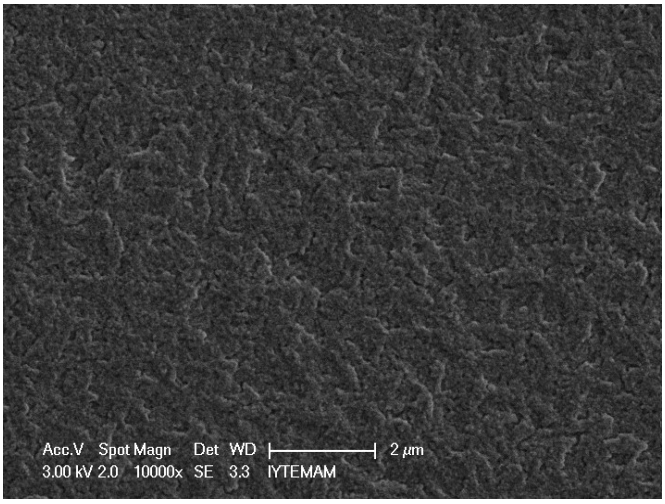

Figure 5.9. SEM image of YD 37 sample (30 sccm Argon 50 sccm Oxygen delivered for 3 hours).

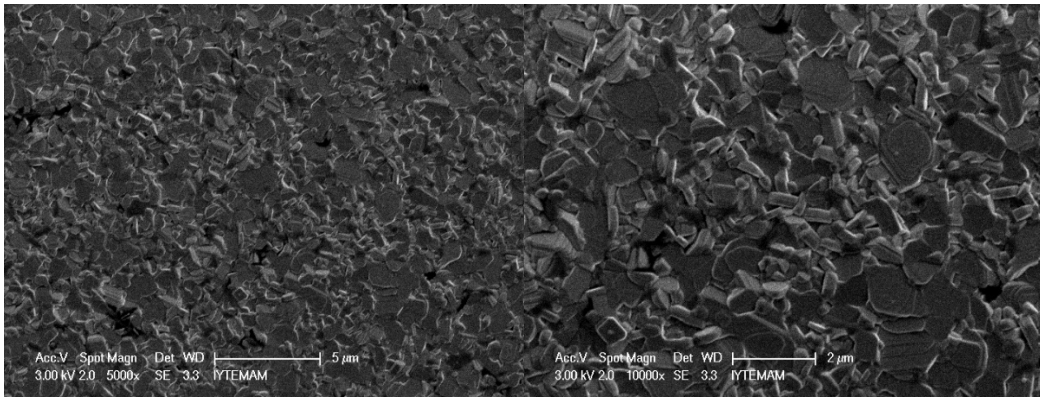

Figure 5.10. SEM image of YD 39 sample (50 sccm Argon 2.5 sccm Oxygen delivered for 3 hours).

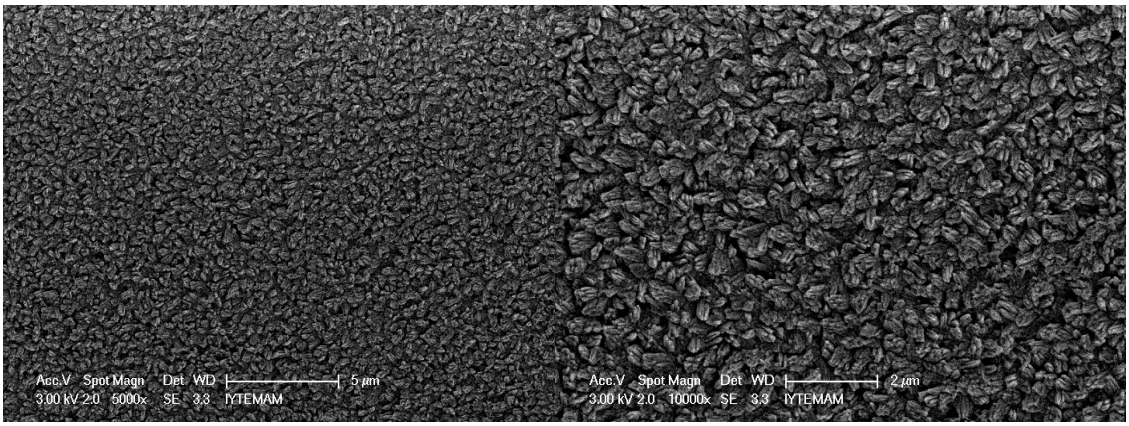

Figure 5.11. SEM image of YD 48 sample (120 sccm Argon 30 sccm Oxygen delivered for 3 hours).

The most important reason of the low transition temperature and critical current density in the layered ceramic superconductors such as Bi2212 are the grained structure (Kim et al., 2002; Baker et al., 1994; Sozeri et al., 2007). So, it is important to have strong bonds between the particles. The granular structures we expected were clearly observed in the SEM images. When we examine the SEM images, it is seen that the particles observed in the thin films are in random contact, and that the particle boundaries are in contact with each other to form weak bonds with each other. This is one of the characteristics of high temperature superconductors. In the case of YD 39, it is observed that there is generally a layered structure in the coated samples, but the homogeneity decreases as the coating temperature decreases. In addition, it appears that the grains formed by the large pieces are randomly oriented, and the small sized clusters are observed, which are also observed in the XRD results. EDX analysis of Bi2212 thin films coated with different parameters, Bi2212 thin films coated with different parameters with the same parameters, and Bi2212 targets produced and purchased are given in Table 5.1., Table 5.2. and Table 5.3.. Referring to Table 5.3, the thin film coating made by sending 120 sccm Argon and 40 sccm oxygen gave the closest result to phase Bi2212.

Table 5.1. EDX analysis of prepared and purchased Bi2212 targets

Element	**(At%) Self-prepared Target (%)**	**(At%) Purchased Target**
Bi	16.41	17.07
Sr	11.78	15.57
Cu	9.43	10.15
O	31.35	34.22
Ca	4.08	5.94
C	26.96	17.05

Table 5.2. EDX analysis of Bi2212 thin films coated with different parameters

Element	(At%) Ar:60 sccm O: - YD12	(At%) Ar:50 sccm O:2.5 sccm YD35	(At%) Ar:120 sccm O:40 sccm YD52	(At%) Ar:120 sccm O:30 sccm YD56	(At%) Ar:30 sccm O:50 sccm YD25
Bi	21.38	19.77	15.31	18.84	15.62
Al	0.52	2.49	6.16	1.47	1.15
Sr	15.19	16.67	15.22	15.44	14.51
Cu	14.20	15.67	15.31	15.57	15.95
O	8.32	39.07	40.11	42.17	46.29
Ca	3.54	6.32	7.89	6.50	6.47

Element	(At%) Ar:30 sccm O:50 sccm YD27	(At%) Ar:30 sccm O:50 sccm YD37	(At%) Ar:50 sccm O:12.5 Sccm YD31	(At%) Ar:150 sccm O:3 sccm YD42	(At%) Ar:70 sccm O: 15 sccm YD46
Bi	3.63	5.65	16.75	21.04	19.76
Al	17.90	5.25	1.63	1.36	4.44
Sr	16.44	18.43	15.99	13.13	14.65
Cu	16.86	19.10	19.05	14.92	15.35
O	41.20	47.45	39.64	43.34	39.44
Ca	3.96	4.12	6.95	6.21	6.35

Table 5.3. EDX analysis of Bi2212 thin films coated on different substrates with the same parameters

Element	(At%) MgO Substrate	(At%) Saphirre Substrate
Bi	3.68	4.76
Al & MgO	30.47	27.65
Sr	10.88	12.99
Cu	13.49	13.75
O	38.53	37.26
Ca	2.95	3.60

5.3.2. XRD Analysis Results

One of the structural characterization methods of coated thin films is the examination of x-ray diffraction measurements. Using these measurements, information about crystal structure of film; lattice parameters, Miller indices can be obtained. It is also necessary to detect different superconducting phases and impurity phases. XRD analysis of target and coated thin films prepared for this purpose was performed. These analyzes were performed at the İzmir Institute of Technology Materials Research Center (MAM) using a CuKα x-ray in the Philips X'pert Pro diffractometer at a range of $20^o \leq 2\theta \leq 70^o$. The XRD analysis of the Bi2212 target we prepared and the Bi2212 thin films we coated are shown in Figures 5.12.-5.14.-5.15.-5.16.-5.17.-5.18.-5.19.-5.17.,5.18.-5.20. respectively. Peaks of high-T_c and low-T_c phases were determined with reference to the reference work (Endo et al., 1992) (Figure 5.13.)

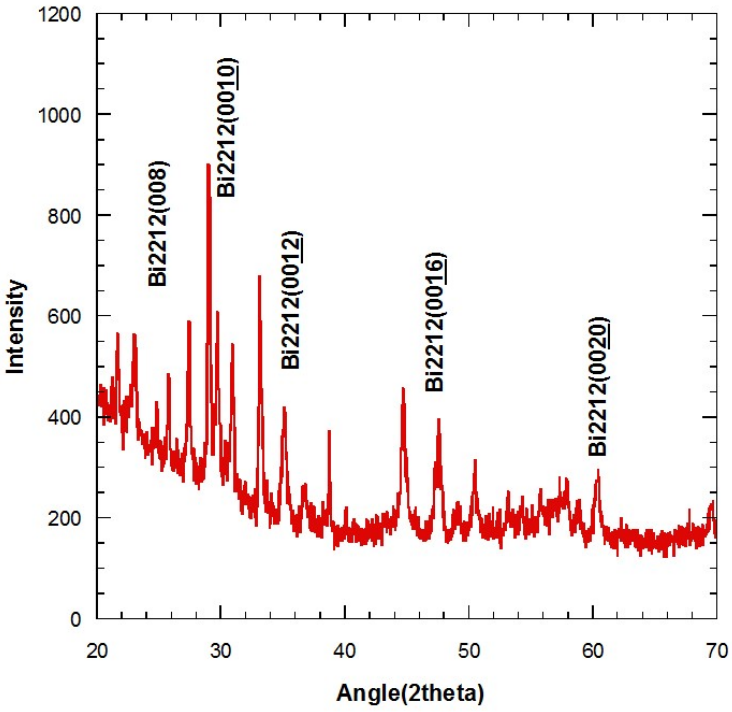

Figure 5.12. Result of XRD analysis of Bi2212 target.

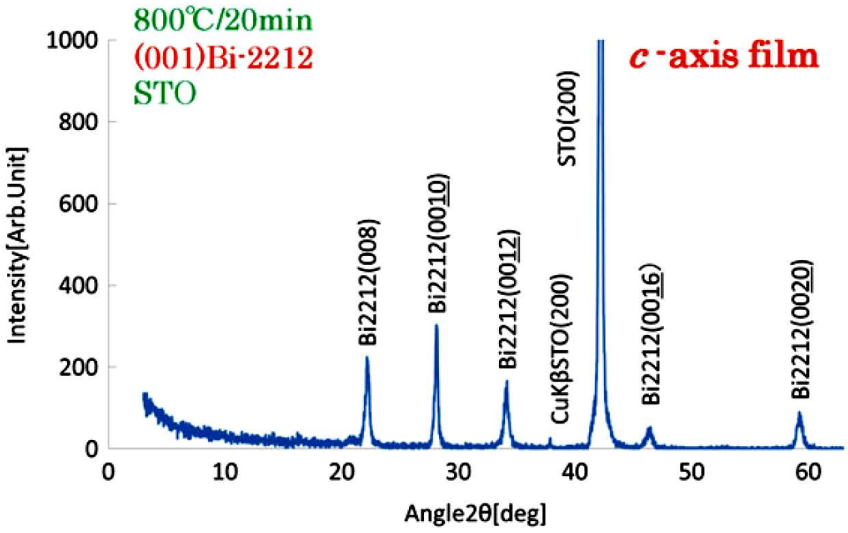

Figure 5.13. XRD analysis of Bi2212 films grown along the reference c-axis. (Source: Endo et al., 1992)

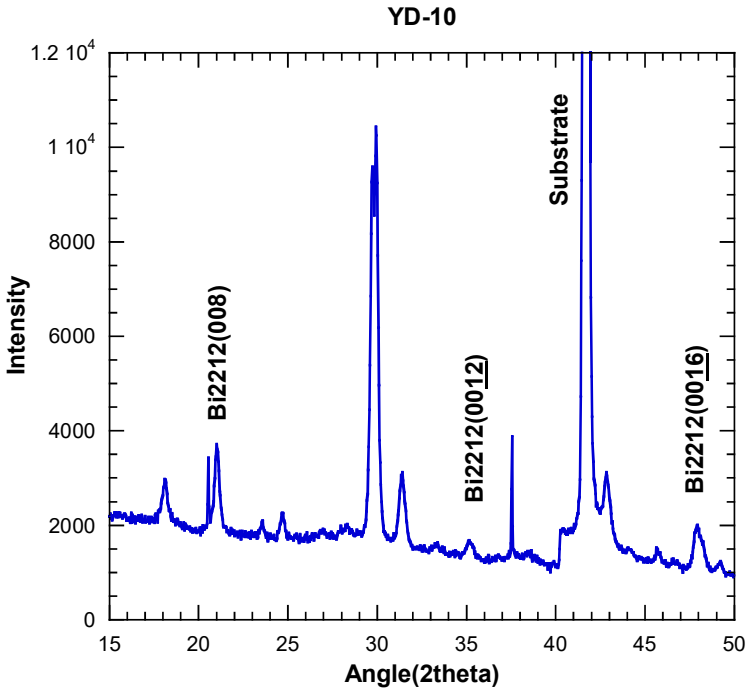

Figure 5.14. The XRD analysis result of the YD 10 sample (50 sccm Argon, 20 sccm Oxygen was delivered for 1.5 hours).

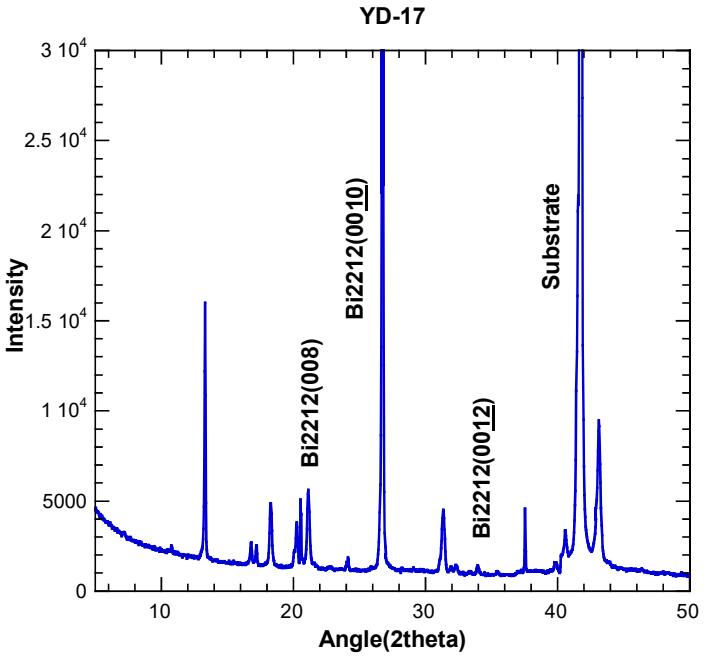

Figure 5.15. The XRD analysis result of the YD 17 sample (30 sccm Argon, 50 sccm Oxygen was delivered for 2 hours).

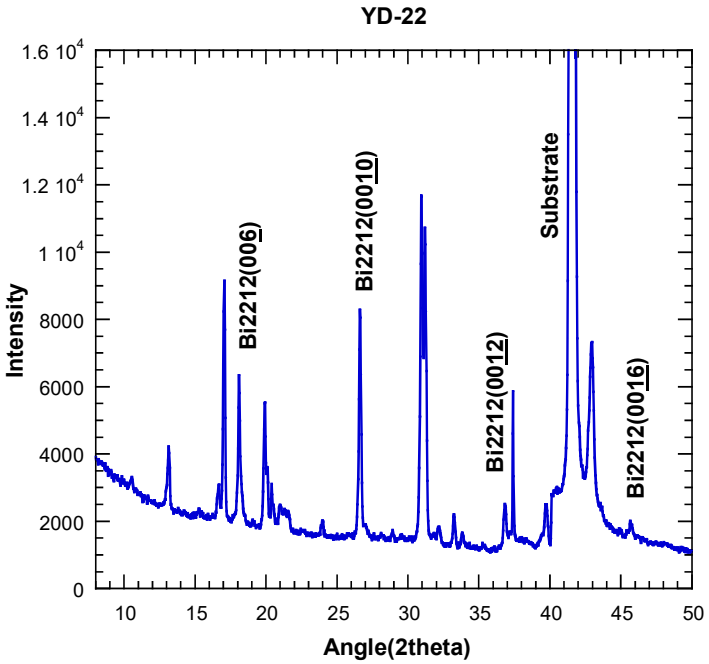

Figure 5.16. The XRD analysis results of the YD 22 sample (20 sccm Argon 50 sccm Oxygen were delivered for 3 hours).

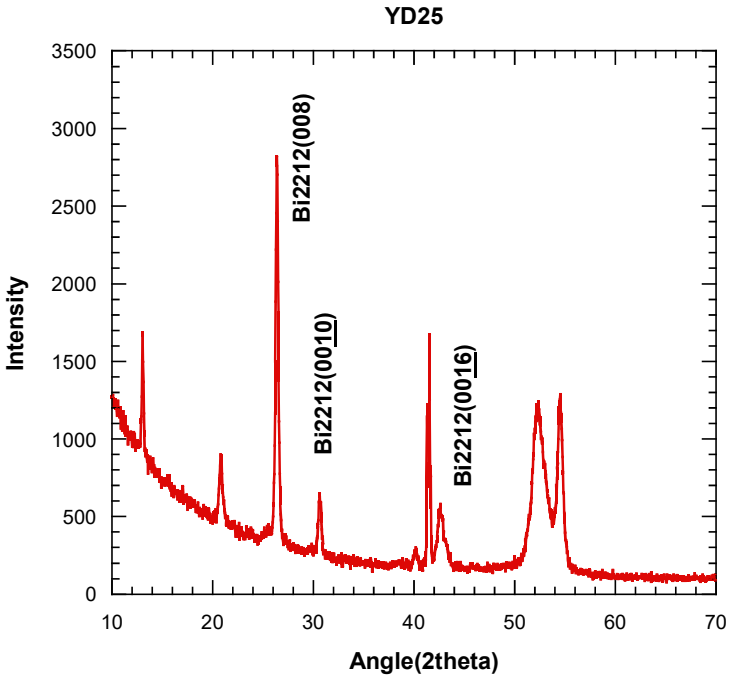

Figure 5.17. Result of XRD analysis of YD 25 sample (30 sccm Argon, 50 sccm Oxygen delivered for 3 hours).

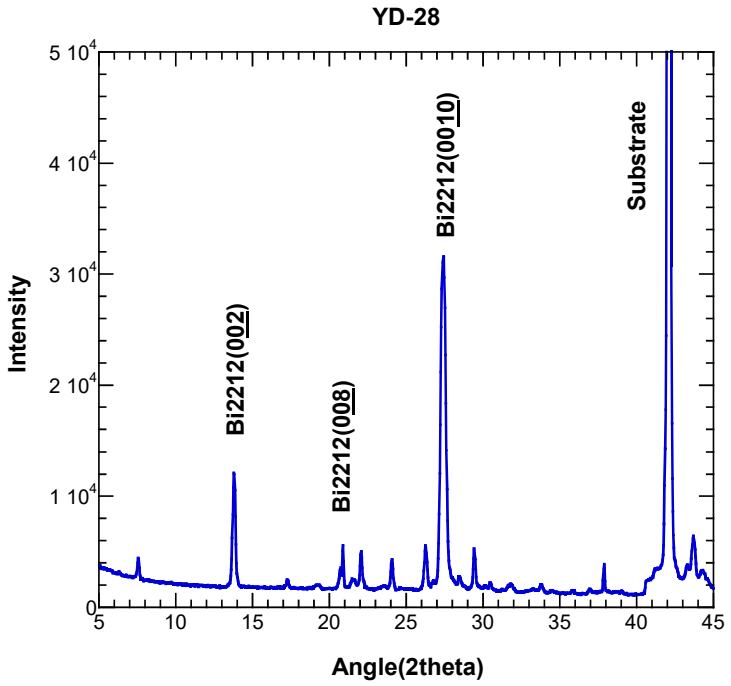

Figure 5.18. XRD analysis result of sample YD 28 (30 sccm Argon 50 sccm Oxygen delivered for 5.5 hours).

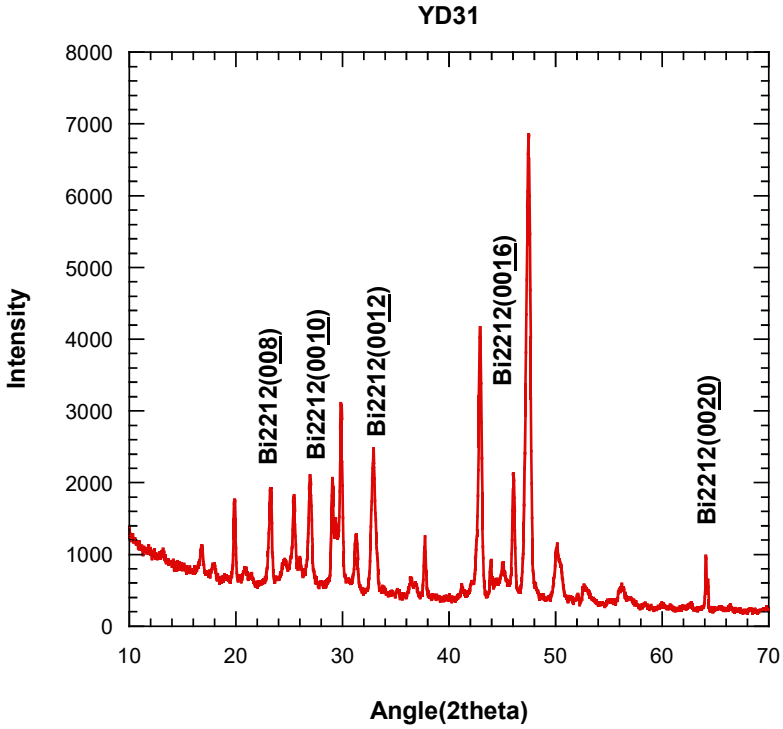

Figure 5.19. XRD analysis result of YD 31 sample (50 sccm Argon, 12.5 sccm Oxygen delivered 5 hours 50 minutes).

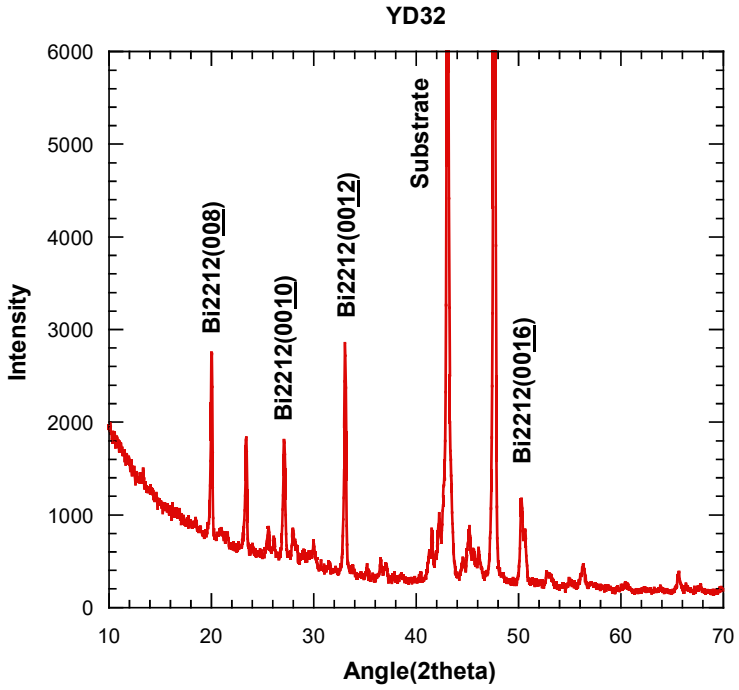

Figure 5.20. XRD analysis result of YD 32 sample (100 sccm Argon, 25 sccm Oxygen delivered for 1.5 hours).

5.3.3. Resistance-Temperature (R-T) Measurements of Bi2212 Thin Films

Resistance-temperature measurements of Bi2212 thin films deposited on sapphire and MgO substrates by DC magnetron sputtering were made by four point method in our closed cycle cryostat system. In addition to the R-T measurements of the thin films, a thinner piece was separated from the Bi2212 target and measured by four point method. Closed-cycle Helium cooling is used to decrease the temperature of superconducting materials below the critical temperature (T_c) and to measure resistance-temperature behavior. The system includes vacuum pump, compressor, water cooling system and temperature controller. The operating principle of the system is based on the expansion of the refrigerant at the cold pressure of the He gas. First the He gas is compressed to 16.5 bar with the water cooling compressor, then the compressed gas is transferred to the cooler by the flexible line. Cooling is produced by compression of the He gas at the cold head (Cold head) and is controlled by the temperature controller. The area between the material holder and the cooler's guard is vacuum pumped to create thermal insulation and keeps the surrounding thermal effects to a minimum. The vacuum must be 10^{-4} or 10^{-5} mbar to achieve the required low temperature. The devices we use can be coordinated with the computer and multiple device controls are controlled by a computer program that includes data analysis and data storage.

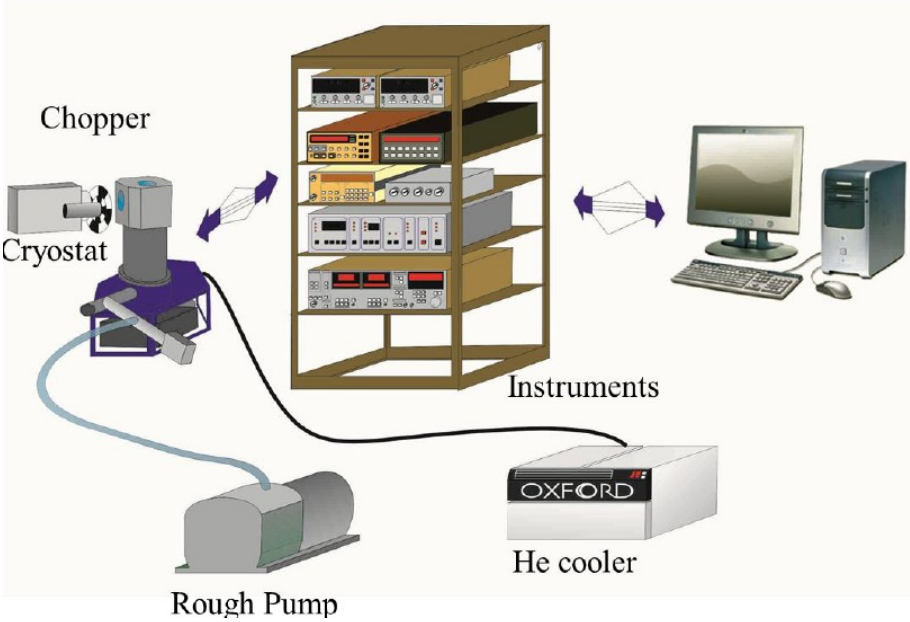

Figure 5.21. Closed-cycle He measurement system.

Figure 5.22 shows the R-T measurement of the Bi2212 target. The transition to superconducting state was observed at around 85 K, indicating that this target is in phase 2212 as expected. A zero resistance value is seen below the T_c value at 4 point measurement.

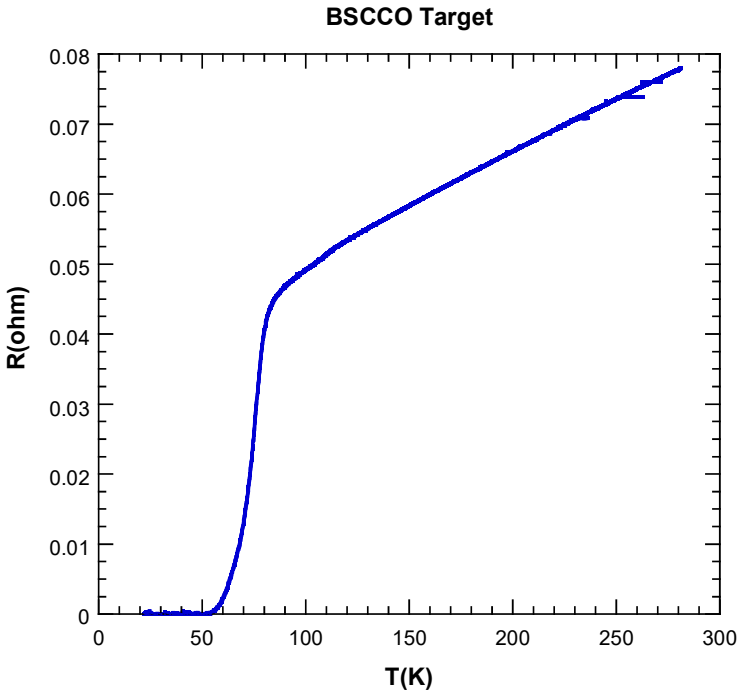

Figure 5.22. R-T measurement of prepared Bi2212 target.

The R-T measurements are necessary to determine the properties such as superconducting phase, transition temperature, and doping level of the thin films. Resistance temperature graphs of annealed samples taken from YD 25, YD 27, YD 37, YD 37-annealed, YD 39, YD 39-annealed samples are shown in Figure 5.25-5.26-5.27-5.28-5.29 respectively. In graphs, superconducting phase transitions are observed at critical temperature, but no zero resistance is expected from 4 point measurement. Observed critical temperature values are between 88 and 91 K.

During magnetron sputtering, the same stoichiometry with the target was not achieved, especially the change in oxygen content and loss of Bismuth were observed. This result can be seen from the EDX analysis in Table 5.4. The annealing procedure shown in Figure 5.23 was used to adjust the oxygen content of the coated Bi2212 films. 200 sccm Oxygen was passed through the heat treatment and annealing steps in Fig. 5.24 were used.

Figure 5.23. Picture of the annealing system in oxygen atmosphere.

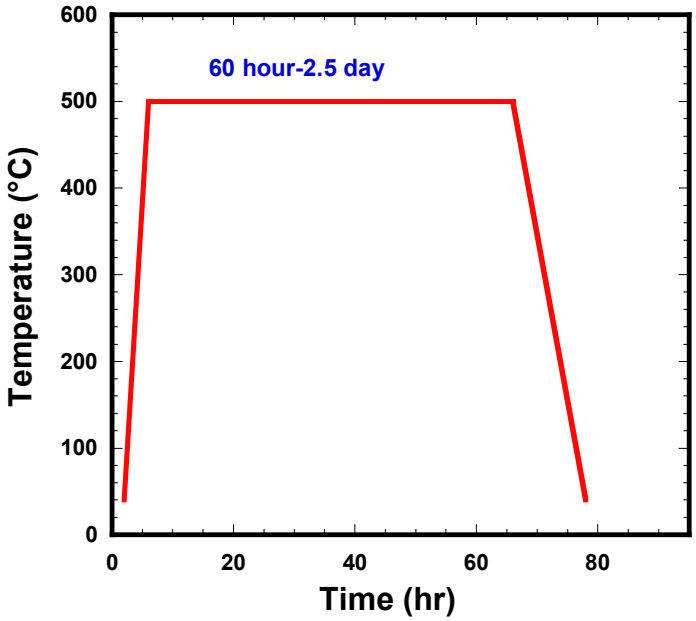

Figure 5.24. Temperature-time graph of annealing system.

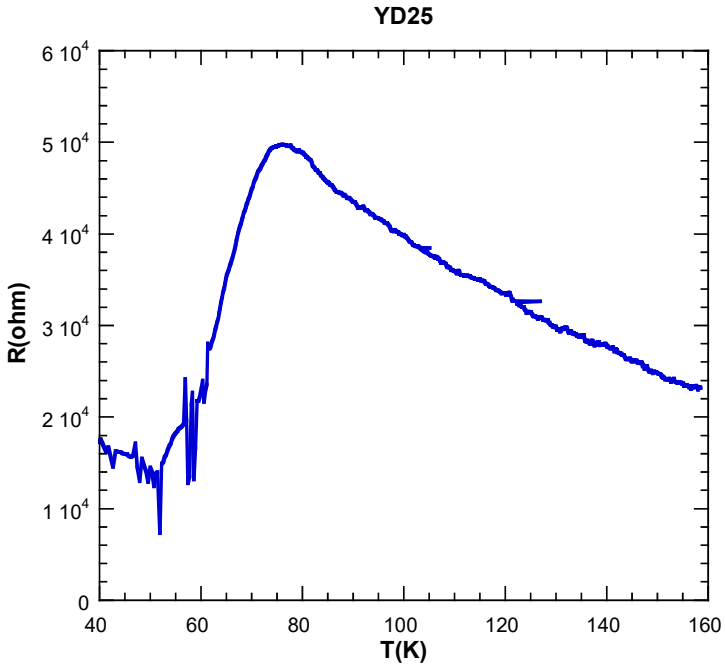

Figure 5.25. R-T measurement of YD25 sample (30 sccm, Argon 50 sccm Oxygen delivered for 3 hours).

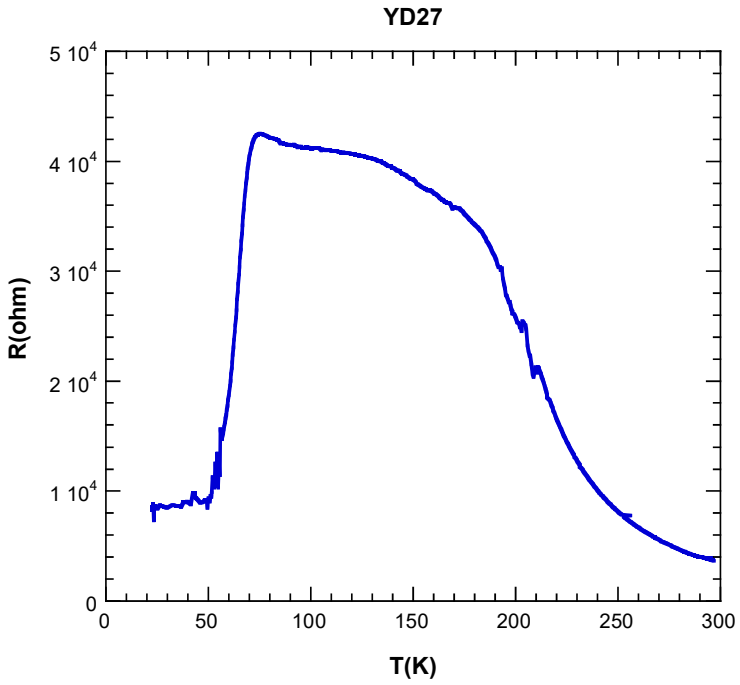

Figure 5.26. R-T measurement of YD 27 sample (30 sccm Argon 50 sccm Oxygen delivered for 3 hours).

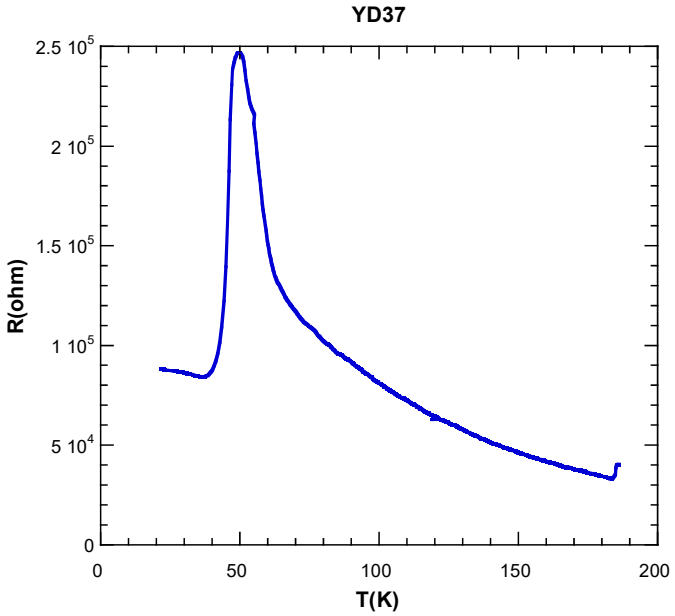

Figure 5.27. R-T measurement of YD 37 sample (before annealing) (30 sccm Argon 50 sccm Oxygen delivered for 3 hours).

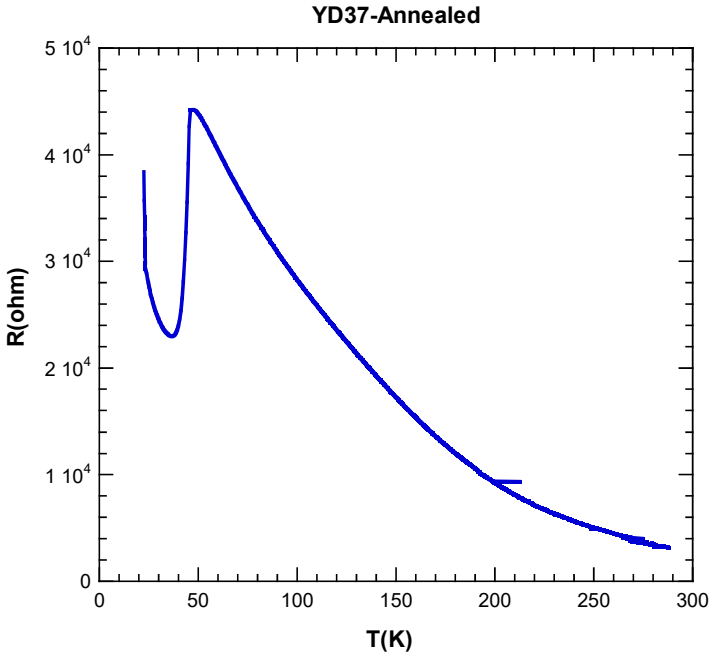

Figure 5.28. R-T measurement of YD 37 sample (after annealing) (30 sccm Argon 50 sccm Oxygen delivered for 3 hours).

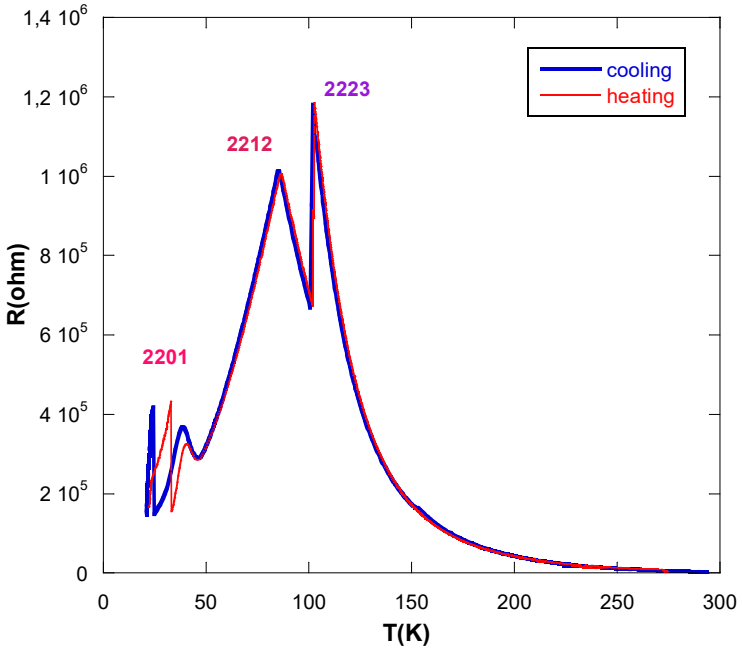

Figure 5.29. R-T measurement (heating and cooling) of the sample YD 56 (120 sccm Argon 30 sccm Oxygen delivered for 2 hours 15 minutes).

The characterization results shows that the quality of the deposited Bi2212 thin films are not suitable for filter fabrication. So, instead of Bi2212 superconducting thin films, commercially available Y123 thin films are used. A unique fourcross metamaterial filter structure was designed for the thesis and fabricated on both gold and YBCO thin

films. In the last chapter of this thesis, the study of quadcross metamaterial filters fabricated from high Temperature superconducting YBCO and Au thin films for Terahertz waves is given.

CHAPTER 6

SUPERCONDUCTING METAMATERIAL FILTERS FOR THE THZ WAVES

A unique and new fourcross shaped metamaterial Terahertz (THz) filter fabricated using two thin films namely, gold thin films and $YBa_2Cu_3O_{7-d}$ high T_c superconducting thin films is presented in this part of the thesis. In order to design and optimize the metamaterial filter structures we utilized a commercial electromagnetic simulation software, CST Microwave Studio. Fourcross shaped rectangular filter structure that is suggested in this study comprises of periodic metallic rings in which strip lines are placed at the sides of the ring.

Utilizing e-beam lithography and ion beam etching techniques, fourcross metamaterial filters are fabricated. The design predictions for the center frequencies and bandwidths of the resonances due to the fourcross structures are formalized by the measurements of terahertz time-domain spectroscopy. Lowering the temperature below the critical transition temperature it was possible to investigate the resonance switching of the transmission spectra. When the filters are produced from metals this resonance switching effect is not utilized. Temperature-dependent resonance property of this novel fourcross rectangular resonator exhibits eminent capacity for active, tunable and low loss THz devices that could be used in imaging, sensing, and detection applications.

6.1. Fourcross-shaped Metamaterial Filters

Since bulk materials typically do not exhibit a strong electromagnetic response in the frequency range between 0.1 and 10 THz, this region usually called the THz gap due to the difficult to develop devices which can interact, generate or detect radiation. There are prominent attempts trying to fill this vacancy in the spectrum (Kadowaki et al., 2008; Wang et al.,2009; Guénon et al.,2010; Demirhan et al., 2015). Since metamaterials (MMs) have electromagnetic properties which could not be attained by their natural bulk material counterparts, they can be designed with a specific functionality for THz

applications and thus have a important role in the fabrication of artificial optical components. In its most fundamnental composition, the metamaterial structure can be considered as electrical circuits much less in size than the wavelength that replace atoms as the basic unit of interaction with electromagnetic radiation.

In recent years there has been important progress in this field (Smith et al.,2004; Soukoulis et al., 2010) which has given rise to the development of electromagnetic MMs and these structures demonstrate novel properties namely magnetic response at terahertz and optical frequencies, negative index of refraction, and huge chirality (Padilla egt al., 2006; Hsieh et al., 2012).

The appreance of THz MMs led to electromagnetic properties and functionality that can not be achieved by the present natural materials an thus allowing a whole new generation of MMs based devices such as, electrically small resonators, compact high selective THz filters, superlenses, cloaks, chiral devices, electromagnetically induced transparency applications and modulators. Consequently, the theoretical and experimental study of THz MMs has attracted great attention (Chen et al., 2006; Chen et al., 2008). In the fabrication of conventional THz MMs either dielectrics or normal conducting metals are used. Sub-wavelength structures based on these conventional materials exhibited low insertion loss at microwave frequencies however one of the key limitations is that there are substantial losses in the terahertz frequency range. Consequently, to minimize the losses there is a great effort to explore novel structures based on novel materials. There are other factors effecting the performance namely; the conductivity of the metamaterial which imposes a severe limit on the device performance in the THz frequency range (the degree of Ohmic loss can be measured by the quality factor Q of the resonance) (Singh et al., 2010). Contrary to usual conducting metals, electromagnetic properties of superconductors can be employed for the purpose of fabricating virtually ideal and novel metamaterial structures. When metallic structures are replaced by superconducting configurations losses can be reduced extensively (Ricci et al., 2007). Compared to metals, complex conductivity properties of superconductors essentially depends on the applied magnetic field and temperature.This permits the feasibility to instantly control the conductivity of the superconducting element regardless of inserting additional elements i.e. an active metamaterial structure (Chen et al., 2010, Zhang et al., 2012). Furthermore, superconductors exhibit superior conductivity at low temperatures and possess the capacity to integrate elements demonstrating quantum behaviour. In these materials,

values of the surface resistance at microwave frequencies are also small (Savinov et al., 2012).

In THz device applications, there are various methods for employing superconducting materials due to their specific properties. Josephson based metamaterials, immediately introduce a great number of significant and appealing posibilities for novel metamaterial structures. The nonlinear response of these materials can allow for parametric amplification (Kurter et al., 2012) of photons and also reduction of losses. Furthermore, due to the changes in the Josephson inductance and depending on magnetic field and temperature, superconducting meta-atoms can exhibit an intrinsic tunability of their resonance frequency. The density of Cooper pairs in other words suppression of the superconducting order parameter gives rise to the tunability. With the help of resonance frequency tuning, in superconductor MMs, the quality factor of the resonance can be modified.

Zhang et al. measured the field-induced nonlinear response of metamaterials and unpatterned films made out of the low-T_c conventional superconductor NbN (Zhang et al., 2013). Here, the gap frequency (f_g) of NbN is given by $f_g = 2\Delta_0/h$, where Δ_0 is the energy gap at 0 K and h is the Planck constant at 1.18 THz (Kang et al., 2011). On the contrary, in the case of broadband response high-T_c superconductors are more suitable due to their larger energy gap. When currents flow in the Cu–O planes, high-T_c cuprate superconducting materials display metallic behavior. On the other hand, for light polarized in the c-direction they have dielectric-like properties. Furthermore, they possess higher transition temperatures, which assure conduction of electrical current without resistance at liquid nitrogen temperatures however, the necessity to provide and sustain a cryogenic environment stands as the main handicap of superconductors.

Measurement of the nonlinear THz transmission through films composed of the high-T_c superconductor $YBa_2Cu_3O_7$ (YBCO) has been carried out by Glossner et al (Glossner et al., 2012). The nonlinear transmission of BSSCO at modest field strengths has been measured by Orenstein et al (Orenstein et al., 1997) which led to finding a characteristic current scale for the nonlinearity on the order of the intrinsic depairing current for $Bi_2Sr_2CaCuO_{8+x}$ (BSSCO) that can be calculated from well-known parameters. Latter works concentrated in minimizing the material losses, by cautiously designing MM structures to match impedances between propagation in different media.

In tuning the negative permittivity wire structures are more advantageous on the other hand when temperature dependent tuning of the negative permeability in the superconducting structure can be accomplished, structures of split-ring resonators type have been shown to be functional (Vendik et al., 1998; Padilla et al., 2006).

In this study, the aim was to design superconducting metamaterial filters with a unique geometry which operates in the THz frequency band. In the patterning of the structures, normal conductive metallic films together with High T_c superconductor YBCO thin films were utilized. It was demonstrated that; modification of the geometrical parameters of the structure and temperature dependent superconducting properties leads to the tuning of the resonance frequency and transmittance at resonance of the metamaterial structure. These properties contribute to the fabrication of very efficient and compact metamaterial-based filters with a high selectivity. These type of extremely specific filters can be used to remove undesirable transmitted signals in pre-defined frequency bands and have imminent applications in the field of THz diagnostics.

6.2. Design and Fabrication of Fourcross Metamaterial Filters

6.2.1. Design and Background Theory

A unique geometry that can be used as a terahertz filter which operates in the sub THz frequency range has been designed. In Figure 6.1., the design of the filter structure is demonstrated in detail.

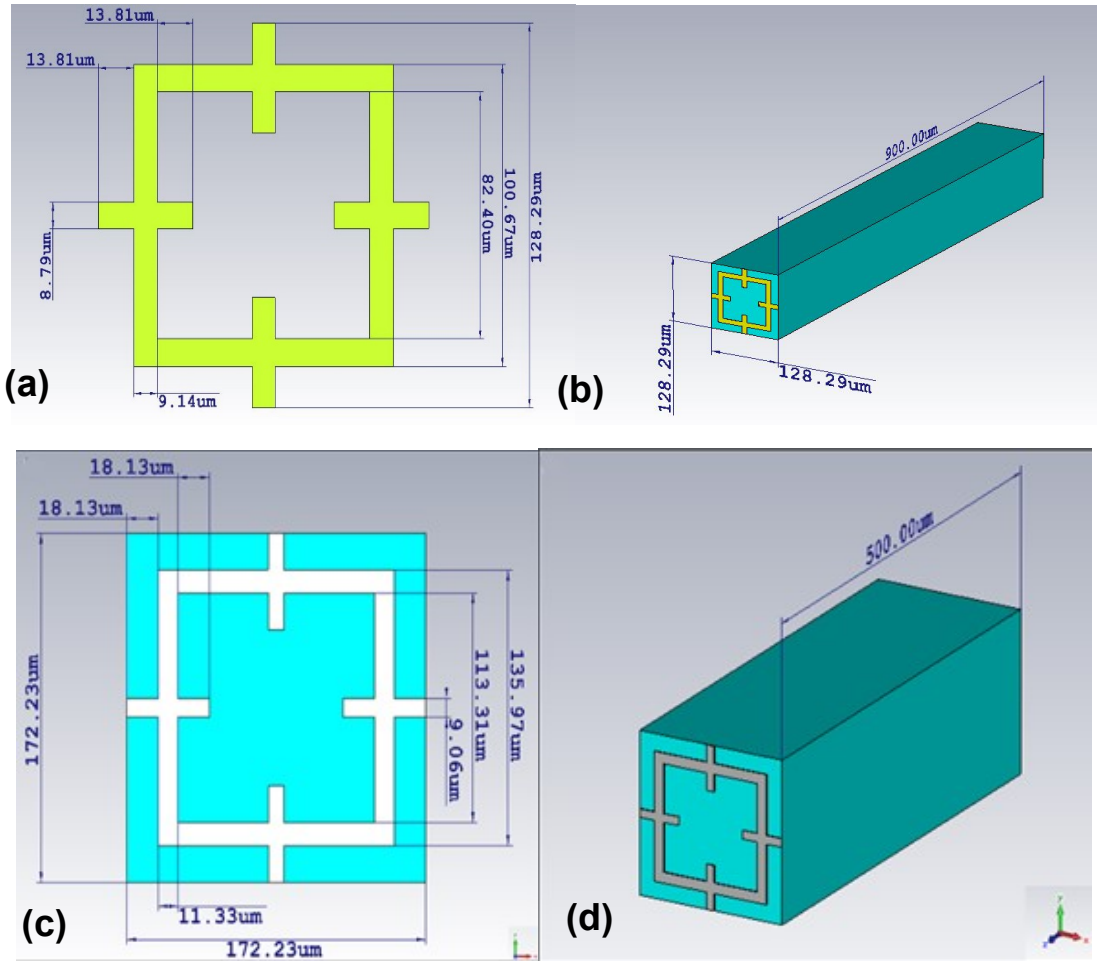

Figure 6.1. (a), (b) Front and perspective view of gold fourcross filter design with the unit cell dimensions; the width of the unit cell (W) was 128.29 μm, the length of the square-loop (L) was 100.67 μm, and the width of the strip line (M) was 8.79 μm. (Source: Demirhan et al., 2017)

A fourcross rectangular resonator which constitutes the structure of the metamaterial, has a rectangular shape where strip lines are located at the sides of the ring on a dielectric substrate (Figure 6.1(a), (c)). The proposed design has not split rings or apparent capacitance elements, this is the combination of square ring with quadruple strips. In order to suggest the resonance behavior of the metamaterial design of the metamaterial structures, generally LC equivalent circuit model can be utilized. The equivalent circuit of the proposed design presented in a simple pattern is given in Figure 6.2. In the disposed structure, the inner gap between the strips behave as capacitor where as the metallic parts operate as inductors. In addition, C represents the capacitance formed by the gap between the mutual strips.

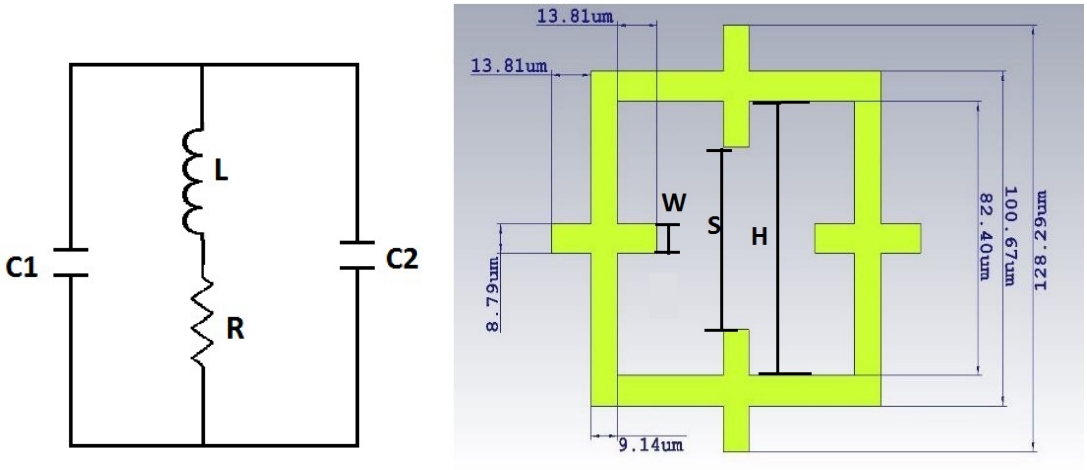

Figure 6.2. Equivalent LC circuit diagram of the designed metamaterial fourcross filter structure. (Source: Demirhan et al., 2017)

Using the parallel plate capacitance formula the total capacitance is given by (Brorson et al., 1996):

$C_1 = KW\varepsilon_0 \frac{2}{\pi} \ln \frac{H}{S}$ (1)

$C_2 = KW\varepsilon_0 \frac{\varepsilon_s - 1}{\frac{s}{h_s}}$ (2)

$C = C_1 + C_2$ (3)

where $K = n\frac{\omega}{c}$, ε_o is the free space permittivity, ε_s represents the dielectric constant of the substrate is the thickness of the substrate, the values and the placement of the symbols used in the equations 1-3 (H,W,S) is given in the Figure 2(b).

With the help of the formula (Vendik et al., 1998)

$$L=\frac{\mu_0 l}{2\pi}\left[\ln\left(\frac{2l}{b}\right)+\frac{l}{2}+\frac{b}{3l}-\frac{b^2}{24l^2}\right] \quad (4)$$

total inductance can be calculated,where the length and the width of the metallic strips are given by the symbols l and b respectively.

The equations 1-4 are used to calculate the values for K, C_1, C_2, L and are given as follows:

$$K=105.19$$

$$C_1=1.94\text{x}10^{-15}\text{F}$$

$$C_2=1.59\text{x}10^{-18}\text{ F}$$

$$L=1.6\text{x}10^{-11}\text{ H}$$

The resonance frequency depends on the total capacitance and the total inductance of the circuit. Using the relation:

$$f_0=\frac{1}{2\pi}\sqrt{\frac{1}{L(C1+C2)}} \quad (5)$$

the resonance frequency is calculated as

f_0=0.90 THz which is in very good agreement with the experimentally measured resonance value 0.92 THz.

Since the observed resonance occurs in the low frequency THz range that is accessible with the small energy gap observed in high-T_c superconducting materials, in the design of the fourcross resonator this fact that is taken into account. We have made use of CST Microwave Studio software frequency domain solvers for the investigation of the transmission profile in order to supply the most appropriate design. There after the devices are patterned on the chosen dielectric substrates where THz Time Domain Spectroscopy (THz-TDS) technique is employed for the measurement process. At the beginning, in order to perform the simulations 130 nm thick patterned gold layer and 80 nm thick patterned YBCO layer deposited on 900 μm thick fused silica and 500 μm thick

sapphire substrates are separately used. These substrates exhibit very small loss at THz frequencies and due to this property they are frequently used in the fabrication of filter structures. For the simulations, the electrical permittivity values are extracted by THz-TDS measurements of the fused silica and sapphire substrates in the THz region. For fused silica the electrical permittivity value is ε_r=3.98 and loss tangent value is tan δ=0.05.On the other hand, for sapphire these values are ε_r=9.6 and tan δ=0.05. The following mesh parameters are used in the design of gold fourcross filters ; the width of the unit cell (W) was 128.29 μm, the length of the square-loop (L) was 100.67 μm, and the width of the strip line (M) was 8.79 μm as shown in Figures 6.1.(a) and 6.1.(c).

In Figure 6.3., the numerical results for terahertz wave transmittance of the gold metamaterial filter on 900 μm fused silica are presented.In the figure, the primary simulated results for the band-stop filter design yield the terahertz wave minimum transmittance peak at 0.92 THz. It is feasible to tune YBCO fourcross by altering the temperature in contradiction to gold fourcross filters.

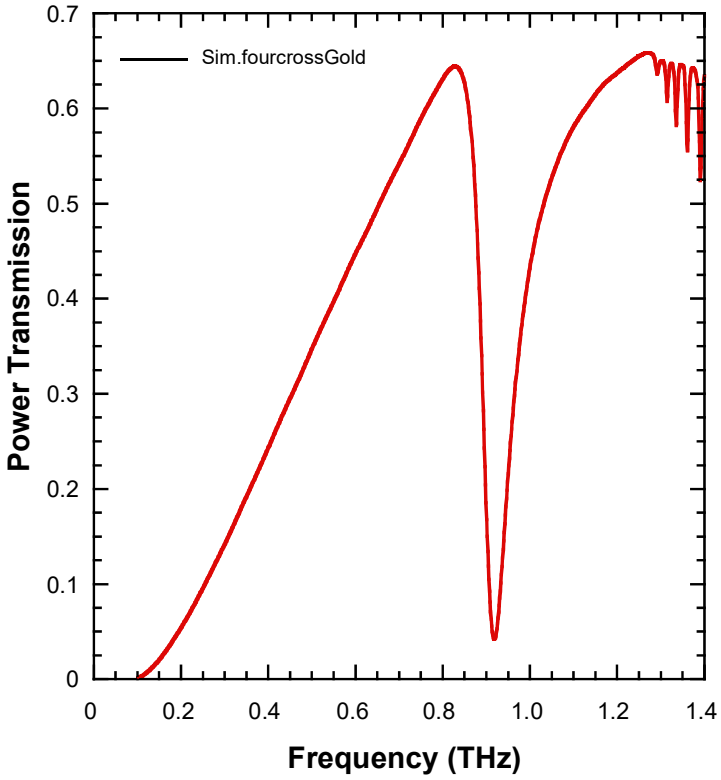

Figure 6.3.The simulated transmission spectrum of gold fourcross filters with designed parameters (solid line). (Source: Demirhan et al., 2017)

Simulations are accomplished at temperatures above and well below T_c with the purpose of verifying the measurements and investigating the temperature-dependent resonance behavior.

The tunable characteristics of THz transmission primarily initiates from the temperature-dependent conductivity in the superconductor material. Using the two-fluid model, the variation in the density of superconducting and normal carriers contributes to the change in the conductivity of the material (Vendik et al., 1998). Increasing the temperature of the superconductor leads to a decrease in the density of superconducting Cooper pairs in comparison to the normal conduction electron population which occurs up to state where the Cooper pair density goes to zero at T_c governing the conductivity of the superconductor. Taking into account the two-fluid model and considering YBCO the normal state carriers make contribution to the real part of the conductivity σ_r since their motion is ruled by the Drude model. However, the superconducting carriers, which obey the London Equation govern the imaginary part σ_i and thus the conductivity of the superconducting carriers is given by the relation $\sigma_i = i(n_s e^2)/(m^* w)$, where n_S is the Cooper pair carrier density, e is the charge of carriers, m^* is the effective carrier mass, and ω is the frequency of operation (Brorson et al., 1996). It is vital to point out that the conductivity emerging from the Cooper pairs is purely imaginary and accordingly the resistivity of the YBCO below T_c is also almost imaginary, and this reality brings about an inductor type behavior under the applied THz field. In the THz regime, it is a well-established reality that, the absolute value of the imaginary conductivity is three orders of magnitude less than the real part and consequently at temperatures higher than T_c the real part of conductivity is superior (Singh et al., 2013). Moreover, at several kelvins under T_c, the imaginary conductivity value increases instantly with decreasing temperatures and then the total conductivity is governed by σ_i.Considering this model the complex conductivity of the superconductor material for different temperature values, is calculated as a function of frequency where the equations given below are used. The surface impedance of the superconducting thin film is obtained by utilizing the calculated conductivity values and thickness of the metamaterial and supplied to the simulation program in order to simulate the transmission of the THz waves through the fourcross YBCO filters. In accordance with the two-fluid model (Vendik et al., 1998), the real and imaginary parts of the conductivity are given by,

(6)

$$\sigma_{re} = \frac{ne^2}{m^*}\frac{f_n(T)\tau}{1 + \omega^2\tau^2} = \frac{ne^2\varepsilon_0}{m^*\varepsilon_0}\frac{f_n(T)\tau}{1 + \omega^2\tau^2} = \omega_p^2\varepsilon_0\frac{f_n(T)\tau}{1 + \omega^2\tau^2}$$

(7)

$$\sigma_{im} = \frac{ne^2}{m^*}\left[\frac{f_n(T)\omega\tau^2}{1 + \omega^2\tau^2}\frac{f_s(T)}{\omega}\right] = \frac{ne^2\varepsilon_0}{m^*\varepsilon_0}\left[\frac{f_n(T)\omega\tau^2}{1 + \omega^2\tau^2}\frac{f_s(T)}{\omega}\right] = \omega_p^2\varepsilon_0\left[\frac{f_n(T)\omega\tau^2}{1 + \omega^2\tau^2}\frac{f_s(T)}{\omega}\right]$$

where n is the carrier density, is the carrier effective mass, and is the quasiparticle relaxation time. The ratio of normal to superconducting carriers is,

(8)

$$f_n(T) + f_s(T) = 1$$

where f_n and f_s are fractions of normal (quasiparticle) and superconducting (superfluid) carriers. The inverse relaxation time is given by,

(9)

$$\frac{1}{\tau(t)} = \frac{1}{\tau(1)}\frac{t}{1 + \alpha(t^{1-\gamma} - t)}$$

where t is the ratio of the temperatures which is defined by,

(10)

$$t = \frac{T}{T_c}$$

and α is an exponent in addition γ is an empirical parameter. With the help of these relations the conductivity and surface impedance of the patterned films are written as,

(11)

$$\sigma = \sigma_{re} + i\sigma_{im}$$

(12)

$$Z_s = R_s + iX_s = \sqrt{\frac{i\omega\mu_0}{\sigma}}\coth\left(d\sqrt{i\omega\mu_0\sigma}\right)$$

Optimized design parameters of YBCO fourcross filters are as follows; the width of the unit cell (W) was 172.23 μm, the length of the square-loop (L) was 135.97 μm, and the width of the strip line (M) was 9.06 μm. After the simulations obtained results are given in Figure 6.4.

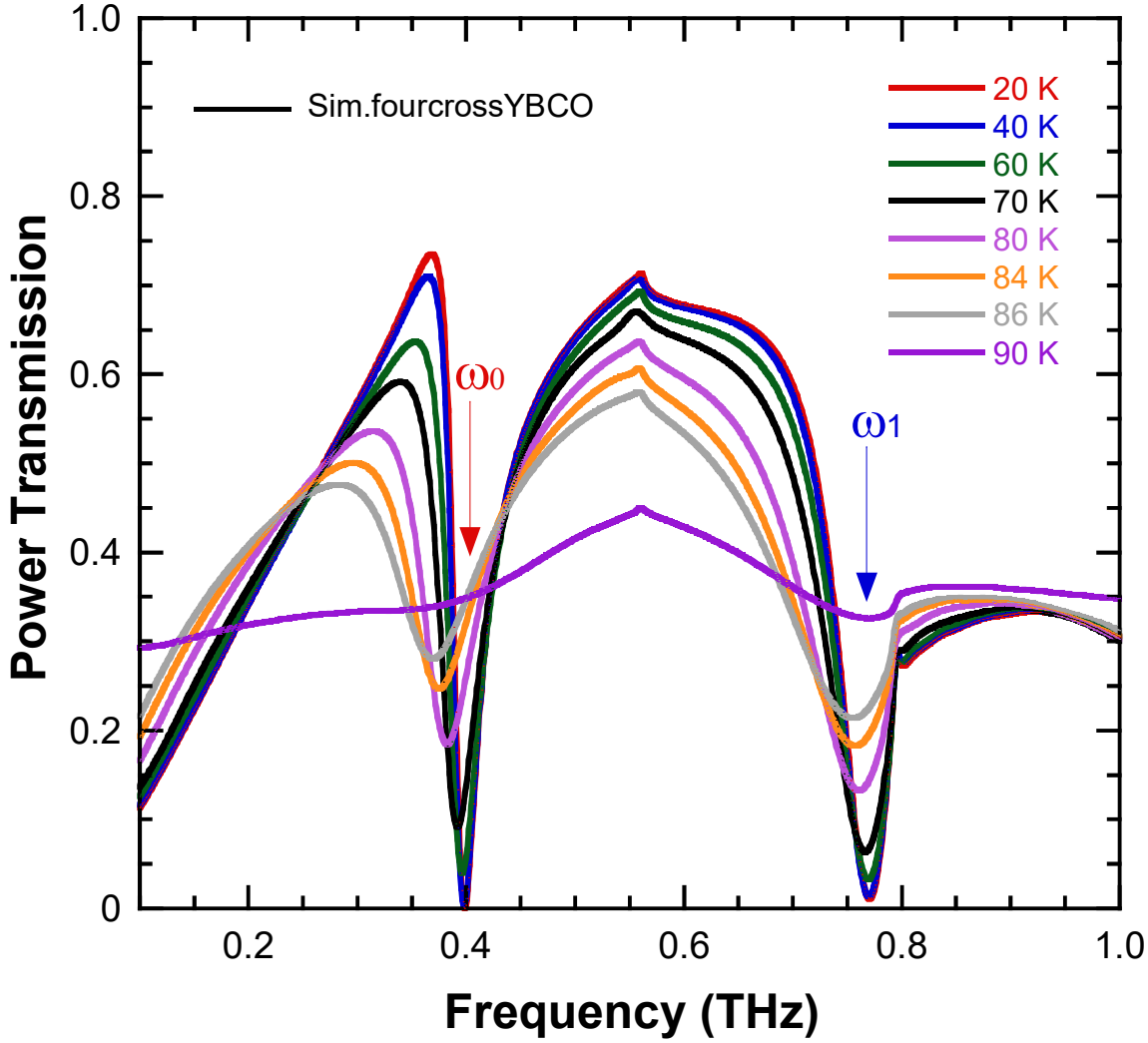

Figure 6.4.The simulated transmission spectrum of YBCO fourcross filters with designed parameters. (Source: Demirhan et al., 2017)

The simulations demonstrate that; at temperatures 20 and 40 K, the resonances reduced to zero transmission. Utilizing the identified mesh dimensions, with the help of the simulated YBCO fourcross filter design a stop band at both ω_0 (0.412 THz) and ω_1 (0.765 THz) for 20 K is created. At 40 K, it was observed that these resonances were

shifted to ω_0 (0.410 THz) and ω_1 (0.760 THz), individually. Moreover, at 60 K a resonance shift to ω_0 (0.390 THz) and ω_0 (0.734 THz) is also observed.

6.3. Fabrication and Measurements

In the case of gold metamaterial samples, a gold metal film with a thickness of 230 nm is deposited by dc magnetron sputtering system taking into account the optimal conditions. We have made use of a commercially accessible 80 nm thick YBCO film grown on sapphire substrates for the superconducting samples (YBCO film is deposited by ceraco ceramic coating GmbH). Using closed cycle He cryostat system, the transition temperature of the YBCO films which were oriented with the *ab* plane parallel to the surface, was measured to be $T_c \cong 90$ K. In the the microfabrication of the metamaterial filters, traditional e-beam lithography, and ion beam etching techniques were adopted. E-beam lithography is a more precise technique when compared to customary optical lithography. In UV lithography process, different imperfections could appear as irregularity in shape rounding etc. It has been established that these the structural variations will influence the spectral properties of the THz filters (Melo et al.,2012). The optical photographs of the cross-shaped filters fabricated from both Au and YBCO thin films are presented in Figure 6.5. It is observed that nearly perfect structures are achieved.

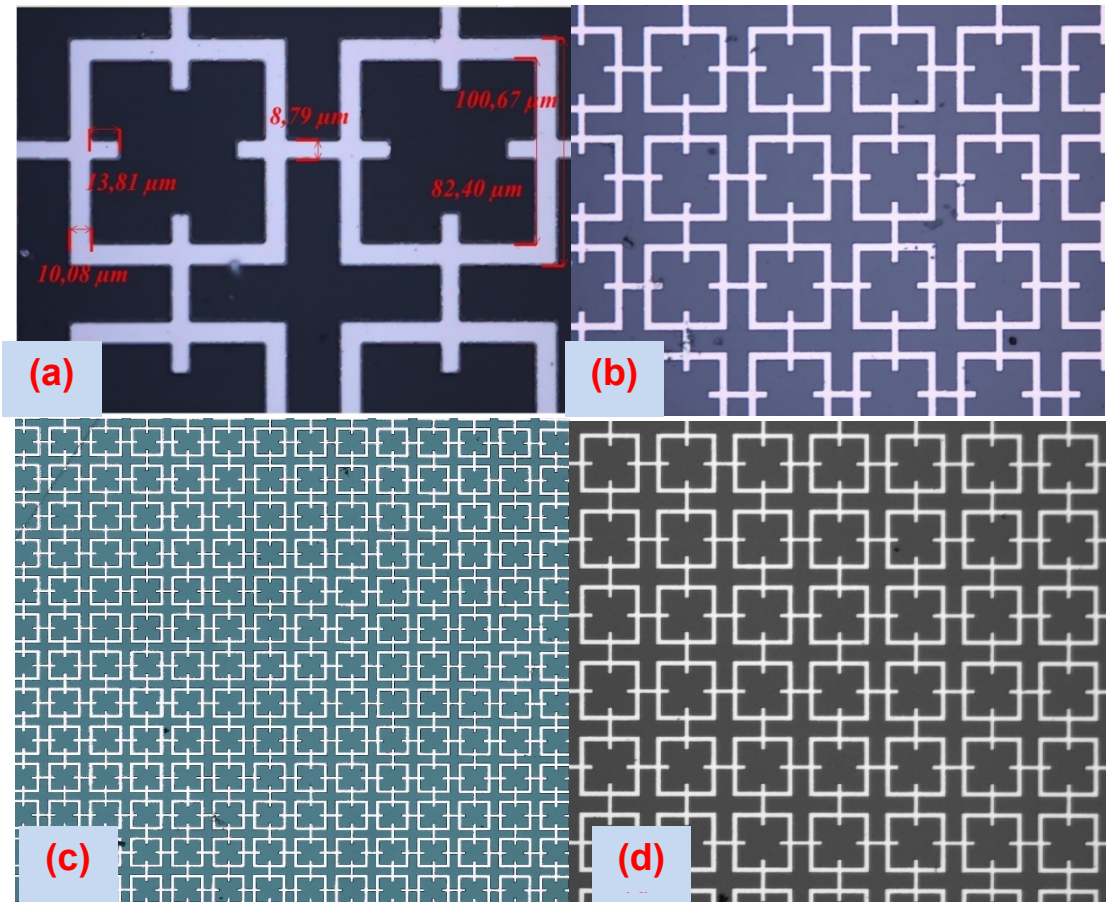

Figure 6.5. (a), Optical microscope images of fabricated gold fourcross filters given with measured dimensions. (b), (c), (d) Optical microscope images of fabricated gold and YBCO fourcross filters which is taken with different magnifications. (Source: Demirhan et al., 2017)

In analyzing the transmission profile of the fourcross filters we have introduced a home built THz–TDS system which is driven by a Ti:Al_2O_3 mode-lock laser. Using a beam splitter, the incoming beam is separated into the generation arm and detection arm of the spectrometer. A s-polarized terahertz beam is generated in the first arm (the generation arm) where a multi-dipole photoconductive antenna is utilized. In order to guide the produced THz within the system, inside the antenna two off-axis parabolic mirrors and two TPX^{TM} polymethylpentene (PMP) lenses are used. On the other hand, in the detection arm for the measurement of THz pulse, electro-optic detection method through a balanced photodiode is established. In the data collection, by making use of a PC and data acquisition software we supplied a lock-in amplifier with the purpose of utilizing phase-sensitive detection.The frequency data is obtained with 40 GHz resolution after applying a Fourier transform to the time-domain data. In the characterization of

uperconducting patterned sample, a closed cycle helium cryostat that was installed inside the terahertz time domain spectroscopy system has been used. The componenets of the cooling system are Sumitomo CH-204SFF coldhead, Sumitomo HC-4A compressor and Vacuubrand RZ 14 vacuum pump. Samples were mounted onto sample holder at the end of the cold head. By two high quality quartz windows the THz radiation is focused through the samples.

6.4. Results and Discussion

In Figure 6.6. on the same plot, for two different gold fourcross samples namely,Fourcross(Au)01 and Fourcross(Au)02, the transmission spectra and the simulation results are demonstrated. It is observed from the graph that; the measured electromagnetic properties of the metamaterials are in agreement with the simulation results. The simulation results indicate that for his structure the resonance frequency has the value 0.92 THz.

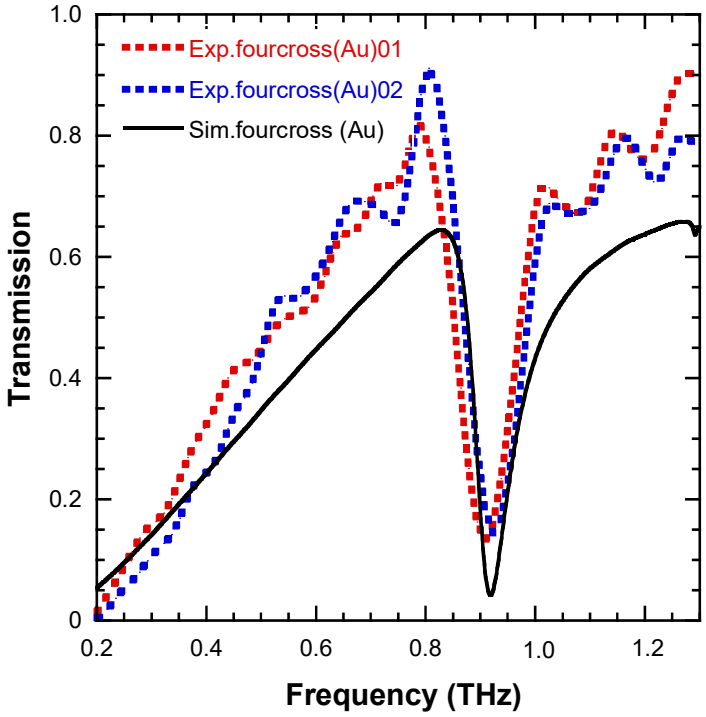

Figure 6.6. THz time-domain measurements of two identical gold fourcross filters (fourcross(Au)01-dashed red line- and Fourcross(Au)02-dashed blue line), plotted with simulation results(solid black line) on the same graph.
(Source: Demirhan et al., 2017)

THz-TDS measurement which is presented in the figure, reveals that the resonance occurs at 0.9 THz for sample 1 whereas at 0.92 for sample 2. The metamaterial structure comprising from rectangular resonator displays bandstop characteristics which is an expected conclusion of numerical analysis. The terahertz transmission of unpatterned single layer 80 nm thick YBCO film at 20, 40, 60, 65, 70, 75, 80, 85, 90, 95, 100, 120 and 298 K is presented in Figure 6.7. (a).

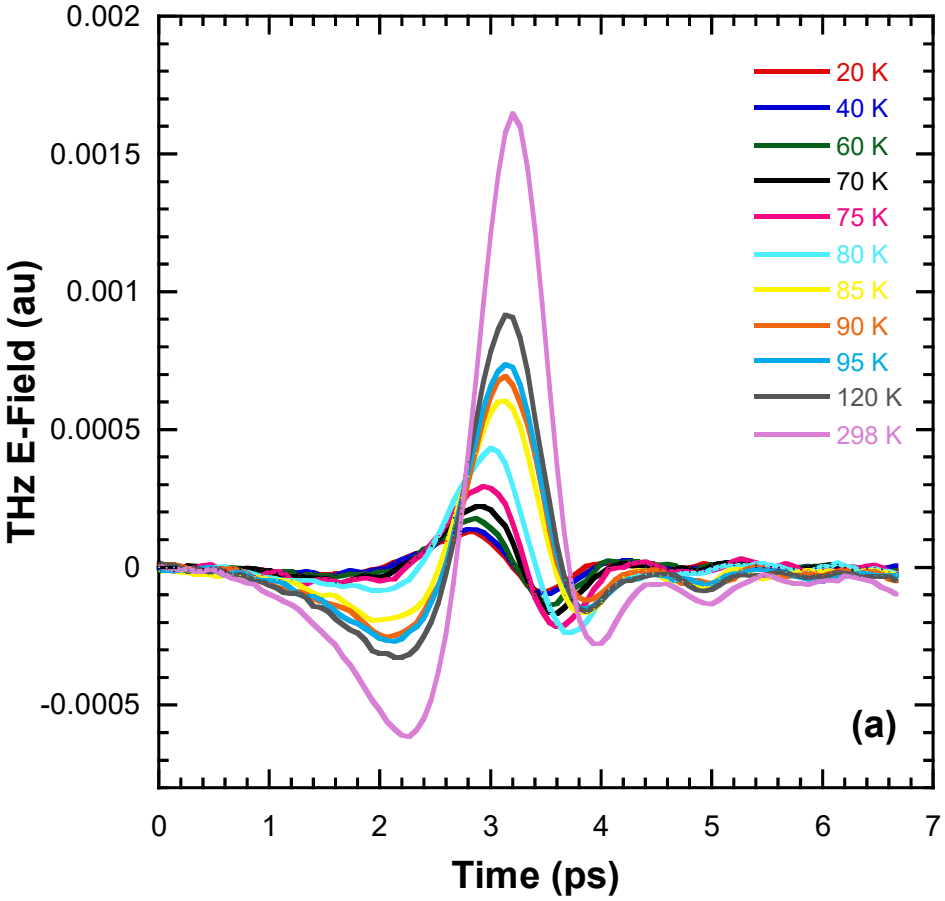

Figure 6.7. (a) The THz transmission of unpatterned 80 nm thick YBCO film at 20, 40, 60, 65, 70, 75, 80, 85, 90, 95, 100, 120 and 298 K.

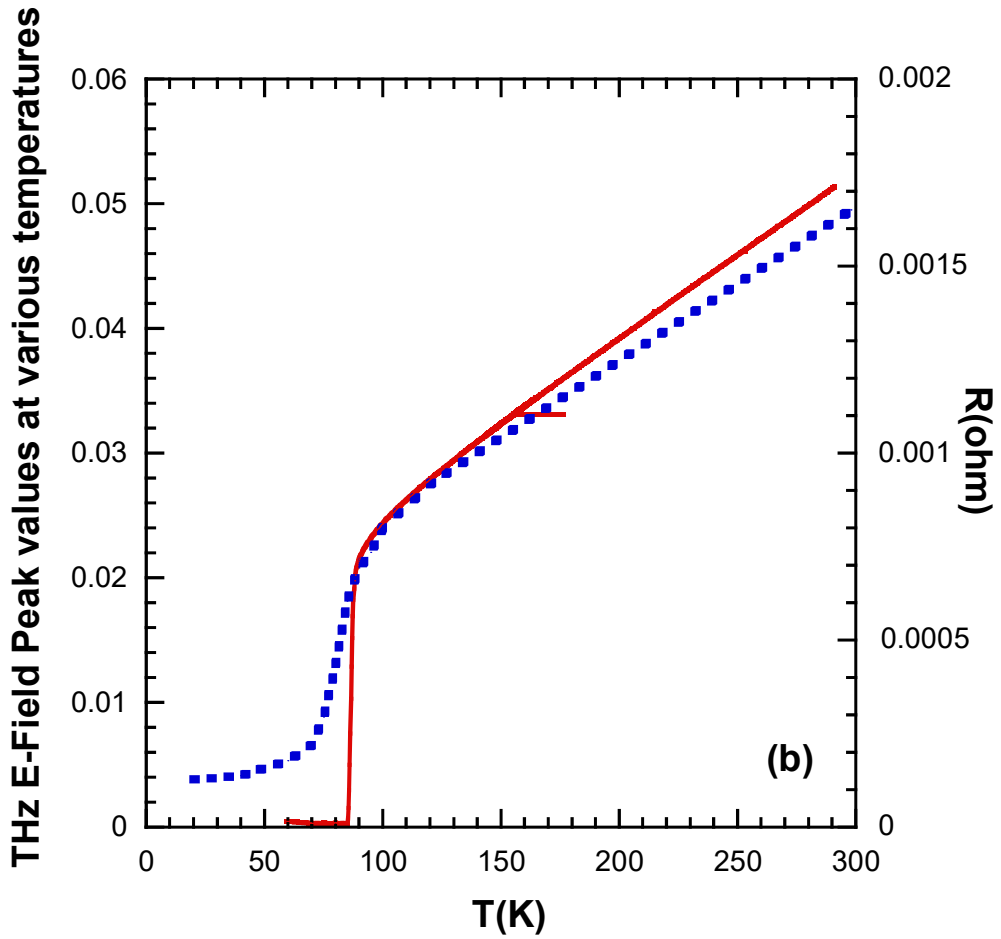

Figure 6.7. (b) The THz E-field peak values versus temperature curve is plotted in order to determine the critical temperature of the superconducting YBCO film (blue curve). R-T measurement of the film is also plotted on the same graph (red curve). (Source: Demirhan et al., 2017)

Under the critical temperature YBCO layer exhibits metallic characteristics and the transmitted signal power is very low. With the purpose of finding out the critical temperature of the superconducting YBCO film, the values of THz E-field with respect to temperature are plotted. In Figure 6.7.(b) the plotted graph is nearly the same to a superconducting phase transition curve received by the R-T measurement of the film and this curve is presented together with the plotted curve. It is understood from the above mentioned graphs that the critical temperature of the sample is nearly 90 K. In Figure 6.8. for different values of the temperature, the transmission amplitude spectra of the fabricated YBCO metamaterial filter structure are given.

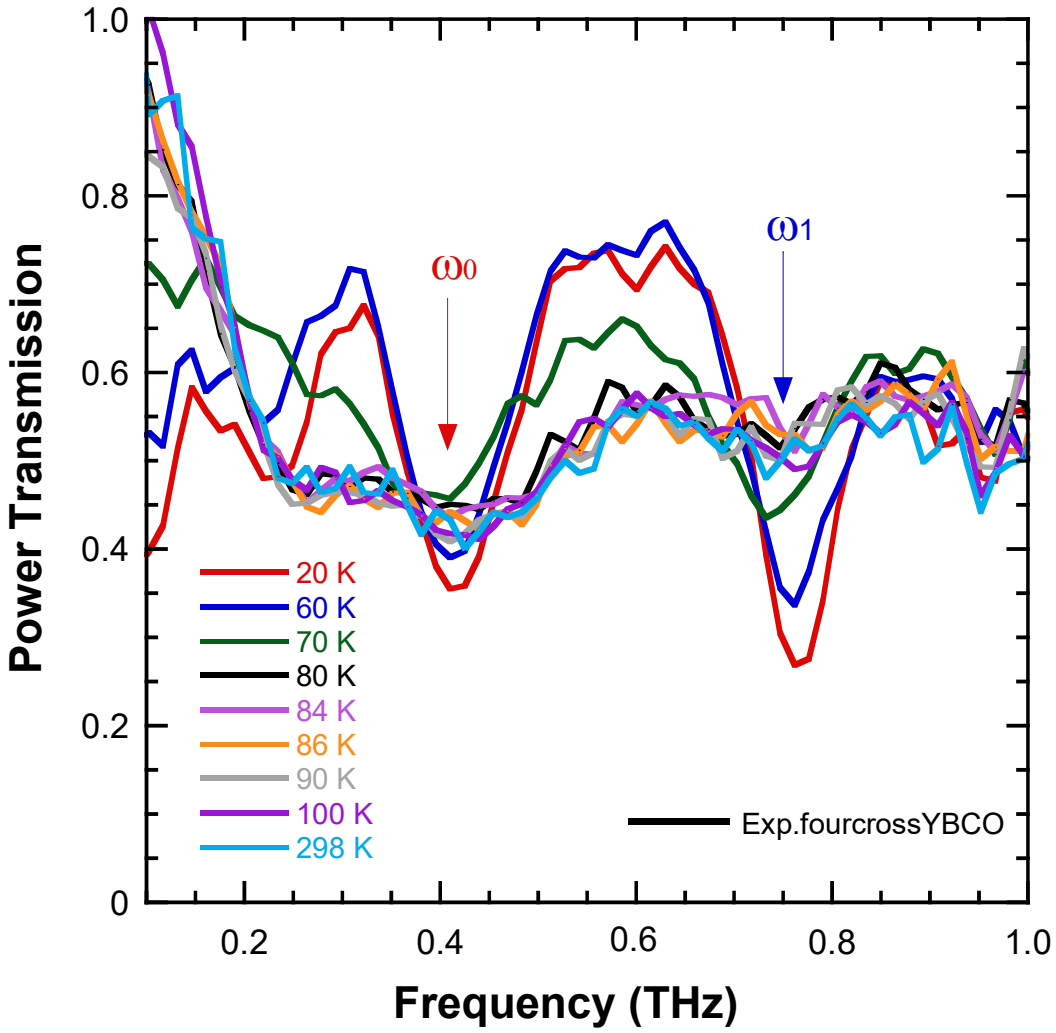

Figure 6.8. THz time-domain measurement of YBCO fourcross filter taken from 298 to 20 K. (Demirhan et al., 2017)

In the graph, the metamaterial transmission spectra is presented where two resonance peaks at ω_0 (0.4 THz) and ω_1 (0.75 THz) are recognized. The sharp THz transmission dip ω_1 with a minimal transmission amplitude of 0.05 at ω_0 (0.61 THz) indicates powerful resonances observed at temperatures below T_c, namely, 20 K which is displayed by the patterned structure.

In the figure, it is observed that; a decrease in temperature lesds to an increase in resonance strength and also a resonance shift to higher frequencies. Accompanying the increase of temperature (from 20 K up to T_c and the room temperature) resonance frequency is blue-shifted and a decrease in resonance strength as a broadening and

reduction in amplitude of the transmission dip is observed. In Figure 6.9.,_THz transmission measurement together with the simulation result of YBCO fourcross filter at 20 K, which is much lower than T_c, are presented on the same plotted graph.

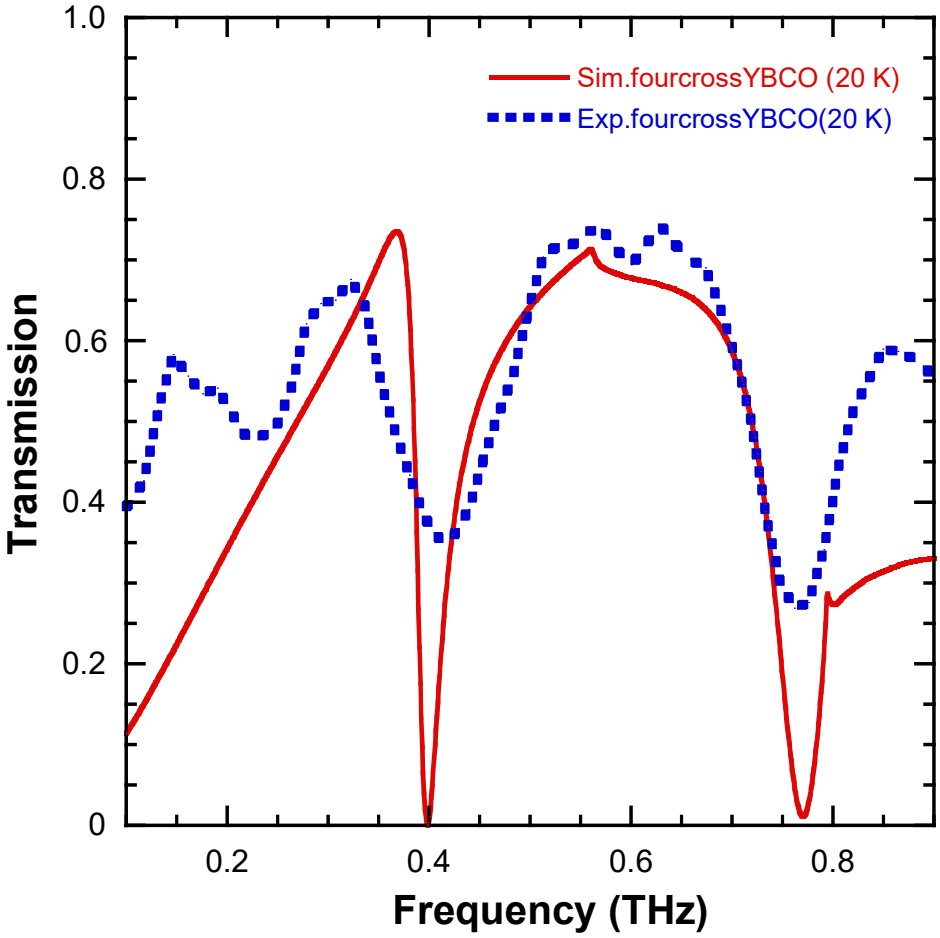

Figure 6.9.THz time-domain measurement of YBCO fourcross filter at 20 K, plotted with simulation result on the same graph. (Demirhan et al., 2017)

In comparison to other temperatures, the metamaterial filter reveals a strong resonance ω_1 at 20 K. After an increase in temperature and when reaching towards T_c, a redshift of the resonance frequency ω_1 (7%) is observed. The THz transmission amplitude of the band stop filters varies from 26 % at 20 K to 53 % at 90 K, displaying about a 51 % change in the amplitude for the ω_1. When compared to the YBCO metamaterials, considering the changes in temperature, the resonance strength and frequency have very small tunability in normal conducting metal films. In a recent work, it is verified that when the metamaterials are produced from thinner YBCO

superconducting films, their resonance frequency will have a low value which leads to more efficient resonance switching and frequency tuning.

CHAPTER 7

CONCLUSION

Terahertz (THz) radiation is a part of the electromagnetic spectrum lying between microwaves and the infrared. This region covers frequencies ranging from 0.3–10 THz and wavelengths from 1 mm to 0.03 mm. Organizations involved in military and defense are requesting the development of many technologies such as hand held THz radar systems that work in this frequency range to remotely detect the presence of explosive materials, poison gases, ceramic weapons, and biological warfare agents like viruses and bacteria. In addition, the medical community has shown that THz waves can detect the presence of cancer, viruses, bacteria, and other diseases instantly without surgery, biopsies, or other expensive procedures making this an ever more important area for further research and development. Together with a great variety of feasible applications from pharmaceuticals to agricultural research, these fields are supplying the requirement to develop compact and tunable coherent THz devices. Since bulk materials typically do not exhibit a strong electromagnetic response in the frequency range between 0.1 and 10 THz, this region is usually called the THz gap due to the difficulty in developing devices which can interact, generate or detect radiation. There are prominent attempts trying to fill this vacancy in the spectrum. Metamaterials (MMs) have electromagnetic properties which could not be attained by their natural bulk material counterparts, they can be designed with a specific functionality for THz applications and thus have a important role in the fabrication of artificial optical components. This field has seen a notable progress in recent years where studies have led to the development of electromagnetic MMs which exhibit novel properties such as magnetic response at terahertz and optical frequencies, negative index of refraction, and huge chirality. The emergence of THz MMs has given rise to electromagnetic properties and functionality that can not be attained by already existing natural materials permitting a whole new family of MM based devices namely, electrically small resonators, compact high selective THz filters, superlenses, cloaks, chiral devices, electromagnetically induced transparency applications and modulators. Consequently, the theoretical and experimental study of THz MMs has attracted great attention. In contrast to normal conducting metals, electromagnetic properties possessed by superconductors can be utilized for the purpose of producing almost ideal and novel

metamaterial structures. If metallic structures are replaced by superconducting structures losses can be greatly reduced. The complex conductivity of superconductors intrinsically depends on the applied magnetic field and temperature in comparison to metals. This allows the possibility to directly control the conductivity of the superconducting element without inserting additional elements i.e. an active metamaterial structure. Moreover, superconductors show superior conductivity at low temperatures and have the potential to integrate elements exhibiting quantum behaviour. In these materials, values of the surface resistance at microwave frequencies are also small. The unique properties of superconducting materials allow them to be utilized in a number of ways for THz device applications. Momentarily, Josephson based metamaterials propose a lot of important and attractive opportunities for novel metamaterial structures. The nonlinear response of these materials can allow for parametric amplification of photons and also reduction of losses.

In this thesis, both normal conducting and superconducting metamaterial filters were designed, numerical analysis was performed by CST microwave studio program and characterization was done in terahertz region using FTIR and Terahertz Time Domain Spectroscopy systems. Filters were designed by using uv-lithography and e-beam lithography, ion beam etching methods using copper, indium tin oxide, titanium, gold and high temperature superconducting YBCO coated films on fused silica and sapphire substrates.

In the first part of this study, Ti, ITO and Cu bandpass filters in the THz frequency range are presented. Unsurprisingly, the transmittance of the bandpass filters increases with increasing conductivity. These characterization methods can be employed in the design of compact, tunable, THz filters since the acquired experimental data are in agreement with the simulations and observed transmission properties. An insertion loss is observed in the measurements which arises from the finite conductivity of the metal films and some loss in the substrate. Owing to the existence of a 350 GHz atmospheric transmission window, ITO coated filter structures with 330 GHz resonant frequency can provide applications in future wireless THz communication. In the removal of unwanted transmitted signals in specified frequency bands metal mesh filters can be utilized which also reveals future applications in the field of THz diagnostics and THz communications.

Thin film deposition studies were accomplished (with the BSCCO target that we prepared and a commercially available target) by dc and rf magnetic sputtering systems for metamaterial filter fabrication. Structural and electrical characterizations of the coated

films were made. As a result of the elemental analysis, the Bi2212 phase was obtained and in the resistance temperature measurements made at 300 K-20 K, the films were superconducting and the 2212 phase specific 80-90 K superconducting transition was observed. However, no zero resistance was observed during the superconducting transition. This is because the superconducting material is not in a single phase and the peaks of phases 2201 and 2223 obtained as a result of XRD analysis are the resultant ones. So, we can not use the BSCCO films that were deposited could not be used in metamaterial filter fabrication.

In addition to the metal mesh filters, it is demonstrated that, a unique metamaterial based on a fourcross patterned above metallic gold films and thin high temperature superconducting YBCO films can be utilized as an active band-stop filter in the THz frequency region. The proposed fourcross shaped rectangular filter structure consists of periodic metallic rings where strip lines are located at the sides of the ring. Fourcross metamaterial filters are fabricated by using e-beam lithography and ion beam etching techniques. Terahertz time-domain spectroscopy measurements validated the design predictions for both the center frequencies and bandwidths of the resonances due to the fourcross structures. The resonance switching of the transmission spectra was investigated by lowering the temperature below the critical transition temperature. This resonance switching effect is not observed in filters made up of metals. The measured electromagnetic properties of the metamaterials are consistent with that of the simulation results. Resonance frequency of this structure is at 0.92 THz according to the simulation results. Sample 1 has a resonance at 0.9 THz, sample 2 has a resonance at 0.92 THz according to THzTDS measurement. As expected from numerical analysis, the metamaterial structure consisting of rectangular resonator exhibits bandstop characteristics. The THz transmission amplitude spectra for the fabricated YBCO metamaterial filter structure at various temperatures are presented. In the metamaterial transmission spectra given by the graph, two resonance peaks are observed at ω_0 (0.4 THz) and ω_1 (0.75 THz). The patterned structure exhibits powerful resonances observed at temperatures below T_c, namely, 20 K which is implied by the sharp THz transmission dip ω_1 with a minimal transmission amplitude of 0.05 at ω_0 (0.61 THz). It is seen that; with a decrease in temperature one observes increase in resonance strength and also a resonance shift to higher frequencies. With the increase of temperature (from 20 K up to T_c and the room temperature) resonance frequenc is blue-shifted and it is observed that

the resonance strength decreases as a broadening and reduction in amplitude of the transmission dip. THz transmission measurement and simulation result of YBCO fourcross filter at 20 K, which is much lower than T_c, is shown. The metamaterial filter exhibits a strong resonance ω_1 at 20 K when compared to other temperatures. A redshift of the resonance frequency ω_1 (7%) is observed as the temperature increases and approaches T_c. The THz transmission amplitude of the band stop filters changes from 26 % at 20 K to 53% at 90 K, exhibiting about a 51% change in the amplitude for the ω_1.

In YBCO fourcross filters, resonance switching and frequency shifting with respect to temperature are observed. It has been demonstrated by the simulated results and THz-TDS measurements that when the YBCO fourcross filters are used under the critical temperature, a noteworthy spectral tunability of the resonance can be realized. Aforementioned investigations evidently confirm the feasibility of temperature switched, low loss, THz active YBCO metamaterial basis devices. The THz metamaterial filters that are produced by using the high temperature superconductors which are incorporated with low cost cooling technology, can be utilized to construct and improve THz sources and detectors.

REFERENCES

Abrikosov A. A., On the Magnetic Properties of Superconductors of the Second Group. *Soviet Physics JETP* 1957, 5:1174

Ade Peter A.R., Pisano G., Tucker C., Weaver, S.: A Review of Metal Mesh Filters. *Proc. SPIE* 6275, 2006, 62750U1-U15

Akimitsu J., Yamazaki A., Sawa H. and Fujiki. H.,. Superconductivity in the Bi-Sr-Cu-O system. *Japanese Journal of Applied Physics,* 26, 1987, 2080.

Alaboz H., Demirhan Y., Yuce H., Aygun G., Ozyuzer L., Comparative study of annealing and gold dopant effect on DC sputtered vanadium oxide films for bolometer applications, *Opt. Quant. Electron*.,49, 2017,238.

Arnone D. D., Ciesla C. M., Coricha A., Egusa S., Pepper M., Chamberlain J. M., Bezant C., Clothier R. and Khammo N., Applications of terahertz (THz) tech-nology to medical imaging. Terahertz Spectroscopy and Applications II, ed. by J. M. Chamberlain, *Proceedings of SPIE*, 3828, 1999, 209–219

Bardeen J., Cooper L. N. and Schrieffer J. R., The Theory of Superconductivity, *Physical Review Letters* 108,1957, 1175

Bednorz J. G. and Müller K. A., Possible high-T_c superconductivity in the Ba-La-Cu-O system. *Zeitschrift Physics B*, 64, 1986, 189.

Brorson S D, Buhleier R, Trofimov I E, White J O, Ludwig C, Balakirev F F, Habermeier H-U and Kuhl J Electrodynamics of high-temperature superconductors investigated with coherent terahertz pulse spectroscop,y *J. Opt. Soc. Am. B.* 13-9, 1996, 1979

Chen H T, Padilla W J, Zide J M O, Gossard A C, Taylor A J, Averitt R D Active terahertz metamaterial devices, *Nature,* 444, 2006, 597-600

Chen H T, O'Hara J F, Azad A K, Taylor A J, Averitt R D, Shrekenhamer D, Padilla W J Experimental demonstration of frequency-agile terahertz metamaterials, *Nat. Photonics,* 2, 2008, 295–298

Chen H. T., Yang H., Singh R., O'Hara J. F., Azad A. K., Trugman S. A., Jia Q. X., Taylor A. J., Tuning the resonance in high-temperature superconducting terahertz metamaterials, *Phys. Rev. Lett.,* 105, 2010, 247402.

Demirhan Y., Saglam H., Turkoglu F., Alaboz H., Ozyuzer L., Miyakawa N., Kadowaki K. Area dependence and influence of crystal inhomogeneity on superconducting properties of Bi2212 mesa structures, *Vacuum*, 120, 2015, 89-94

Demirhan Y., Alaboz H., Ozyuzer L., Nebioglu M. A., Takan T., Altan H., Sabah C. Metal mesh filters based on Ti, ITO and Cu thin films for terahertz waves, *Opt*

Quant Electron, 48, 2016. 170.

Demirhan, Y., Alaboz, H., Nebioglu, M. Mulla, B., Akkaya, M., Altan, H., Sabah, C. Ozyuzer,, L. Fourcross shaped metamaterial filters fabricated from high temperature superconducting YBCO and Au thin films for terahertz waves, 2017. *Superconductor Science and Technology*, 30, 7

Du J., Hellicar A.D., Li L., Hanham S.M., Nikolic N., Macfarlane J.C. et al. Terahertz imaging using a high-Tc superconducting Josephson junction detector, *Superconductor Science and Technology*. 21, 2008, 125025

Ebbesen T. W., Lezec H. J., Ghaemi H. F., Thio T., Wolff P. A., Extraordinary optical transmission through subwavelength hole arrays, *Nature,* 391, 1998, 667-669

Ferguson B, Zhang X-C, Materials for terahertz science and technology, *Nature Mater.,* 1, 2006, 26–33

Fischer B., Hoffmann M., Helm H., Modjesch G. and Jepsen P. U. Chemical recognition in terahertz time-domain spectroscopy and imaging. *Semiconductor Science and Technology*, 20, 2005, S246–S253

Grady N K et al., Nonlinear high-temperature superconducting terahertz metamaterials *New Journal of Physics,* 15, 2013, 105016-12

Ginzburg V. L. and Landau L. D., On the theory of superconductivity, *Journal of Experimental and Theoretical Physics,* 20, 1950, 1064.

Glossner A, Zhang C, Kikuta S, Kawayama I, Murakami H, Muller P and Tonouchi M Cooper pair breakup in YBa2Cu3O7−under strong terahertz fields *arXiv*:1205, 2012, 1684v1

Guénon S, Grünzweig M, Gross B, Yuan J, Jiang Z, Zhong Y, Iishi A, Wu P, Hatano T, Koelle D, et al., Interaction of hot spots and THz waves in Bi2Sr2CaCu2O8 intrinsic Josephson junction stacks of various geometry, *Phys. Rev. B,* 82, 2010, 214506

Hazen R. M., Finger L. W., Angel R. J., Prewitt C. T., Ross N. L., Hadidiacos C. G., Heaney P.J., Veblen D.R., Shenh Z.Z., Ali A. El and Hermann A.M., 100 K superconducting phases in the Tl-Ca-Ba-Cu-O system, *Physical Review Letters* 60,1988,1657

Hsieh F. J., Wang W. C., Chang, C L., Full Extraction Methods to Retrieve Effective Refractive Index and Parameters of a Bianisotropic Metamaterial Based on Material Dispersion Models, *J. App. Phy.* 112, 2012, 064907

Hu Q., Richards P.L., Design analysis of a high Tc superconducting microbolometer, *Appl. Phys. Lett.,* 55, 1989, 2444-2446

Ma Y., Khalid A., Drysdale T. D., Cumming D. R. S., Direct fabrication of terahertz optical devices on low-absorption polymer substrates, *Optics Letters*, 34;10,

2009,1555–1557

Kadowaki K., Tsujimoto M., Yamaki K., Yamamoto T., Kashiwagi T., Minami H., Tachiki M., Klemm R. A., Evidence for a Dual-Source Mechanism of Terahertz Radiation from Rectangular Mesas of Single Crystalline Bi2Sr2CaCu2O8+δ Intrinsic Josephson Junctions, J. *Phys. Soc. Jpn*.,79, 2010, 023703

Kadowaki K, Yamaguchi H, Kawamata K, Yamamoto T, Minami H, Kakeya I, Welp U, Ozyuzer L, Koshelev A, Kurter C, Gray K E, Kwok W K. Direct observation of terahertz electromagnetic waves emitted from intrinsic Josephson junctions in single crystalline Bi2Sr2CaCu2O8+δ, *Physica C: Superconductivity,* 468 2008, 634-639

Kang L, Jin B. B., Liu X. Y., Jia X. Q., Chen J., Ji Z. M., Xu W. W., Wu P. H., Mi S. B., Pimenov A., Wu Y. J., and Wang B. G., Suppression of superconductivity in epitaxial NbN ultrathin films, *J. Appl. Phys.* 109(3), 2011, 033908

Kaufmann P., Marcon R., Marun A., et al., Selective spectral detection of continuum terahertz radiation. in Millimeter, Submillimeter, and Far-Infrared Detectors and Instrumentation for Astronomy, *Proceedings of SPIE, San Diego, Calif, USA, July* , 7741, 2010.

Kawayama I., Zhang C., Wang H. & Tonouchi M., Study on terahertz emission and optical/terahertz pulse responses with superconductors, *Supercond. Sci. Technol.,* 26, 2013, 093002

Kawase K., Terahertz imaging for drug detection & large scale integrated circuit inspection, *Optics & Photonics News,* 15, 2004, 34–39

Knobloch J, Padamsee H and Hays T RF Superconductivity for Accelerators, *New York: Wiley*, 1998

Koseoglu H., Turkoglu F., Demirhan Y., Ozyüzer L., The Fabrication of THz Emitting Mesas by Reactive Ion-Beam Etching of Superconducting Bi2212 with Multilayer Masks, *J. Supercond. Nov. Magn.,* 24, 2011, 1083.

Kimand D. H., Choi J. I., Design of amultiband frequency selective surface, *ETRI Journal,* 28;4, 2006, 506–508

Kleine-Ostmann T., Nagatsuma T., A review on terahertz communications research, *J. Infrared Millim. THz Waves,* 32, 2011, 143–171

Kleiner R., Steinmeyer F., Kunkel G., Müller P., Intrinsic Josephson effects in Bi2Sr2CaCu2O8 single crystals, *Phys. Rev. Lett.,* 68, 1992, 2394

Koseoglu H., Turkoglu F., Kurt M., Yaman M. D., Akca F., Aygun G., Ozyuzer L., Improvement of optical and electrical properties of ITO thin films by electro-annealing, *Vacuum*,120, 2015, 8-13

Kurter C., Tassin P., Zhuravel A. P., Zhang L., Koschny T., Ustinov A. V., Soukoulis C. M., Anlage S. M., Switching nonlinearity in a superconductor-enhanced metamaterial, *Applied Physics Letters,* 100, 2012, 121906

Linden S. Enkrich C., Wegener M., Zhou J., Koschny T., Soukoulis C. M., Magnetic response of metamaterials at 100 terahertz, *Science,* 306, 2004, 1351–1353

Maeda H., Tanaka T., Fukutomi M. and Asano T., A New high-Tc oxide superconductor without a rare earth element, *Japanese Journal of Applied Physics,* 27, 1988, L209.

Martin-Moreno L., Garcia-Vidal F. J., Lezec H. J., Pellerin K. M., Thio T., Pendry J. B., Ebbesen T. W., Theory of Extraordinary Optical Transmission through Subwavelength Hole Arrays, *Phys. Rev. Lett.,* 86;6, 2001,1114-1117

Melo A.M., Kornberg M.A., Kaufmann P. et al., Metal mesh resonant filters for terahertz frequencies, *Applied Optics,* 47, 2008, 6064–6069

Melo A. M., Angelo L. G., Piazzetta Maria H. O. , da Silva M. P. A., Cross-Shaped Terahertz Metal Mesh Filters: Historical Review and Results, *Advances in Optical Technologies,* 2012, 2012, 530512- 12

Nebioglu M., Takan T., Altan H., Demirhan Y., Alaboz H., Ozyuzer L., A., Sabah C. An indium tin oxide metasurface filter for terahertz applications: Design, fabrication, and characterization, *Modern Physics Letters B,* 31, 2017, 8, 1750074-2

Onnes H. K. Disappearance of the electrical resistance of mercury of Helium temperature. *Akad. Van Wetenschappen (Amsterdam)* 14,1911, 113

Orenstein J., Bokor J., Budiarto E., Corson J., Mallozzi R., Bozovic I. and Eckstein J. N., Nonlinear electrodynamics in cuprate superconductors, *Physica C,* 282–287, 1997, (Pt 1) 252–5

Ozyuzer L., Koshelev A. E., Kurter C., Gopalsami N., Li Q., Tachiki M., Kadowaki K., Tamamoto T., Minami H., Yamaguchi H., Tachiki T., Gray K. E., Kwok W. K. and Welp U., Emission of coherent THz radiation from superconductors, *Science* 318, 2007, 1291

Ozyuzer L., Simsek Y., Koseoglu H., Turkoglu F., Kurter C., Welp U., Koshelev A. E., Gray K. E., Kwok W. K., Yamamoto T., Kadowaki K., Koval Y., Wang H. B., and Müller P., Terahertz wave emission from intrinsic Josephson junctions in high-T_c superconductors, *Superconductor Science & Technology* 22,2009,114009

Padilla W. J.. Taylor A. J., Highstrete C., Lee M. and Averitt R. D., Dynamical Electric and Magnetic Metamaterial Response at Terahertz Frequencies, *Phys. Rev. Lett.,* 96, 2006. 107401

Park H.R., Park Y.M., Kim H.S., Kyoung J.S., Seo M.A., Park D.J., Ahn Y.H., Ahn K.J. ,

Kim D.S., Terahertz nanoresonators: Giant field enhancement and ultrabroadbandperformance, *Appl. Phys. Lett.* 96, 2010, 121106

Paul O., Beigang R., Rahm M., Highly selective terahertz bandpass filters based on trapped mode excitation, *Opt. Express*,17, 2009, 18590-1859

Pendry J. B., Holden A. J., Robbins D. J., Stewart W. J., Magnetism from conductors and enhanced nonlinear phenomena, *IEEE Trans. Microwave Theory Tech.,* 47, 1999, 2075-2084.

Pendry J. B., Negative Refraction Makes a Perfect Lens, *Phys. Rev. Lett.*,85, 20003699.

Pickwell E., Wallace., V. P. Biomedical applications of terahertz technology, *J. Phys. D.,* 39, 2006, R301–R310

Porterfield D., W., Hesler J. L., Densing R., Mueller E. R., Crowe T. W., Weikle II R. M., Resonant metal-mesh bandpass filters for the far infrared, *Applied Optics,* 33,1994, 25, 6046–6052

Rogalskii A. and Sizov F., Terahertz detectors and focal plane arrays, *Opto−Electronics Review*, 19, 2011, 346-404.

Romano P., Chen J. and Zasadzinski J. F., Josephson and Quasiparticle Tunneling in SIS Junctions Bi2Sr2CaCu2O8 and Bi2Sr2CuO6, Physica C, 295,1998.15

Ricci M. C., Anlage S. M., Single superconducting split-ring resonator electrodynamics, *Appl. Phys. Lett.,* 88, 2006, 264102.

Ricci M.C., Xu H., Prozorov R., Zhuravel A. P., Ustinov A. V. and Anlage S. M., Tunability of superconducting metamaterials, *IEEE Trans. Appl. Supercond*., 17 2007, 918–21

Rice J.P., Grossman E.N., Rudman D.A., Antenna- coupled high-T_c air- bridge microbolometers on silicon, Appl. Phys. Lett., 65, 1994, 773- 775

Sabah C. and Roskos H. G., Numerical and experimental investigation of fishnet-based metamaterial in a X-band waveguide, *Journal of Physics D: Applied Physics*, 44, 2011, 255101.

Savinov V., Fedotov V. A., Anlage S. M., Groot P. A. J., Zheludev N. I., Modulating sub-THz radiation with current in superconducting metamaterial, *Phys. Rev. Lett.,* 109, 2012, 243904

Semerci T., Demirhan Y., Miyakawa N., Ozyuzer L., Thin film like terahertz bolometric detector on Bi2212 single crystal, *Opt. Quant. Electron*., 48, 2016,340.

Shelby R.A., Smith D.R., Schultz S., *Science,* 292 (5514) ,2001, 77.

Shen N.-H., Kenanakis G., Kafesaki M., Katsarakis N., Economou E. N., and Soukoulis

C. M., *JOSA B,* 26, 12, 2009, B61-B67

Schilling A., Cantoni M., Guo J. D., and Ott H. R., Superconductivity above 130 K in the Hg-Ba-Ca-Cu-O System, *Nature,* 363,1993, 56.

Smith D. R., Pendry J. B., Wiltshire M. C. K., Metamaterials and Negative Refractive Index, *Science,* 305, 2004,788

Siegel P.H. Terahertz technology in biology and medicine, *IEEE Trans Microwave Theory Tech.,* 52,2004, 2438–2447

Singh R., Chowdhury D. R., Xiong J., Yang H., Azad A. K., Taylor A. J., Jia Q. X. and Chen H. T., Influence of film thickness in THz active metamaterial devices: A comparison between superconductor and metal split-ring resonators, *Applied Physics Letters,* 103, 2013, 061117

Singh R., Tian Z., Han J., Rockstuhl C., Gu J., and Zhang W., Cryogenic temperatures as a path toward high-Q terahertz metamaterials, *Appl. Phys. Lett.* 96(7), 2010,071114

Soukoulis C. M. and Wegener M. Materials science: Optical metamaterials--more bulky and less lossy, *Science,* 330, 2010,1633

Tarasov V.D., Gromov G.D. Bogomolov E.A. Otto L.S. Fabrication and characteristics of mesh bandpass filters, *Kuzmin, Instrum. Exp. Tech.,* 52, 2009, 74–78

Takan T., Keskin H., Altan H., Low-cost bandpass filter for terahertz applications, *Opt. Quant. Electron.,* 47, 2015,953–960

Talanov V. V., Mercaldo L. V., Anlage S. M. and Claassen J. H., Measurement of the absolute penetration depth and surface resistance of superconductors and normal metals with the variable spacing parallel plate resonator*, Rev. Sci. Instrum.,* 71, 2000, 2136–46

Tonouchi M., Cutting-edge terahertz technology, *Nature Photonics*, 97, 2007,105

Turkoglu F., Ozyuzer L., Koseoglu H., Demirhan Y., Preu S., Malzer S., Simsek Y., Wang H.B., Muller P., Emission of the THz waves from large area mesas of superconducting Bi2Sr2CaCu2O8+d by the injection of spin polarized current, *Physica C Superconductivity,* 491, 2013,7

Turkoglu F., Koseoglu, H., Demirhan Y., Ozyuzer L., Preu S., Malzer S., Simsek Y., Muller P., Yamamoto T., Kadowaki K., Interferometer measurements of terahertzwaves from Bi2Sr2CaCu2O8+d mesas.*Supercond.Sci.Technol.*25,2012, 125004

Vendik O. G., Vendik I. B. and Kaparkov D. I., Empirical model of the microwave properties of high-temperature superconductors, *IEEE Trans. Microw. Theory. Tech.,* 46, 5, 1998, 469–478

Voisiat B., Biciunas A., Kašalynas I., Raciukaitis G., Bandpass filters for THz spectral range fabricated by laser ablation, *Appl. Phys. A.,*104, 2011, 953–958

Wang H. B., Guénon S., Yuan J., Iishi A., Arisawa S., Hatano T., Yamashita T., Koelle D., and Kleiner R., Hot Spots and Waves in Bi2Sr2CaCu2O8 Intrinsic Josephson Junction Stacks-a Study by Low Temperature Scanning Laser Microscopy, *Phys. Rev. Lett*. 102, 2009, 017006

Wesche R., High Temperature Superconductor Materials, Properties, and Application. *Boston: Academic Publishers,* 1998.

Winnewiser, C., Lewer, F., Weinzier, J., Helm, H.: 1999.Transmission features of frequency selective surface compoments in the far infrared determined by terahertz time domain spectroscopy. Applied Optics 38;18

Wild J., Macl J., Sichova H., Bohacek P., Pracharova J., Janu Z., Civis S., and Kubat P., *Supercond. Sci. Technol.,* 11,1998, 1341–1343

Woodward R. M., Cole B.. Wallace V. P., Pye R. J, Arnone D., Linfield E. H. and Pepper M., Terahertz pulse imaging in reflection geometry of human skin cancer and skin tissue, *Phys. Med. Biol.* 47, 2002, 3853-3863

Wu M. K., Ashburn J. R., Torng C. J., Hor P. H., Meng R. L., Gao L., Huang Z. J., Wang Y. Q. and Chu C. W., Superconductivity at 93 K in a New Mixed-Phase Y-Ba-Cu-O Compound System at Ambient Pressure, Physical Review Letters, 58*, 1987,* 908

Yamasaki H. and Endo K, *Supercond. Sci. Technol.* 27, 2014, 025014

Yazici S., Olgar M. A., Akca F. G., Cantas A., Kurt M., Aygun G., Tarhan E., Yanmaz E., Ozyuzer L.,Growth of Cu2ZnSnS4 absorber layer on flexible metallic substrates for thin film solar cell applications, *Thin Solid Films,* 2015, 589.

Yurgens A., Winkler D., Zavaritski N. V. and Claeson T., Strong temperature dependence of the c-axis gap parameter of Bi2Sr2CaCu2O8+x intrinsic Josephson junctions, *Physical Review B,* 53,1996a.,R8887.

Zhang C. H., Wu J. B., Jin B. B, Ji Z. M., Kang L., Xu W. W., Chen J., Tonouchi M. and Wu P. H. Low-loss terahertz metamaterial from superconducting niobium nitride films, *Opt Express*, 20, 2012, 42–7

Zhang C. et al., Nonlinear response of superconducting NbN thin film and NbN metamaterial induced by intense terahertz pulses, *New J. Phys.,* 15, 2013,055017

Zhang C., Jin B., Han J., Kawayama I., Murakami H., Wu J., Kang L., Chen J., Wu P. and Tonouchi M., Terahertz nonlinear superconducting metamaterials, *App. Phys. Lett.* 102, 2013,081121

VİTA

Yasemin Demirhan was born in İzmir, Turkey, on June 4, 1985, the daughter of Prof. Dr. Ahmet Doğan Demirhan and Necla Demirhan. After finishing İzmir Atatürk Anatolian High School, she went on to the İzmir Institute of Technology and she completed a Bachelor of Science in Physics in June of 2008. In September 2008, she entered the graduate school at İzmir Institute of Technology. She received an M.Sc. degree in June 2011 in Physics and Ph.D. degree in July 2017 in Materials Science and Engineering from İzmir Institute of Technology. She worked as a research assistant between 2009 and 2017 in İzmir Institute of Technology. She has also experience on e-beam lithography and various deposition techniques such as evaporation and magnetron sputtering technique, and characterization techniques such as electrical and optical characterization.

Selected Publications:

Y. Demirhan, H. Alaboz, M. Nebioglu, B. Mulla, M. Akkaya, H. Altan, C. Sabah, L. Ozyuzer, *Superconductor Science and Technology*, **30**, 7 (2017).

Y. Demirhan, H. Alaboz, L. Ozyuzer, M. A. Nebioglu, T. Takan, H. Altan, C. Sabah, *Opt. Quant. Electron*. **48**, 170 (2016).

Y. Demirhan, H. Saglam, F. Turkoglu, H. Alaboz, L. Ozyuzer, N. Miyakawa, K. Kadowaki, *Vacuum* **120**, 89-94 (2015).

M. A. Nebioglu, T. Takan, H. Altan, **Y. Demirhan**, H. Alaboz, L. Ozyuzer, C. Sabah, *Mod. Phys. Lett. B* **31**, 1750074 (2017).

T. Semerci, **Y. Demirhan,** N. Miyakawa, H. B. Wang, L. Ozyuzer, *Opt. Quant. Electron.* **48**, 340 (2016).

F. Turkoglu, L. Ozyuzer, H. Koseoglu **Y. Demirhan,** S. Preu, S. Malzer, Y. Simsek, H.B. Wang, P. Muller, *Physica C: Superconductivity* **491**, 7-10 (2013).

F. Turkoglu, H. Koseoglu, **Y. Demirhan,** L Ozyuzer, S Preu, S Malzer, Y Simsek, P Müller, T Yamamoto and K Kadowaki, *Superconductor Science and Technology* **25**, 125004 (2012).

H. Alaboz, **Y. Demirhan,** H. Yuce, G. Aygun, L. Ozyuzer *Opt. Quant. Electron*. **49**, 238 (2017).

T. Semerci, **Y. Demirhan,** N. Miyakawa, H. B. Wang, L. Ozyuzer, *Springer:* THz for CBRN and Explosives Detection and Diagnosis **Book Chapter**, pp 75-83 (2017).